IoT Based Sodar Network for Estimation of Atmospheric Boundary Layer

A Thesis

Submitted in fulfillment of the requirements for the Degree

of

Doctor of Philosophy

in

Electrical and Instrumentation Engineering Department

by

PARAG CHOUREY
(901704007)

Under the Guidance of

Dr. Kirti Soni
Principal Scientist
CSIR-NPL, Delhi

Dr. Nirbhow Jap Singh
Associate Professor, EIED
TIET- Patiala

Dr. Ravinder Agarwal
Professor, EIED
TIET-Patiala

Electrical and Instrumentation Engineering Department
Thapar Institute of Engineering & Technology, Patiala
(Declared as Deemed-to-be-University us 3 of the UGC Act., 1956)
Punjab (India)

September 2022

Dedicated to my parents

Shri. D. P. Chourey

&

Smt. Maya Chourey

DECLARATION

I hereby certify that the work which is presented in the dissertation entitled, "**IoT Based Sodar Network for Estimation of Atmospheric Boundary Layer**", in partial fulfilment of the requirements for the award of the degree of Doctor of Philosophy submitted to the Electrical & Instrumentation Engineering Department of Thapar Institute of Engineering and Technology, Patiala is an as authentic record of my work carried under the supervision of Dr. Ravinder Agarwal, Dr. Nirbhow Jap Singh, and Dr. Kirti Soni.

The matter contained in this thesis has not been submitted elsewhere for the award of any other degree in India or Abroad.

Place: Patiala
Date: 23/05/2023

(Parag Chourey)
Reg No.: 901704007

It is certified that the above statement made by the student is correct to the best of my knowledge and belief.

(Kirti Soni)	(Nirbhow Jap Singh)	(Ravinder Agarwal)
Principal Scientist	Associate Professor	Professor

ACKNOWLEDGEMENT

Every goal is achievable with firm determination and true guidance. Giving up is our greatest weakness and the most certain way to achieve success is to try again. The meaning of life is to gain knowledge from every possible source and the purpose is to serve it back to nature and society. I am fortunate to have had the assistance of so many individuals in achieving my goal. I am thankful for their direct and indirect contributions to my life.

Before expressing my deepest appreciation to all of my mentors, I would like to thank my greatest teacher, ***God, and my parents****, who have given me the ability to believe in myself and the drive to pursue this study. I could never have accomplished this without their blessings.*

I would like to express my deep gratitude to my supervisors ***Dr. Ravinder Agarwal****, Electrical and Instrumentation Engineering Department, Thapar Institute of Engineering and Technology, Patiala,* ***Dr. Nirbhow Jap Singh****, Electrical and Instrumentation Engineering Department, Thapar Institute of Engineering and Technology, and* ***Dr. Kirti Soni****, Council of Scientific and Industrial Research – National Physical Laboratory, for their consistent encouragement and support. I am extremely fortunate to have had the opportunity to work under their supervision. The completion of this project would not have been possible without their foresight and encouragement, for which I am extremely grateful.*

I would like to thank ***Dr. Prakash Gopalan****, Director TIET, Patiala, and* ***Dr. Dinesh K. Aswal****, Director, CSIR-NPL, New Delhi for providing facilities for current research work. I am also truly thankful to* ***Dr. R. S. Kaler****, the department head, and the members of my doctoral research committee for providing insightful feedback throughout the course of this research. Sincere thanks to* ***Dr. Sanjay Yadav****, Head of Division, Physico-Mechanical Metrology, CSIR-NPL, New Delhi, and* ***Dr. Mahavir Singh****, Head, Acoustics and Vibration Metrology, CSIR-NPL, New Delhi, for their invaluable advice and attentiveness at every stage of my studies.*

I am also mighty thankful to my fellow researchers ***Nishant Kumar, Rohan Kamra*** *and all lab mates of Biomedical Research Lab, TIET, Patiala and A&V Metrology, CSIR-NPL, New Delhi for always being an excellent support to me. I also like to extend my sincere thanks to* ***Dr. Rohit Gupta*** *for their fruitful technical discussions during the entire journey.*

I am grateful to ***my parents*** *for inculcating seeds of knowledge in me and for standing by me throughout my life. They have been the primary source of energy and motivation for completing this thesis. I would like to thank my sister* ***Yamini Chourey*** *and brother* ***Pankaj Chourey*** *from the bottom of my heart for their unconditional support and belief throughout this journey.*

Although I have tried to express my gratitude to everyone who has contributed directly or indirectly to this work, it is possible that I have overlooked someone. Last, but certainly not the least, I would like to thank such souls.

(Parag Chourey)

Table of Contents

Summary

The advancement in connected and interactive networks such as the Internet of Things (IoT) has paved the way for the networking of various meteorological sensors to study and research in atmospheric science. Nowadays, it is important to consider regional meteorological parameters for planning and management the air quality of a defined area. The atmospheric boundary layer (ABL) is one of the essential components of meteorology and is utilized to estimate the emission and dispersion of air pollution. An integrated network of meteorological sensors using IoT expedites real-time monitoring of critical parameters. These networks facilitate regulatory authorities in enhancing their decision-making and planning in the fields of atmospheric science and air quality management.

Remote sensing techniques have dominated the field of lower atmospheric parameter monitoring. Sonic Detection and Ranging (SODAR) is a robust technique to estimate the ABL structures. SODAR is a remote sensing technique that relies on acoustic backscattered signals to plot echogram structures. The ABL height is estimated by echogram structures which are interpreted as standard atmospheric conditions such as convection, inversion and *etc.* based on the echogram patterns. In the modern era of the Internet and informatics, the combination of ground-based and remote sensing meteorological sensors provides a new paradigm for ABL estimation.

In this research work, an IoT-based SODAR network has been created for estimation and monitoring of the ABL height. Monostatic SODAR is used to measure the ABL height. The air quality of a region depends on the local pollutants and environmental conditions along with the pollutants transported through the region. The transport of hazardous gases and particulate matter has a significant impact on the quality of the air. The primary goal of this research is to develop an IoT-based SODAR network (IoT-SN) for measuring the ABL height at various locations in Northern India. The development process initiates with designing of an analog signal conditioning system for Monostatic SODAR followed by creation of an IoT-SN and integration of meteorological sensors with the IoT-SN. Furthermore, an attempt has been made to determine the relationship between the ABL height and other meteorological parameters such as temperature, relative humidity, wind speed, and wind direction.

In the initial phase of research, an ultra-low-noise amplifier (ULNA) and dual-amplifier band-pass (DABP) filter have been designed for analog signal conditioning of SODAR. The designed analog signal conditioning system features improved gain and high signal-to-noise ratio (SNR) of 65 dB and 92 dB, respectively. The results have been then compared to the existing analog signal conditioning system. The existing analog signal conditioning stage consists of single low-noise amplifier (SLNA) and state variable (SV) narrow band-pass filter. It has been observed that the updated system has significant advantages in terms of gain and narrow band-pass response. The updated SODAR system has been deputed to capture the echogram structures. The resulting echogram structures demonstrate the efficiency in capturing the well-known standard structures of ABL.

The second phase of research focuses on designing a digital signal processing and data processing system for SODAR in order to make it suitable for IoT networking. The updated SODAR system has been installed at the different locations of Northern India which includes Delhi, Roorkee, Aligarh, Alwar, Hisar, and Sangrur. The IoT-SN data has been validated against the local station data. The analysis yielded encouraging results, with a network accuracy of 99.74 % and ABL height estimation accuracy of 95.57 % from the IoT-SN.

Subsequently, meteorological sensors namely wind sensor (MeteoWind-2), temperature, and relative humidity sensor (MeteoTemp + RH) have been integrated with the IoT-SN. The IoT network consists of SODAR and meteorological sensors has been designated as IoT-SMSN. To maintain the system's reliability, calibration and testing of the sensors has been accomplished at the CSIR-National Physical Laboratory, New Delhi (National Measurement Institute, India). The data received from the IoT-SMSN have exhibited a promising level of accuracy, with a 95 % rate and an uncertainty range of 0.1 to 0.3. In the final phase of the research, correlation between SMSN parameters of all installation sites have been analyzed. In addition, key pollutant data has been collected from the Central Pollution Control Board (CPCB), India, and the relationships between SMSN parameters and air pollutants of each location have been investigated. It has been observed that the proposed system is reliable and accurate and offers distinct advantages in air quality management and planning of a region.

NOMENCLATURE

The main symbols and notations used in this study are listed below. Sometimes a symbol may have an alternate meaning but in such a case; the context is sufficient to avoid confusion.

ABL	Atmospheric Boundary Layer
ADC	Analog to Digital Convertor
AI	Artificial Intelligence
API	Application Programming Interface
AWS	Amazon Web Services
S3	Simple Storage Service
B&K	Brüel & Kjær
BW	Bandwidth
$C_V{}^2$	Wind Structure
$C_T{}^2$	Temperature Structure
CIPM	Comité International des Poids et Mesures
DABP	Dual-Amplifier Band-pass
DSP	Digital Signal Processing
ECG	Electrocardiogram
EIA	Environment Impact Assessment
FIR	Finite impulse response
GPRS	General Packet Radio Service
GSM	General System Mobile
HTTP	HyperText Transfer Protocol
IAM	Identity, Access Management
IAPh	Institute of Atmospheric Physics
IC	Integrated Chip
IoT	Internet of Things
SMSN	SODAR and Meteorological Sensor Network
SN	SODAR Network
LIDAR	Light Detection and Ranging
LTE	Long Term Evolution
MFBP	Multiple-Feedback Band-pass
ML	Machine Learning
MQTT	Message Queue Telemetry Transport
NAMP	National Air Quality Monitoring Programme
NBP	Narrow Band-pass
NMI	National Measurement Institute

Q	Quality Factor
RADAR	Radio Detection and Ranging
RASS	Radio Acoustic Sounding System
SLNA	Single Low Noise Amplifier
SNR	Signal-to-Noise Ratio
SODAR	Sonic Detection and Ranging
SQL	Structured Query Language
SV	State Variable
UAF42	Universal Active Filter 42
ULNA	Ultra Low Noise Amplifier

Chapter 1
Introduction

Science and innovation play a big part in achieving a sustainable environment. The Atmospheric Boundary Layer (ABL) is instrumental in determining the air quality of an environment. It is a lower part of the troposphere where all human and biological activities take place. The ABL behavior dictates whether highly concentrated pollutants are widely dispersed, passed to the free atmosphere, or redeposited at the surface. Due to the high turbulence and nonlinear behavior of the atmosphere in this region, the study of the boundary layer of the atmosphere has always been challenging. The developments of remote sensing techniques such as Sound Detection and Ranging (SODAR) expedite the process of continuous monitoring/studying of the atmospheric boundary layer. The evolution of modern networking tools and techniques, such as the Internet of Things and cloud services, has enabled the expansion of SODAR's application domains, particularly in the study of the atmospheric boundary layer.

1.1 Atmospheric Boundary Layer

The troposphere is the lowest atmospheric layer. The troposphere contains approximately 75-80 % of the mass of the atmosphere. The troposphere contains the majority of cloud types, and all weather phenomena take place in this layer. The atmospheric boundary layer (ABL) is the lowest portion of the troposphere that is directly affected by the earth's surface [1]. The origin of the boundary-layer theory can be traced back to the twentieth century. Since then, significant efforts are devoted to this field, and the resulting progress is truly remarkable. The ABL has strong surface inhomogeneities in the form of thermal heat, momentum, and water vapor fluxes [2]. The amount of surface radiation varies diurnally and also seasonally [3]. The ABL structures and their growth are affected by the corresponding changes in surface temperature [4]. The atmospheric boundary layer influences human lives in many ways including environment, climate, and air quality for survival. Since the majority of the pollutants are emitted or formed in the boundary layer, variations in the boundary layer play a crucial role in determining the dispersion of pollutants. The ABL structure and ABL height data have been utilized to measure the

sources of emission [5] and pollution dispersion [6] for Airshed management and planning. Airshed management and planning is a process of maintaining the air-quality in a geographical area within which the air frequently is confined and complete location is subject to similar conditions of air pollution. The thermal heat, momentum, water vapors fluxes, and air pollutants determine the depth of the boundary layer. The boundary layer height ranges from tens of meters to several kilometers, followed by free atmosphere as depicted in Figure 1.

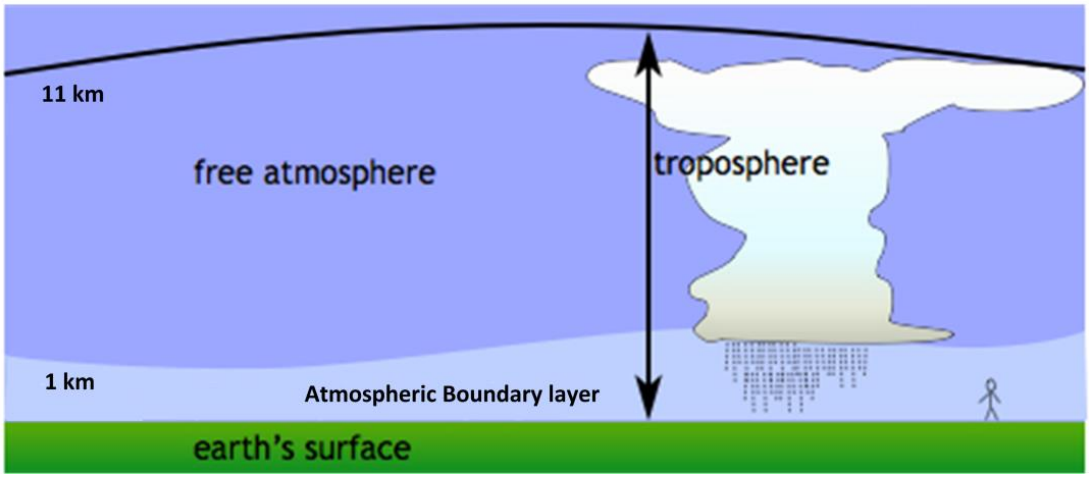

Figure 1.1: Region of atmospheric boundary layer and free atmosphere in troposphere

1.1.1 Measurement Technique of ABL

Prediction and comprehension of the local environment require knowledge of the boundary layer. In particular, the boundary layer is crucial for predicting a variety of parameters. These parameters include near-surface wind and turbulence, daily maximum and minimum temperatures, visibility and fog, and the dispersion of pollutants and other substances. There are two methods for measuring ABL structure, *i.e.,* indirect and direct. The direct method (in-situ measurement) is defined as the process where the instrument is close to the object being measured [7]. In contrast, with the indirect method (remote sensing measurement), the measuring instrument is located at a distance from the object being measured. Radiosonde, meteorological towers, aircraft-based instruments, and balloon-based instruments are the direct measurement techniques for ABL parameters [2, 7]. On the other hand, systems such as Sonic Detection and Ranging (SODAR), Radio Detection and Ranging (RADAR), Radio Acoustic Sounding System (RASS), and Light Detection and Ranging (LIDAR) are utilized to remotely describe the ABL structure [8].

The in-situ techniques provide a detailed profile of the atmospheric boundary layer's height in space. However, one of the major limitations of these techniques is that these instruments do not provide continuous data, which is required for the uninterrupted monitoring of an area's air quality conditions. Due to this limitation, direct measurement methods are ineffective for a comprehensive examination of ABL parameters, which is essential for air quality monitoring [9 - 10].

Table 1.1: Comparative analysis of remote sensing devices for ABL monitoring [11]

Devices	Applications	Operating Frequency / Wavelength	Range	Strengths	Limitations
Monostatic SODAR (Acoustic Sounder)	Atmospheric research, meteorological systems, wind Profiling, air quality studies	1000 Hz – 5000 Hz	10 m to 3 Km	• Low cost • Strong turbulence • Finer vertical resolution • Continuous sampling of data	• Interferences may occur due to acoustic noise • Less reliable output in low humidity and high wind conditions
RADAR (Wind Profiler)	Weather analysis and forecasting, aviation, atmospheric research, air quality studies	915 MHz – 1290 MHz	30m to 50 Km	• Not as sensitive to high wind and acoustic noise as SODAR • Continuous sampling of data • Moderate Cost	• Interference due to objects like a bird, aeroplane • Disturbances due to ground-based radio signal • Performance degrades in a low humid environment
RASS	Air quality studies, temperature profiling	915 MHz – 1290 MHz	50 m to 1 Km	• Can measure virtual temperature profile in ABL • Can work with SODAR	• Conversion is needed for actual temperature measurement • Interference may occur due to ground clutter • Data fluctuate with high wind speed • High Cost
LIDAR	Atmospheric research, wind profiling	0.3 µm – 10 µm	0.15 km to 100 km	• A continuous sample of data • High spatial resolution • No interference due to acoustic and electromagnetic waves	• Performance degrades during fog, clouds, and high aerosol concentration, • High Cost

The continuous measurement of ABL parameters is useful for a variety of applications, including meteorological monitoring, short-term weather forecasting, and estimating the air pollution emission and dispersion. In order to develop an effective air quality management and planning system, there is a need for sensors that can provide data on meteorological variables remotely and consistently. Compared to in-situ techniques, remote sensing instruments offer several advantages, including continuous measurement with minimal manual effort, high-resolution data, and the ability to measure a wide variety of parameters. Temperature, humidity, wind, cloud particles, precipitation, gaseous pollutants, turbulence spectrum, and momentum flux are among the most important parameters measured via remote sensing techniques [9 - 11].

There are number of remote sensing instruments used to measure ABL height. Table 1.1 outlines the advantages and disadvantages of various remote sensing instruments for ABL parameter monitoring. SODAR is regarded as one of the most effective remote sensing instruments and is strongly recommended for the monitoring of ABL parameters.

1.2 Theory of Sound Detection and Ranging (SODAR)

Since the mid-1970s, SODAR is used to measure ABL structures [5, 20]. SODAR works on the principle of acoustic signal scattering in the open atmosphere. The intensity of the scattered acoustic signal at the scattering angle θ depends on the wind and temperature fluctuation in the atmosphere as shown in Equation 1.1.

$$\sigma(\theta) = 0.03k^{\frac{1}{3}}\cos^2\theta\left(\frac{{C_V}^2}{C^2}\cos^2\frac{\theta}{2} + 0.13\frac{{C_T}^2}{T^2}\right)\left(\sin\frac{\theta}{2}\right)^{-11/3} \quad 1.1$$

where, $k = 2\pi/\lambda$ is the acoustic signal's wave number, C is the mean velocity of sound, T is the mean temperature of the scattering volume, and ${C_V}^2$ & ${C_T}^2$ are the wind velocity structure and thermal structure of the atmosphere. The mathematical expression for ${C_V}^2$ & ${C_T}^2$ is given in Equation 1.2.

$${C_V}^2 = \frac{u(x) - u(x+r)^2}{r^{1/3}}\ ; {C_T}^2 = \frac{T(x) - T(x+r)^2}{r^{1/3}} \quad 1.2$$

where, x is a distance and u and T are wind and temperature profiles as a function of x and $x + r$ distance. As the monostatic SODAR receives the scattered acoustic signal at an

angle of 180º backscattered intensity becomes the exclusive function of thermal structure [13].

Figure 1.2 depicts the SODAR system's block diagram. It operates on the backscattered acoustic signal. An antenna, transmitting-receiving (T-R) switch, preamplifier, power amplifier, and computer are the primary components of SODAR. The antenna comprises an acoustic shield, a parabolic dish, and an acoustic transducer. During transmission and reception, the acoustic transducer converts electrical signals to acoustic signals and vice versa. The acoustic shield eliminates surrounding noise, while the parabolic dish transmits acoustic signals perpendicularly into the atmosphere [14].

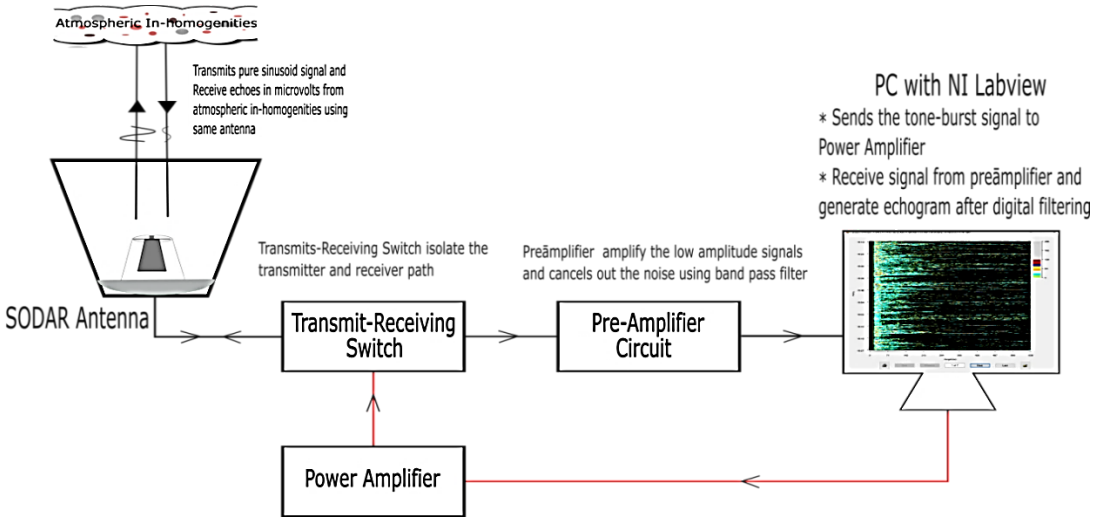

Figure 1.2: Block diagram of monostatic SODAR

A programmable, fixed-frequency, high-tone audio burst signal is transmitted into the atmosphere during the transmission stage. The backscattered acoustic waves from turbulent regions along the propagation path are received and transferred to the T-R switch using the same antenna. The T-R switch reroutes the signal to the preamplifier circuit for analog signal conditioning. The backscattered signals are then plotted in the form of an echogram to estimate the ABL structure [14 - 16].

The reflective index of the acoustic signals with the inhomogeneities of the lower atmosphere is much stronger than that of electromagnetic waves and optical waves [10 - 11]. SODAR is a very economically viable option as well. SODAR-recorded ABL structures are capable to identify the presence of thermal convection, inversion, elevated inversion, advection, subsiding air mass, sudden gust, and other phenomena. SODAR provides valuable data regarding the development of coastal boundary layer occurrences

as well (sea/land breeze) [19]. These data have been utilized to evaluate and comprehend the signal performance of real-time communication links. During the day, the air in the upper atmosphere is colder than the air near the earth's surface. This makes it more buoyant and lighter. This vertical movement is detected by SODAR (dense inverted cones) in the form of thermal plumes. SODAR is one of the most effective instruments to measure ABL height up to 3000 meters altitude [10].

1.3 Internet of Things (IoT)

In this decade, the Internet of Things (IoT) emerged as a revolutionary technology. It offers a very efficient, effective, and user-friendly networking model. Therefore, IoT has received the attention of almost every section of the research community. Many industries and emerging entrepreneurs have contributed to the development of IoT networks for various applications including meteorological weather forecasting. IoT is an advanced automation and analytics system that uses networking, sensing, big data, and artificial intelligence to provide comprehensive product or service systems. It is a system of interconnected computing devices, mechanical and digital machines, objects, animals, and people with unique identifiers and the ability to transfer data over a network.

1.3.1 Major Components of IoT

Things or physical devices, sensors/ actuators, gateway, cloud services, analytics, and user interface are the major IoT components as depicted in Figure 1.3. The things are any physical devices that has capability of exchanging data [20]. In IoT, sensors and actuators are measuring and controlling components of physical devices. Gateway established local and remote connections and shares information with the cloud. Cloud services store all shared data with remote users who have security credentials. Based on the applications, the analytics and user interface provide a meaningful representation of the data [21].

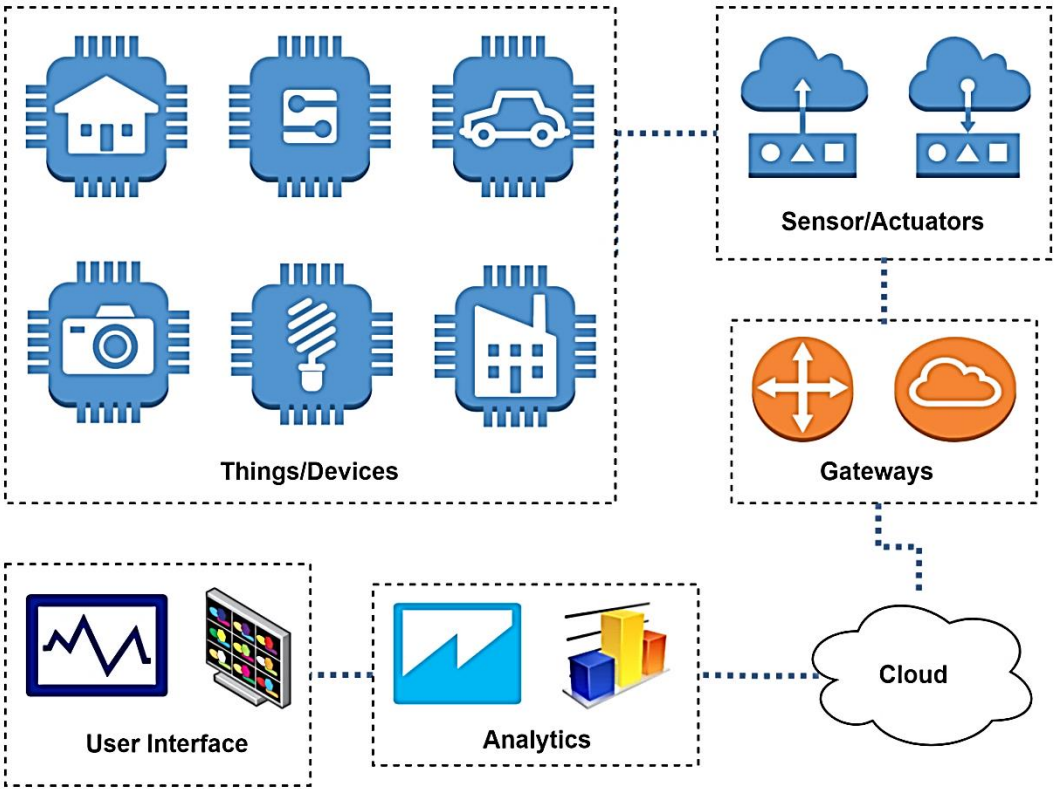

Figure 1.3: Major components of IoT

1.3.2 IoT Architecture

The devices, network structure, and cloud technologies that enable IoT devices to communicate with one another are all part of IoT architecture. Figure 1.4 depicts the basic IoT architecture, which consists of four layers namely sensing, network, data processing, and application. These layers provide information collection and processing to the IoT devices. This architecture goes beyond the Open Systems Interconnection (OSI) model by incorporating data transformation into usable data [22 - 24].

1.3.2.1 Sensing Layer

Sensing layer components include sensors, actuators, and devices. These sensors or actuators receive data (physical/environmental parameters), process data, and transmit data via network.

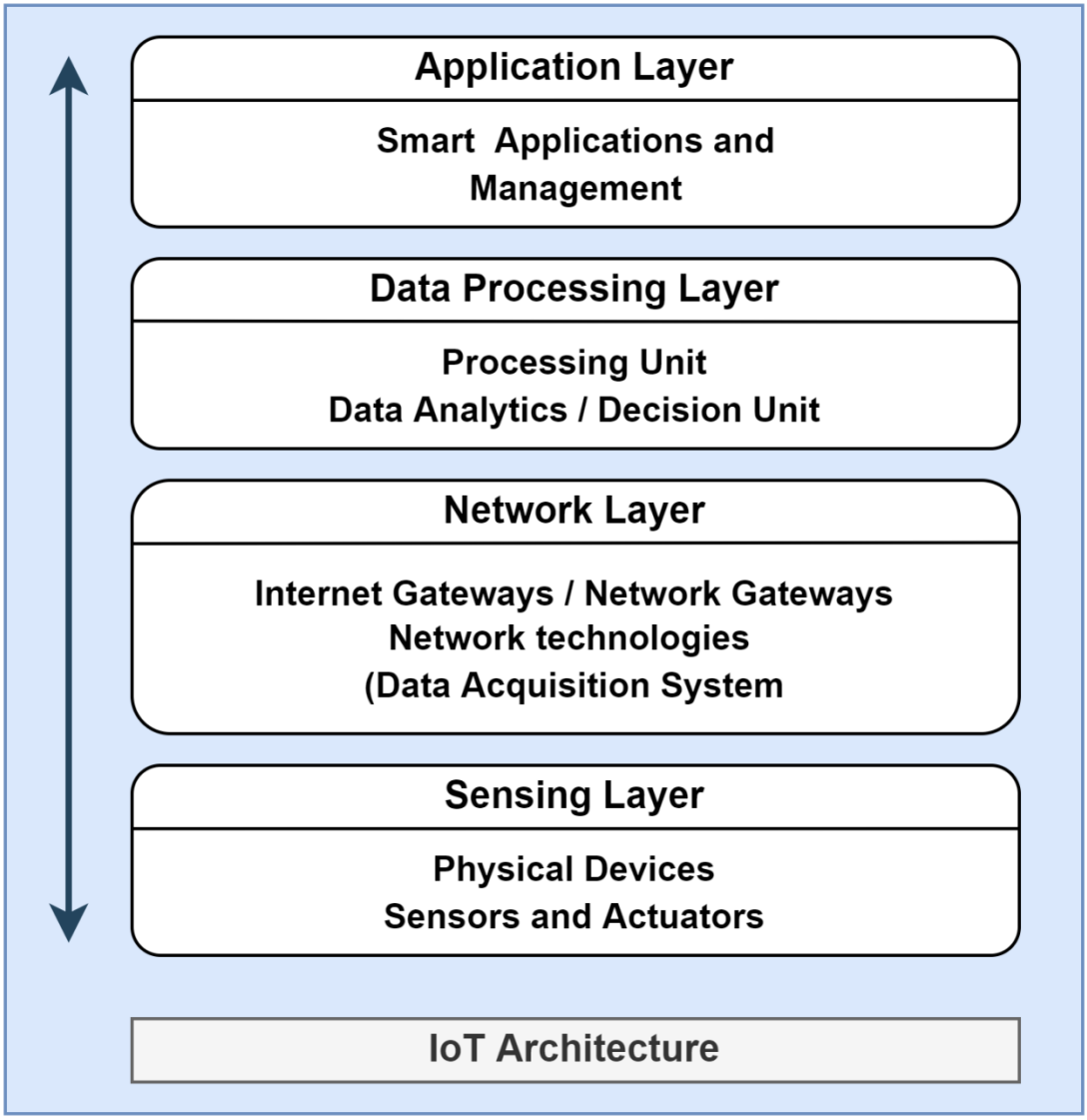

Figure 1.4: Fundamental IoT architecture

1.3.2.2 Network Layer

This layer contains internet/network gateways and data acquisition System. It is responsible for data aggregation and conversion (collecting data and aggregating data then converting analog data of sensors to digital data *etc.*). advanced gateways, whose primary function is to establish a connection between sensor networks and the internet, also perform several fundamental gateway functions, such as malware protection, data filtering, and decision-making based on inputted data, among others.

1.3.2.3 Data Processing Layer

In the data processing layer, data is analyzed and pre-processed before being sent to a data center, from which it is accessed by software applications, often referred to as business applications, where it is monitored, and managed. The Edge information technology plays a crucial role in the IoT architecture.

1.3.2.4 Application Layer

In this layer, data management occurs in data centers or the cloud, where data is managed and used by end-user applications such as agriculture, health care, aerospace, defense, *etc.*

1.4 Objectives and Organization of the Thesis

The main difficulty with SODAR is that the backscattered signals are extremely low in amplitude and highly susceptible to environmental noise [25]. Continuous ABL height measurement and data sharing with regulatory authorities is crucial for regional-level monitoring and planning [26]. The IoT has been used in the last decade to describe the Internet's capability to affect people's everyday life through a wireless network of uniquely identified things [23]. The IoT technique improves governing authorities' decision-making to predict and promote the entire process and planning for long-term growth [27].

1.4.1 Research Objectives

The research work intends to investigate the solution of multi-location data acquisition and collection systems by developing the IoT-based SODAR network for the estimation of ABL height. The research objectives of the work are:

a) To develop an IoT-based SODAR network for ABL height measurement
b) To acquire the data from the IoT-based SODAR network
c) To estimate the ABL height from data collected using the IoT-based SODAR system
d) To validate the results of estimated ABL height at different locations with the established system

1.4.2 Organization of Thesis

This research work intends to develop an IoT-based network for SODAR to estimate the ABL height. A novel signal conditioning stage has been designed for the preamplifier circuit of the SODAR. Thereafter, Labview-based data acquisition software has been used for digital signal processing and IoT networking.

The notable milestones in the measurement methods of the Atmospheric Boundary layer along with the introduction of SODAR, IoT architecture, and development of IoT network are presented in **chapter 1**. The application of SODAR and IoT-based meteorological sensor networks are reviewed addressing their salient features and limitation for the application of air shed management and air pollution monitoring. The significant contributions of various authors related to SODAR signal processing development and relevant topics have also been briefly reviewed in **chapter 2**.

Chapter 3 describes the overall implementation methodology and design theory for IoT-based SODAR networking. This chapter contains three distinct sections. The first section describes the evolution of SODAR's signal conditioning system. It also describes the components and methodology employed. The SODAR analog signal conditioning system includes amplifiers and a band-pass filter. In the second section, the development of the SODAR network utilizing IoT and its applications in airshed management and planning has been analyzed. It begins with the design of digital signal processing and data manipulation that will enable SODAR to monitor the ABL structure in real time. Afterwards, the installation and commissioning of SODAR at multiple locations throughout Northern India have been described. Subsequently, data has been collected from the IoT-enabled SODAR network, and validation methods have been discussed. The final section describes the incorporation of meteorological sensors such as temperature, humidity, and wind into the SODAR network enabled by the Internet of Things. It describes the design of a combined digital signal processing for the SODAR-based meteorological sensor network (SMSN) with IoT functionality. SMSN parameter data validation methods have been also subsequently described.

Chapter 4 describes the experimental analysis, testing, results, and discussions of the IoT Network of SODAR. The initial portion of the results and discussions is centered on the selection of the optimal analog signal conditioning circuit for the SODAR. The

experiments and results of the IoT-based SODAR network and its applications for airshed management and planning are presented in the later section. In addition, meteorological sensors have been integrated with the IoT-based SODAR network and its potential application for effective air quality monitoring systems in defined areas is explored.

Chapter 5 presents brief summary and conclusion of the research undertaken and discusses its potential future recommendations.

Chapter 2
Literature Survey

This chapter provides an exhaustive summary of the research work on atmospheric boundary layer, SODAR, and IoT and their application in air quality monitoring. It begins by providing an overview of the atmospheric boundary layer and air quality followed by the development of SODAR, its signal processing, and its application of SODAR in air pollution studies. Later, the IoT and its applications in meteorological studies are discussed.

2.1. Atmospheric Boundary Layer and Air Quality Monitoring

The Atmospheric Boundary Layer is the lowest portion of the atmosphere, located between 100 and 6000 meters above the earth's surface. The ABL-height estimation measures the capacity of the environment to disperse atmospheric pollutants. The topography of the earth's surface has a direct effect on the behavior and characteristics of atmospheric pollutants. It significantly carries a higher amount of air pollutants than the rest of the atmosphere. The evolution of the ABL structure has significant impacts on the diffusion, transmission, and disappearance of pollutants in the lower atmosphere [28]. The diurnal variation in temperature and humidity affects dispersion and diffusion in the atmosphere. The earth's surface cools faster than the atmosphere due to emitting long-wave radiation at night; therefore, the temperature increases with height [29]. The nocturnal stable boundary layer is the technical term for this temperature inversion, which lowers the atmospheric turbulence [30].

Temperature stratification discontinuities between the upper and lower layers of the atmosphere cause discontinuous turbulence, which results in the formation of a mixing layer. The atmospheric mixing layer is a significant meteorological parameter. The critical advantage of studying the height of the mixing layer, also referred to as mixing-height is its capability to present the transition time characteristics of the day. It defines the characteristics of the large pollutants variability along with ambient temperature and humidity values between the well-mixed boundary layer and the stable free troposphere [10]. It affects the vertical diffusion of environmental pollutants and water vapor concentrations. It impacts the formation and dissipation of air pollutants [9]. The real-

time observation of mixing-height is beneficial for improving the parameterizations and optimizing the air pollution models.

2.1.1 Estimation of ABL/Mixing-Height

The unstable ABL during the daytime is also referred as the convective boundary layer or the mixing-layer and measurement of ABL height during this time is called mixing-height of the atmosphere. The primary methods for the estimation of ABL height are meteorological radiosonde, airplane surveys, and ground-based remote sensing techniques. The radiosonde is the most convenient method to determine quality ABL height data. However, the discrete nature of observations at a higher cost makes radiosonde unable to provide sufficient temporal resolution of the evolution of ABL height in real-time. Therefore the radiosonde technique is less preferable for air pollution monitoring [10]. As an alternative, airplane surveys are excellent at providing high-resolution ABL height data and accurate weather and pollutant profiles. The significant constraints with airplane surveys are air-traffic control, weather conditions, and observation costs. These constraints limit airplane surveys for shorter periods only [31]. Therefore, the ground-based remote sensing technique is the most advanced and reliable method to acquire continuous observations with a high spatial and temporal resolution of ABL height/mixing-height.

SODAR, LIDAR, and RADAR devices are the three popular ground-based remote sensing methods to estimate ABL height [10]. Doppler wind radar obtains variations of the wind vectors at different altitudes. It identifies the ABL height through wind shear data. The limitation of the wind radar is its lower limit of height detection, which is usually above 200 m, and the vertical resolution is limited to $50 - 250$ m. This limitation interprets wind radar data as less faithful.

Similarly, the LIDAR obtains the vertical profile of the aerosol concentration and discerns the atmospheric ABL height by calculating the height at which sudden changes in the profile occur. The high cost of LIDAR technology makes it less preferable. The SODAR has the best refractive index for the backscattered signals and more sensitivity towards atmospheric echoes. Additionally, SODAR is a very economically viable option. It makes SODAR a more suitable and preferred choice for the continuous measurement of mixing-height [32].

The continuous measurement of ABL height data and some meteorological parameters is one of the critical challenges for the regulatory authorities in the regional level monitoring of air pollution [33]. The air pollutants' transportation and dispersion take place on a wide range of geographical scales. International organizations deal with global issues such as climate change, stratospheric ozone depletion, and inter-continent transport. Similarly, it is a nation's duty to plan and manage all stakeholders and regulatory agencies in accordance with a regional perspective [34]. In India, the Central Pollution Control Board (CPCB) provides ambient air quality information through the National Air Quality Monitoring Programme (NAMP) [32 - 34]. The NAMP determines the violated air quality standards of all Indian cities and takes corrective measures. The local pollution is observed by estimating the different pollutants, such as Carbon Monoxide (CO), Sulphur Dioxide (SO_2), Nitrogen Dioxide (NO_2), Ozone(O_2), Ammonia (NH_3), and Particulate Matter 2.5 (PM2.5) [38 - 39]. However, effective air pollution monitoring is only achievable when the measurement is not limited to the local pollutants.

Northern India, especially Delhi, is the epicenter of air pollution and is listed among the top polluted cities in the world. The literature study gives an insight into the megacities like Delhi that air pollution in big cities primarily relies on the transported aerosols from the surrounding atmosphere [40 - 41]. The literature study also states that the local and transported pollutants are equally responsible for the poor air quality in Delhi [42]. Especially agriculture residue burning is one of the significant sources of black carbon, aerosol, trace gases, and other pollutants in Delhi [43]. Therefore, it is essential to measure the dispersion and diffusion process of the whole region for air pollution monitoring in the city. Several meteorological parameters impact the air pollution dispersion process. The mixing-height, wind profile, ambient temperature, and relative humidity are significant parameters for monitoring dispersion [44].

2.1.2 Air Pollution and Meteorology Monitoring Systems

The key contributing factors to atmospheric pollution comprises burning fossil fuels, mining processes, industrial activities, transportation systems, and agricultural activities. The air quality of an atmosphere is decided by the measurement of NOx, SO_2, O_3, CO, PM2.5, and PM10 [39 - 40]. The significant environmental parameters affecting atmospheric pollutants are temperature, humidity, altitude, wind speed, and pressure [36]. Therefore, an effective monitoring system to combat all these factors is necessary for

accurate measurement. Since environmental pollution is dependent on the atmospheric dispersion and diffusion process and its distribution is not uniform, the source of location and its vigilant selection becomes critical for measurement [47]. To cover all dimensions of a defined area, multiple sensors and multiple sensing nodes with advanced networking techniques are required [21, 42].

The conventional monitoring stations consist of local air pollutants measuring sensors to observe the contaminated air. These stations are very consistent, precise, and capable of counting a widespread group of impurities through analytical instruments, like gas chromatograph-mass spectrometers [49]. Although the established monitoring systems use different approaches, the overall goal and general architecture of these systems are similar and continuous monitoring of transported pollutants is still missing from the system [50]. The fundamental process of air monitoring systems comprises three main processes, *i.e.*, sensing, analyzing, and decision-making [51]. The later section discusses the significant advancements in the conventional air pollution monitoring systems' hardware, software, and communication protocols.

There is a vast literature on the hardware and software tools for air pollution monitoring systems. The Arduino board is widely used as a sensor node for this application. Lobur *et al.* used the Atmel 8-bit AVR microcontroller to measure essential pollutants such as CO, PM 2.5, CO2, temperature, and humidity in real-time [52]. Dhingra *et al.* [53] proposed the gas sensor kit along with Arduino and Wi-Fi module to monitor the air pollution on the IoT networks. In this, the Arduino module fetches the sensor data and transmits it to the cloud via a Wi-Fi module.

Similarly, Guanochanga *et al.* [54] and Malhotra *et al.* [55] also utilized Arduino as a data acquisition and transmission controller. While Guanochanga *et al.* [54] and Kiruthika [56] added the Raspberry Pi with an air monitoring system as an IoT Gateway for data communication to the cloud. Singh *et al.* deployed the Raspberry pi 3 and Arduino UNO as sensing nodes. They used the ThingSpeak IoT application for real-time data monitoring of the sensor network. Generally, Arduino, GSM module, Raspberry Pi, and other micro-controller boards are utilized as an IoT gateway.

The software and cloud services for user application development and data management include Labview, MATLAB, Android, Structured Query Language (SQL), DBMS (database-management), AWS (Amazon web services), ThingSpeak, *etc.* The

communication protocol is critical for the sensor network [57]. Generally, two different communication protocols are required in any sensor network, first, for the local networking between the sensors done by a wireless sensor network, and second for the data communication between sensor nodes to monitoring stations done by IoT gateways [58]. The protocols such as Zig-Bee and Bluetooth are widely used for short-distance data communications whereas, Wi-Fi, General Packet Radio Service (GPRS), Long Term Evolution (LTE) Network, GSM (General System Mobile), and radiofrequency communication protocols are used for long-distance data communication [59]. Additionally, the data communication over the web is done by the HyperText Transfer Protocol (HTTP) and Message Queue Telemetry Transport (MQTT) protocols [49].

Moreover, low measurement accuracy is the main obstruction to the reliable deployment of the meteorological sensors network. Several researchers found the error sources after testing and analyzing the sensor and signals over the years and categorized errors into two main categories internal and external. Internal errors include the working mechanism of sensors which depend on the dynamic boundaries such as systematic errors, nonlinear response, and signal drift [60]. While the significant sources of external errors are environmental circumstances that depend on the site selection. The calibration of the sensors from authentic organizations before installation becomes extremely important to form a trust-worthy sensor network [55 - 56].

2.1.2 Role of ABL in Airshed Management and Planning

Nowadays, Airshed management planning is one of the significant methods to improve air quality in a specific area. The air quality of an area is influenced by various factors like emission sources, pollution dispersion, regional wind profiles [63], and the decision of regulatory organizations. Therefore, maintaining the air quality index requires collaborating efforts from all the stakeholders. SODAR is recommended by the Environment Impact Assessment (EIA) in the United States and is also considered among the mandatory list of instruments for air quality measurement index by Central Pollution Control Board (CPCB), India [8]. SODAR is used worldwide to estimate various atmospheric parameters like wind velocity [25], temperature profile, stability parameters [15], ventilation coefficients [26], and pollution dispersion [64]. For Airshed management planning, the ABL structure and height data are used to measure the emission sources [5] and pollution dispersion [6].

2.2 Sound Detection and Ranging (SODAR)

In recent years, there is a growing interest in the study of the lower atmosphere, as it provides information on vital parameters such as aerosol, inversion/convection, ABL height, *etc*. [65]. Due to its high refractive index [64 - 65] and ability to capture continuous temporal data in real-time from the atmosphere, SODAR has distinct advantages among others [11].

2.2.1 History of SODAR Development

In this section, the research contributions and studies related to SODAR are summarized. In 1941 Obukhov [68] proposed the principal of SODAR. In the late 1950s, Obukhov initiated the practical studies of backscattering sound by turbulence and the application of SODAR in the field of the ABL at the Institute of Atmospheric Physics (IAPh) [69]. A SODAR antenna with a vertical beam was the first working model and was utilized to study atmospheric turbulence [18]. In 1975, Singal [13] developed a conventional monostatic SODAR at CSIR-National Physical Laboratory (CSIR-NPL), New Delhi for measuring the ABL depth and structure. Several researchers have contributed to the development of SODAR for different applications. A significant contribution in the field of SODAR is designing the doppler SODAR in bi-static [70] and monostatic mode [69 - 70] for wind profile measurements. The results from the doppler SODAR have also been compared with the various in-situ wind sensors at different heights to establish the correlation among them [73]. Moulsley [74] and Elisei [75] have introduced the deployment of loud-speaker arrays for lower atmosphere measurements.

In 1980-90s, monostatic SODAR was utilized in several meteorological studies *viz.*, temperature structure [15], pollution dispersion and stability classification [1, 74], monitoring air pollution [77], and dispersion capacity of the environment [72]. In 1993, Gera [78] upgraded the SODAR with a microcomputer and an offline echogram facility. In the late 1990s, high-frequency SODAR also called mini-SODAR have been designed and employed for the measurement of the wind profile in the lower atmosphere [77, 78]. In 1997, Asimakopoulos have proposed significant advancements in data processing and high-resolution visualization with color display [81]. This technique displays the echoes in different color coding for each level with lower and higher amplitude signals presented by the darker and brighter colors respectively. Sabine [86 - 87] designed a transponder

prototype for the comparison of different SODAR models with measurement methods of beam patterns to improve data accuracy.

In 2011, Gera [78] designed an upgraded version of SODAR in CSIR-NPL using improved digital signal processing with faster response, and a more efficient data visualization technique. This design has a single amplifier and state-variable type filter for analog signal processing. In 2008, CSIR-NPL implemented a SODAR system with a single amplifier and a state-variable narrow band-pass (NBP) filter designed by Gera *et al.* [78]. This conventional SODAR is installed at the CSIR-NPL as well as the CPCB, New Delhi, and it is being utilized effectively for various ABL studies in real-time. Saha *et al.* [26] observed the ventilation coefficient of the atmosphere, an essential parameter for determining the dispersion of air pollutants, using eight years of ABL data. Similarly, Kumar *et al.* [25] utilized the SODAR data from Delhi in 2013-2014 to estimate the various classes of atmospheric stability. SODAR has been constantly used in Greece [84], Moscow [85], Japan [86], and Russia [87] for atmospheric research and studies.

SODAR operates in an open atmosphere and is exposed to different types of noises. Noise management is a difficult task in SODAR. Noise can be broadly classified into two categories: intrinsic and extrinsic noise. The predominant sources of extrinsic noise are automobiles, birds, aeroplanes, and other ambient sounds. In contrast, intrinsic noise is produced by the SODAR's internal electronic components [85 - 86]. Both intrinsic and extrinsic noises require separate analyses and efforts, and both are equally important. The acoustic properties of the antenna's design and installation location mitigate the SODAR's extrinsic noise. While it is crucial to design an effective analog conditioning system for its fragile backscattered signals [90].

The climate, geographical location, meteorological parameters, and nearby elevated structures of measurement sites have a significant impact on the spectral characteristics of extrinsic noise. As a result of these variables, the noise spectrum varies considerably based on location. This noise spectrum distinguishes backscattered acoustic signals from air turbulence, making it difficult to extract information from unprocessed backscattered signals. Therefore, it is essential to conduct a noise mapping analysis of the installation site to determine the maximum noise level in the frequency spectrum.

In the preceding two decades, researchers have conducted a variety of studies for extrinsic noise evaluations of SODAR and identified methods for its mitigation. Recently, in 2021,

Kumar *et al.* [14] investigated the characteristics of atmospheric noise and developed a SODAR antenna with enhanced acoustic properties. The comprehensive study on the acoustic testing was performed in the Department of Acoustics and Vibration metrology section of CSIR-National Physical Laboratory, New Delhi (National Measurement Institute, India). The analysis report elucidated the improved performance of the antenna's essential acoustic properties, such as the sound absorption coefficient and noise reduction coefficient. In 1998, Gennaro *et al.* [91] investigated the impact of ambient background noise on SODAR performance. The acoustic shield has been utilized to control the active ambient noise and to isolate the side lobe energy of the transmitted acoustic pulse [92]. The majority of prior research has focused on noise reduction. These techniques effectively enhance the signal-to-noise ratio (SNR). However, these methods of noise cancellation are not applicable to intrinsic noise.

2.2.2 Signal Processing for SODAR

Analog signal processing is a critical part of the SODAR system. As the backscattered acoustic signal intensity is highly sensitive to atmospheric noise, a robust preamplifier design with higher noise reduction is of utmost importance. In 2011, Gera *et al.* [78] presented a study in which a preamplifier based on a single low-noise amplifier (SLNA) and state-variable (SV) technique has been used for amplification and filtering purposes to improve the system's SNR performance. In addition, a real-time active noise cancellation algorithm has been created to extract ambient noise directly. The low-noise amplifier and the NBP filter play a crucial role in enhancing the SNR performance of the SODAR system.

Low-noise amplifiers are used in a variety of applications, including communication systems, medical signal processing, and remote sensing systems. [89 - 90]. It has the remarkable advantage of being susceptible to low-amplitude signals [91 - 92]. Low-noise amplifiers are popular in acoustic signal processing [97]. In addition, it is observed in the literature that the parallel combination of the low-noise amplifier configured as a summing amplifier, also known as the "Ultra-Low-Noise Amplifier" (ULNA), has an even better gain and SNR response than the SLNA [94 - 96]. The N-Stage ULNA configuration improves the SNR by $\sqrt{N}$ times, where N is the number of the parallel amplifier connected in the summing configuration [96 - 97]. It is also utilized for the signal conditioning stage in acoustic applications [102].

Designing a narrow band-pass filter with a high quality factor (Q) and stable response is another essential aspect of the SODAR's analog signal processing [107 - 108]. The universal active filter (UAF42) from Texas Instruments (TI) is a prominent integrated chip (IC) for designing the SV topology [105]. It has been utilized in many applications, including biomedical instrumentation [100 - 101], intelligent wearable [108], fibre optics and laser technologies [109], and audio signal processing [112]. The SV filter realisation method provides sufficient stability and is temperature insensitive. Due to its reliance on circuit components, however, this method is less suitable for high Q filter designs [111]. Similar to SV technology, the multiple-feedback band-pass (MFBP) filter realisation technique offers substantial benefits for NBP filter realisation [112]. This topology is ideally suited for high-frequency filtering techniques due to its low dependence on the performance of operational amplifiers (op-amps). In addition, the MFBP has significant drawbacks in terms of its over-dependence on the passive components of the circuit and is therefore deemed inappropriate for high Q filter designs [113].

However, many researchers also employed the dual-amplifier band-pass (DABP) method to create NBP filters [114]. Ikeda [115] uses DABP topology to design a high Q filter for the broadcast signal reception system. Moreover, Ikeda [116] implements the DABP technique in the antenna input tuning circuit to enhance the filter response's selectivity. The DABP technique has substantial advantages, such as a stable output response, low sensitivity, and the ability to design high Q filters [111 - 112]. DABP also permits the adjustment of the central frequency without affecting the Q value of the filter [119].

Further, the output signal from analog signal processing stage required digital signal processing for suitable data presentation. The first stage of digital signal processing is analog to digital conversion (ADC). The in-built ADC of the computer in computer-aided applications is highly useful due to its fast sampling rate i.e., $44.5\,Khz$. The high sampling rate allows to gather more data points and more granular information is obtained about the echogram received from SODAR. Data processing and manipulation is a significant task and the peak-detection method plays a crucial role to extract crucial data points and peaks for better monitoring of signals in the time domain [120]. The last stage of signal processing is digital filtering which eliminates the data points outside the desired frequency range [121]. The digital Finite impulse response (FIR) band-pass filter is one of the popular filtering techniques to eliminate the undesired frequency signals in the acoustic field [122].

2.2.3 Application of SODAR in Air Pollution

The Atmospheric Boundary Layer is considered a circulatory system of the biosphere. It lies in the boundary layer where photosynthesis and respiration activity of plants and animals takes place. It also helps to remove the waste product and thus to cleanse the atmosphere using photochemical reactions. This layer disperses the heat and moisture gathered at the earth's surface horizontally and vertically. This process effectively improves the air quality of the biosphere and provides a conduit for the propagation of weather systems on all scales [28]. An acoustic sounder is a proven technology for estimating the ABL structures. This section briefly discusses the application of acoustic sounder/SODAR in air pollution estimation and modelling [72].

In the examining process of ABL height estimated by SODAR during turbulent stable boundary layer, it is noted that the SODAR measured ABL height is in the lower range than the height required for the air pollution modelling by Koracin and Berkowicz [123]. The main reason for the SODAR measured ABL height depends on the velocity fluctuations in the nocturnal stable boundary layer for pollutants dispersion. In contrast, the monostatic SODAR is sensitive to the temperature coefficient only. The magnitude of the temperature fluctuations decreases much faster with height than the velocity fluctuations. Nevertheless, the lack of other reliable techniques for continuous ABL height measurement makes the SODAR the best option to measure ABL height for the study of the turbulent stable boundary layer. Likewise, Caughey [124] also reported the importance of qualitative pictorial representation of the turbulent stable boundary layer from the acoustic sounder.

The direct determination of the daytime ABL height is limited to heights within the SODAR probing range. In contrast, the ABL height is higher than the probing range for most sites. Singal and his associates [125] studied the stable layer structure of SODAR to determine ABL height. Based on the Holzworth model [126] using radiosonde data of Delhi, the studies of the convective boundary layer height have been established. The ABL height is obtained on a daily basis from radiosonde and compared with the corresponding SODAR measured depth of the thermal plumes. These comparison results have been used to develop an empirical relation to determine the ABL height from the SODAR observed thermal plume height [28], as shown in Equation 2.1.

$$y = 4.24x + 95 \qquad 2.1$$

Here y is the estimated ABL height as per the Holzworth model, and x is the SODAR measured thermal plume height.

Gera and Singal [77] proposed a technique to determine the dispersion coefficient using the monostatic SODAR. The echogram structures from SODAR installed at the sounder at Chittorgarh (India) have been used to observe the vertical dispersion when the plume is passing over the sounder. Similarly, Coulter and Underwood [127] have also observed the potential application of SODAR while taking measurements of temperature structure parameters and estimated the relative dispersion coefficients of the cooling tower plume. In this research, the linear relation between the width of the cooling tower plume and the distance from the tower is demonstrated. SODAR can measure ABL and is used to determine related dispersion parameters and is therefore considered as a high potential technique to now-cast the hazardous events related to air pollution. In the following, the efforts to estimate the pollution concentration at a place under different stability conditions using monostatic SODAR are discussed.

Jensen and Petersen [128] proposed a simple box model based on the mixing-height measured by SODAR to calculate SO_2 concentrations in Gladsaxe, Denmark. Moulsley and Cole explored the acoustic sounder application to measure methane plumes in the air and provide information about its size, behavior, and concentration structure [12], [129]. It also helps to measure the wind velocity structure parameters of the methane plume from acoustic scattering measurements. These measurements showed a good relationship between the plume dimensions derived from sounder measurements and predictions of simple diffusion theory. Brusasca *et al.* [130] observed the improvement in the simple Gaussian model by including the remote sensing system has the potential to benefit the more complex atmospheric diffusion model. Gera *et al.* [131] studied the convective conditions air pollution dispersion model in a power station located area. Using acoustic-sounding data for a preferred dispersion model is essential for understanding the convection at complex substandard locations.

Singal and his associates [72] developed a SODAR-based model to predict pollution concentration due to emission over Delhi, India. They have proposed to adopt the normal Gaussian dispersion model for estimating the downwind pollution concentration. The particulate matter concentration to distance from the cement factory located at Nimbahera (Chittorgarh) in Rajasthan, India, has been computed by Singal *et al.* [28] to observe the

dust contribution of the cement factory in that area. The prediction model calculated values have been found in a similar range to the observed particulate matter values. Additionally, the diurnal variations of the computed particulate matter data correlate with the SODAR-determined mixing-height value. As expected, a high rise in particulate matter is observed during the fumigation period.

The linkage between the concentration of the pollutants and locally measured mixing-height in Moscow, Russia, is demonstrated by Pekour and Kallistratova [4]. In this research work, the pollutants variations in time are measured using SODAR and a correlation with the observed air pollutants are estimated. This positive correlation elucidates the practical use of the SODAR-determined parameters such as mixing-height and stratification of the atmospheric boundary layer for air pollution meteorology.

There is significant advancement in acoustic-sounding technique since the initial work of McAllister [25] and Little [66]. It evolved as a valuable tool for remotely probing the information of the atmospheric boundary layer. Besides the many qualitative studies of atmospheric phenomena like inversions, thermal plumes, mixing-height, fog, and sea breeze it provides quantitative information on many important atmospheric pollutants and their dispersion and diffusion coefficient in the atmosphere.

2.3 Internet of Things (IoT) in Meteorological Studies

In this decade, the Internet of Things emerged as a revolutionary technology. It offers a very efficient, effective, and user-friendly networking model. Therefore, IoT has received the attention of almost every section of the research community. Many industries and emerging entrepreneurs have contributed in the development of IoT networks for various applications including meteorological weather forecasting [132], smart irrigation [133], and air pollution monitoring [134]. Dietrich's [135] used IoT based network to measure thermodynamic parameters and predict the frost event using machine learning. In 2019, keswani used the IoT-enabled smart irrigation technique with neural networking and pattern classification to optimize agriculture mechanism [136]. In 2015, Xia [137] presents an alternative IoT and neural network-based technique for the air monitoring system. The Tran-Dang highlighted the challenges of IoT networking in applications consisting of big data [138].

The IoT-based network consists of four basic stages. The sensor and/or actuators, data acquisition system, Internet gateways, and cloud data center. The selection of sensors, data acquisition system, and Internet/gateway is application dependent. In contrast, the selection of cloud services is contingent on the needs of the various data processing techniques and cloud storage. Microsoft Azure, IBM IoT, Xively, SensorCloud, Temboo, Amazon web service (AWS), ThingsSpeak are among the many cloud service providers. Many of these service providers offer features like machine and deep learning tools to deploy models to build end-to-end workflow pipelines apart from the simple storage and visualization facility [138].

The AWS simple storage service (AWS-S3) is a Web services interface that offers access to the same highly scalable, fast, inexpensive, and reliable data storage that Amazon uses to run its own global network of Web sites. The easy storage facility of large data in the S3 is suitable for the research community, as it offers access and management of data remotely. The cost associated with server maintenance or storage availability is reduced [129 - 130]. Bitzer [141] used the NI-Labview and AWS-S3 cloud storage to monitor and control the smart grid operations. The NI-Labview is a well-known graphical programming language that offers advantages of ease of interface, better data visualization, user-friendly programming & debugging environment, and parallel processing. The NI-Labview is widely used in various remote sensing and low-noise applications. In 2020, Sharma [142] designed the real-time data acquisition of Electrocardiogram (ECG) signals using Labview.

Mayancela and Eduardo [143] developed a remote monitoring solution for wind resources using SODAR. This work is focused on creating a telemetry system consisting of Raspberry Pi and Long-range wide area network (LoRAWAN) for IoT Networking of remotely placed SODAR. The SODAR data was utilized for monitoring the wind profile.

The literature compiled in this chapter asserts that the estimation of ABL height has significant benefits in the field of atmospheric science, particularly in the monitoring of air quality in a specific region. Evidently, SODAR is a crucial instrument for determining the height of the ABL, based on the available literature. Literature suggests that efficient analog signal conditioning for SODAR is essential. It was also observed that IoT is an effective tool for effective monitoring and decision-making in meteorological research. Integration of SODAR with IoT has significant benefits for enhancing the effectiveness of ABL height and other meteorological data in air quality management.

Chapter 3
Methodology and Theory

This chapter describes the methodology opted to create an IoT-enabled SODAR network for estimating ABL height. Figure 3.1, shows the complete methodology opted to fulfil the objectives. The first section discusses the analog signal conditioning system for SODAR's theory and design. In the second section, the methods and architecture of the IoT-based SODAR network, as well as its digital signal processing and data processing steps, have been described. Later section describes the incorporation of meteorological sensors into SODAR's digital signal processing. In addition, an IoT-enabled SODAR and meteorological sensor network has been created for monitoring air pollution in Northern India.

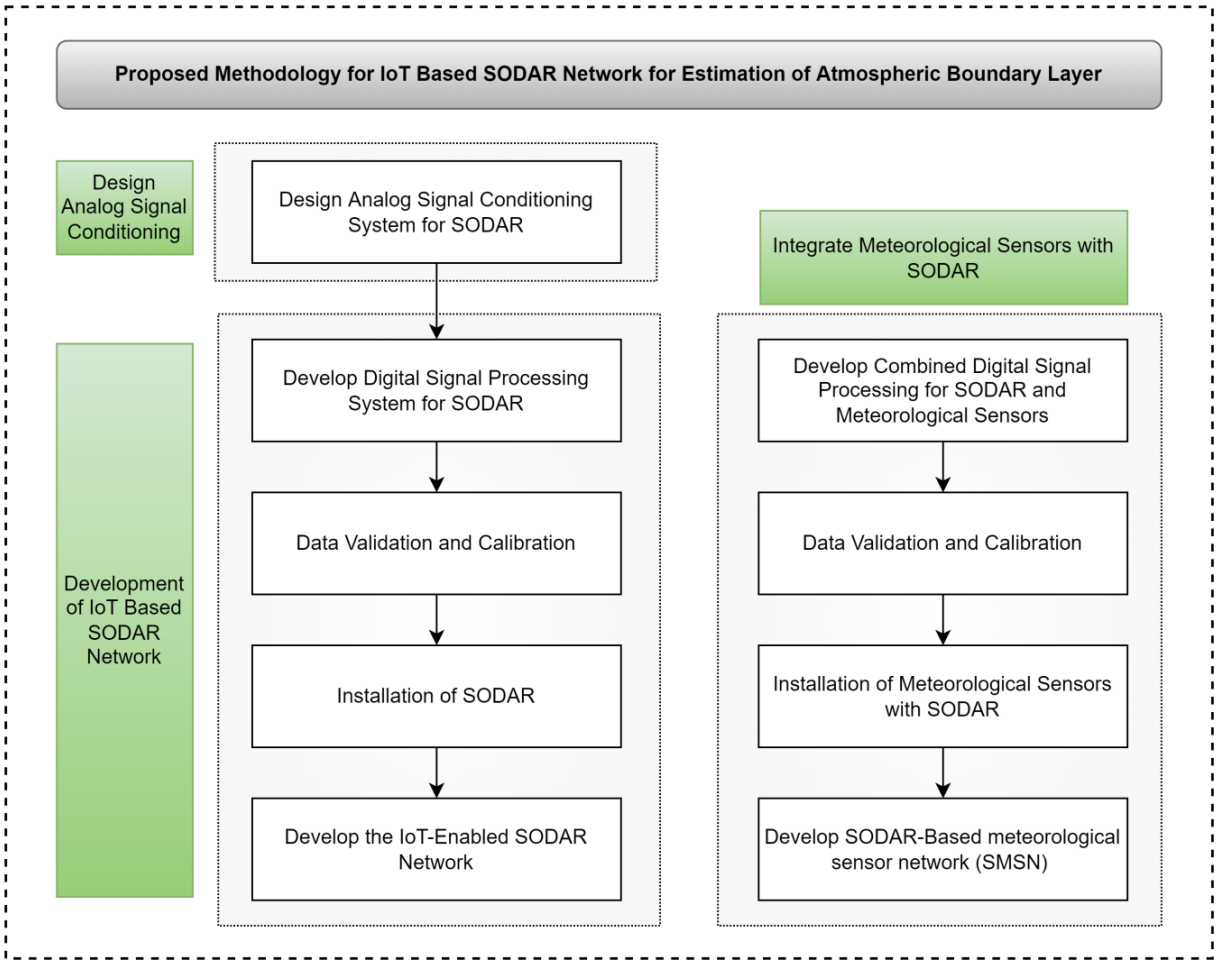

Figure 3.1: Proposed methodology

3.1. Analog Signal Conditioning System for SODAR

The SODAR device is widely used to measure the ABL. SODAR is based on an acoustic principle and uses air-backscattered signals to generate an ABL structure. These signals have extremely low amplitude and are highly susceptible to environmental noise. A novel signal conditioning circuit with high gain, low noise, and a high Q (Quality Factor) has been designed for the SODAR preamplifier. The primary components of this signal conditioning circuit are ULNA and DABP. The designed preamplifier circuit has been implemented and installed with SODAR at the CSIR-NPL, New Delhi. The electrical characteristics of the designed system have been compared to the existing design of a single low-noise amplifier and state variable filter (SLNA-SV) system.

3.1.1. SODAR Analog Signal Conditioning System

The investigation of the lower atmosphere has received more attention, as it provides information on essential parameters such as aerosol, inversion/convection, mixing layer height, *etc.* [65]. Remote sensing is a well-known method for monitoring the temporal and spatial characteristics of the lower atmosphere. SODAR is one of the most well-known remote sensing techniques for ABL structure monitoring [11]. Due to its high refractive index [63 - 64] and ability to capture continuous temporal data from the atmosphere in real time, SODAR has distinct advantages over other technologies [11].

The primary components of SODAR are an antenna, transmitting-receiving (T-R) switch, preamplifier, power amplifier, and central processing unit. An acoustic shield, parabolic dish, and acoustic transducer comprise the antenna. The acoustic transducer converts electrical signals to acoustic signals and vice versa during transmission and reception. The acoustic shield eliminates ambient noise, while the parabolic dish transmits acoustic signals into the atmosphere perpendicularly [14]. The backscattered signals are represented in the form of an echogram to estimate the ABL structure [14 –16].

In the majority of studies, SODAR is deployed in urban areas to monitor the air quality of a region [62, 80]. In certain instances, SODAR is also deployed in coastal or mountainous regions to monitor the behaviour of the ABL [86]. Delhi's CSIR-NPL and CPCB have utilized SODAR for decades to study atmospheric disturbances. CSIR-NPL implemented a SODAR system with a single amplifier and a state-variable NBP filter

designed by Gera *et al.* in 2008 [78]. This conventional SODAR is being effectively utilized for various ABL studies in real-time. Using eight years of ABL data from New Delhi, Saha *et al.* [26] observed the ventilation coefficient of the atmosphere. Ventilation coefficient is an essential parameter for determining the dispersion of air pollutants. Similarly, Kumar *et al.* [25] used SODAR data from Delhi in 2013-2014 to estimate the different classes of atmospheric stability. SODAR has been consistently used by various researchers for measuring and predicting atmospheric parameters.

In a literature survey, it was found that a limited work has been published on the analog signal conditioning of SODAR. This research aims to develop a novel signal conditioning circuit for SODAR that employs ULNA and DABP filtering techniques to achieve a better electrical response. Additionally, the existing SLNA-SV designs are also explored and considered for the comparative study [78].

3.1.2 Theory and Design of Analog Signal Conditioning System

Figure 1.2 depicts the development of a variable-width, programmable, high-power acoustic pulse with repeated transmissions. The Ahuja BR 250M power amplifier has been used to increase the transmitted signal from a few watts to between 40 and $60\ watts$. Later, the T-R switch of the preamplifier transfers this pulse to the acoustic transducer. The acoustic transducer (Ahuja AU60 speaker) converts the electrical signal to an acoustic signal with a power of approximately $130 - 140\ dB$. At the reception, the same acoustic transducer collects backscattered signals from air turbulence, and the T-R switch routes them to a preamplifier circuit for additional amplification and filtering. To generate the echogram from the processed analog signal, the data acquisition system then digitally processes the signal. Consequently, this investigation focuses solely on the design strategy and filter techniques for the proposed amplifier.

3.1.2.1 Ultra-Low Noise Amplifier

SODAR captures reflected signals from the open atmosphere. These backscattering signals have low amplitude and are susceptible to noise [65]. The intrinsic noise from the amplifier and the extraneous noise from the circuit and atmosphere are two of the most challenging aspects of designing an ULNA [85 - 86]. The ULNA design has been implemented to reduce the intrinsic noise of the circuit. ULNA's operational amplifier is chosen based on the input's noise spectral density.

The noise spectral density is measured in watts per hertz and is defined as the noise power per unit of bandwidth. The measurement of noise voltage density and noise current density is crucial for calculating noise spectral density. Low source-impedance instruments require an amplifier with low noise voltage density, while high source-impedance instruments require an amplifier with low noise current density [144]. The AU60 has a low input impedance of 16 Ω [145], and operational amplifiers with a lower noise voltage density have been chosen. Equation 3.1 has been used to calculate the noise voltage density of the input source.

$$\frac{Noise\ Voltage\ Density}{\sqrt{Hz}} = \sqrt{4KTR} = \frac{0.514\ nV}{\sqrt{Hz}} \qquad 3.1$$

where K is the kelvin constant (1.38×10^{-23}) in joules/kelvin, T is the room temperature in kelvin (300 K), and R is the source impedance in ohms (16 Ω). Since the source noise voltage density is $0.514\ nV$, an amplifier with an input noise voltage density less than $0.514\ nV$ has been chosen for the amplification stage. The ULNA design's summing amplifier configuration, shown in Figure 3.2, decreases noise voltage density by N while increasing SNR by the same amount. The Texas Instruments (TI) operational amplifiers *i.e.* OPA27 and OPA37 are ultra-low noise and high precision amplifiers. The OPA37 is chosen for a parallel branch of first-stage amplification, while the OPA27 has been selected for second-stage amplification. The intrinsic noise voltage density of parallel configuration of OPA37 and OPA27 amplifiers is approximate $0.87\ \mathrm{nV}/\sqrt{\mathrm{Hz}}$ [101].

The source-to-amplifier impedance match is also an essential aspect of the preamplifier's design. The mismatch in impedance levels between the source and amplifier affects the amplifier's noise performance and reduces the ULNA's overall noise handling capacity. Impedance matching guarantees signal integrity. An audio transformer has been used to increase the source impedance so that it matches the impedance of the amplification stage [146].

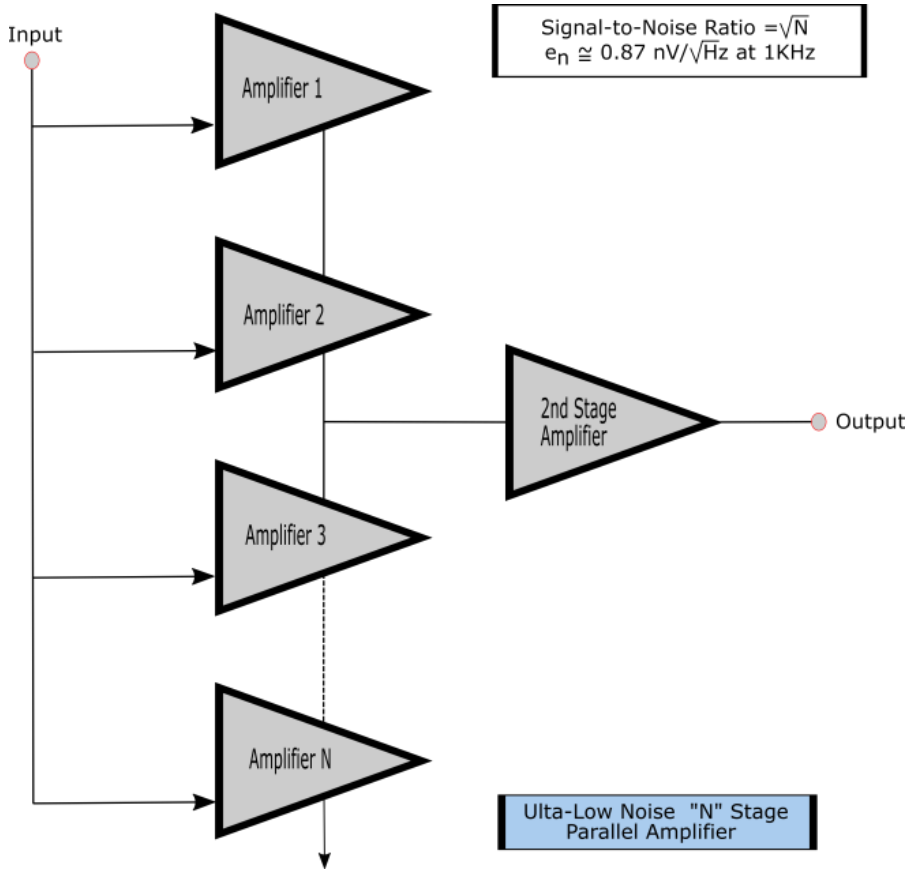

Figure 3.2: Multistage ultra-low-noise amplifier (ULNA)

3.1.2.2 Narrow Band-Pass Filters

The primary task of designing the band-pass filter is providing maximum gain at the selected operating frequency (f_C) of the SODAR and attenuates the signals outside the operating frequency range. The noise mapping analysis of specific location has been conducted to identify the frequency band where atmospheric noise is the lowest. The ISO 1996-2 [147] standard operating procedure has been applied to noise mapping analysis using a Bruel & Kjaer (B&K) type 2270 sound level analyzer. The frequency range between $2 - 2.5$ kHz exhibited the least amount of atmospheric noise. This frequency band has been selected for the CSIR-NPL SODAR's operating frequency. Three NBP filters with good selectivity, stable frequency response, and high SNR have been outlined. The specifications for designing the NBP filters to obtain the desired frequency response from the signal conditioning stage of SODAR are presented in Table 3.1.

Table 3.1: Designed specifications for designing NBP filter for SODAR signal conditioning unit

Center Frequency (KHz)	2.25
Pass band Bandwidth (BW) (Hz)	50
Stop band Bandwidth (Hz)	200
A_s *	4
Q **	45
Pass band Attenuation (dB)	-3
Stop band Attenuation (dB)	-20

* Steepness Factor (A_s) = $\frac{\text{Stopband Bandwidth}}{\text{Passband Bandwidth}}$

** Quality factor (Q) = $\frac{\text{Center frequency}}{\text{Passband Bandwidth}}$

A. MFBP Filter

Figure 3.3(a) shows the MFBP filter circuit diagram. This configuration has the benefit of a simple design, but its response is more sensitive at higher Q values. The transfer function of the MFBP is given by

$$T(s) = \frac{sC/R}{s^2C^2 + 2sC/R_2 + 1/RR_2} \qquad 3.2$$

In this equation, the input resistor R is divided into R_1 and R_3 to create a voltage divider that controls the gain of the circuit. To maintain the resonant frequency, the resistance value of the parallel combination of R_1 and R_3 is kept equal to the input resistor R. The following equations have been used to calculate the designing parameters Q, R and R_2:

$$Q = \frac{f_c}{BW}\ ; R_2 = \frac{Q}{\pi\, f_c C}\ ; R = \frac{R_2}{4Q^2}$$

For the design of the filter, the constant values $f_c = 50$ Hz, $C = 0.01$ µF, and second-order butterworth attenuation characteristics have been considered [111]. This work presents the use of a multistage (4-stage) MFBP filter for achieving a stable and low-noise frequency response in filtering stage of analog signal conditioning stage of SODAR.

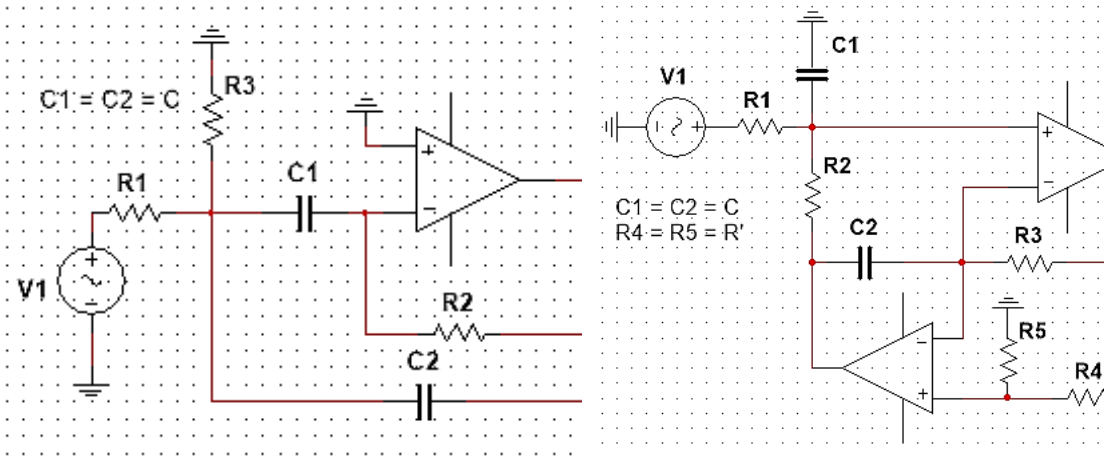

(a) (b)

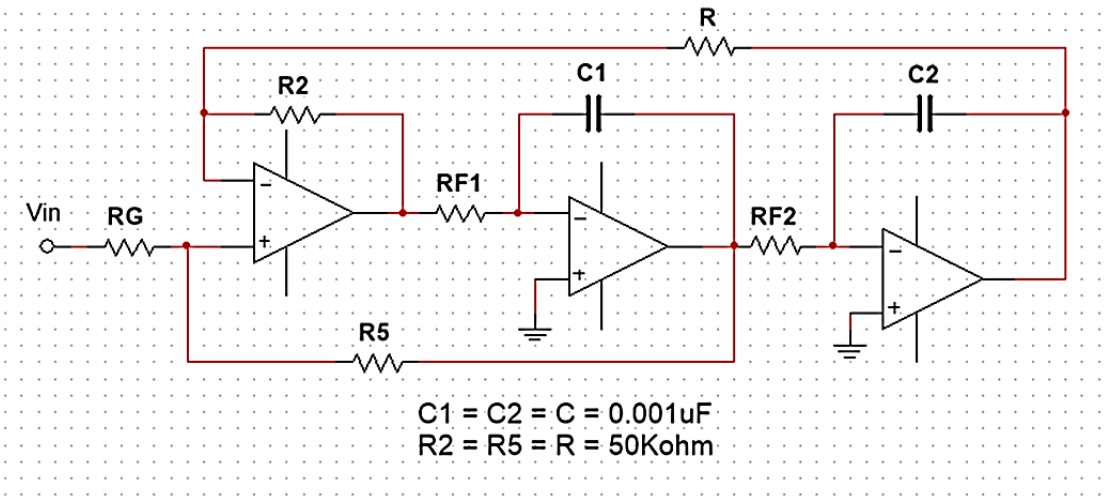

(c)

Figure 3.3: Schematic diagram of (a) multiple feed-back band-pass (MFBP), (b) dual-amplifier band-pass (DABP) and state variable (SV)

B. DABP Filter

The DABP filter is initially introduced by Sedra and Espinoza [111]. Figure 3.3(b) displays the fundamental circuit diagram of the DABP. The DABP exhibits remarkable performance in terms of its high Q and low-temperature sensitivity. In addition, DABP allows the resonance frequency to be modified without affecting its Q value. The mathematical expression for a fundamental DABP structure is:

$$T(s) = \frac{2R_1Cs}{s^2 + s/R_1C + 1/R_2R_3C^2} \qquad 3.3$$

The designing parameters Q, R_1, R_2, and R_3 are calculated using the following equations:

$$Q = \frac{f_c}{BW}\ ; R_2 = \ R_3 = \frac{1}{2\pi f_c C}\ ; R_1 = \ QR$$

Here, the value of $f_c \ = \ 50$ Hz, $C \ = \ 0.01$ µF and $R_2 = \ R_3 = 10$ kΩ is considered with the second-order 2-stage Butterworth attenuation characteristics for designing the filter.

C. SV Filter

The SV is a multiple-feedback filter that generates low-pass, high-pass, and band-pass responses from the same configuration. SV is an active second-order resistor-capacitor (RC) filter. It provides the benefit of designing a filter with a stable gain and a high Q. Figure 3.3(c) depicts the standard SV configuration. The response transfer function of an SV all-pass filter has been denoted by the following expression:

$$T(s) = \frac{sC/R_G}{s^2 + \ s/R_2C + \ 1/R_{F1}RC^2} \qquad 3.4$$

The designing parameters Q, R_G, R_{F1} and R_{F2} are calculated using the following equations:

$$Q = \frac{f_c}{BW}\ ; R_{F1} = \ R_{F2} = \frac{1}{2\pi f_c C}\ ; R_G = \frac{R}{A_{BP}}$$

Here, A_{BP} represents the desired gain from the SV filter. With the second-order Butterworth attenuation characteristics, the designing parameter values $f_c = 50$ Hz, $C \ = \ 0.001$ µF and $R \ = \ R_2$ and $R_5 \ = \ 10$ KΩ have been considered for the filter.

The MFBP filter configuration is appropriate for Q (Quality Factor) less than 5. However, the slight drift in filtering element values changes the MFBP filter's response. The SV filter has been considered adequate with high Q filters due to its stable response. The SV filters have limitations with their complex design and dependencies on a large number of components. In contrast, the DABP technique is more robust and designs a filter with a stable response and a higher Q. To improve the performance of the proposed designs, op-amps with essential characteristics such as low response time, large frequency bandwidth, manufacturing tolerance, and minimal drift have been selected. Op-amps OPA209 and TL052ACP have been chosen for the simulation study of MFBP and DABP, while IC UAF42 has been chosen for the SV design.

3.2 Developing IoT Network of SODAR

IoT plays a crucial role in real-time monitoring and helps in enhancing the decision-making processes of controlling authorities. This section discusses the theory and design methods for developing an IoT-based SODAR Network (IoT-SN). This network links six SODAR installed at Northern India. Later, the data validation steps of the ABL structure and ABL height have been also discussed to ensure the reliability of the proposed IoT-SN's.

3.2.1 IoT Network of SODAR

The Internet of Things has emerged as a revolutionary technology in this decade. It offers a networking model that is highly efficient, effective, and user-friendly. Consequently, IoT has garnered the interest of virtually all sectors of the research community. The development of IoT networks for diverse applications, such as meteorological weather forecasting [132], smart irrigation [133], and air pollution monitoring [134], is aided by contributions from numerous industries and emerging entrepreneurs.

The majority of IoT network work is focused on meteorological parameters. The integration of SODAR and IoT enhances the capability to manage and access remotely placed data with a storage facility, which is highly beneficial for the research community working in the meteorological field. SODAR in association with sophisticated analog signal processing and equipped with IoT networking is highly helpful for Airshed management and planning. Airshed management planning is imperative across the world for better air-quality management. It is a major concern for the research community to develop an effective, fast and continuous monitoring system for planning and decision-making for Airshed Management. In this section, the theory and implementation design methods of IoT-SODAR Network (IoT-SN) have been discussed. Finally, the data validation approach of data received from multiple locations using IoT-SN has been described.

3.2.2 Theory and Design of IoT-Network of SODAR

Figure 3.4 depicts a five-step sequential process for developing the IoT-SODAR Network (IoT-SN) to acquire and analyse data. The first stage of the proposed IoT-SN is advanced analog signal processing, having features of better noise and gain performance already discussed in chapter 3.1. The second stage is focused on the integration of digital signal processing and IoT for the SODAR network. The third stage of the designed methodology aims for the installation, commissioning, and networking of the SODAR. The SODAR designing, development, and installation work are carried out in CSIR-NPL, New Delhi, and funded by Central Pollution Control Board (CPCB), India. In the fourth stage, real-time data acquisition and presentation at the central station have been developed and implemented for IoT-SN. In the last stage, the data acquired from the IoT-based SODAR network has been validated with the local station data.

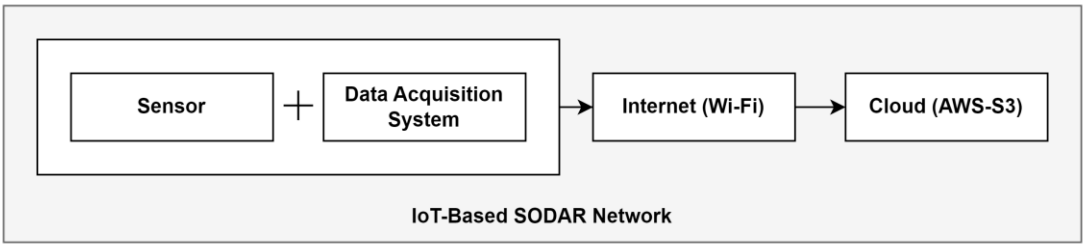

Figure 3.4: Process flow chart of IoT-based SODAR networking

3.2.1.1 Analog Signal Processing

The analog signal processing of SODAR consists of a transducer, T-R switch, impedance matching circuit, amplifier, and analog filters as shown in Figure 3.5.

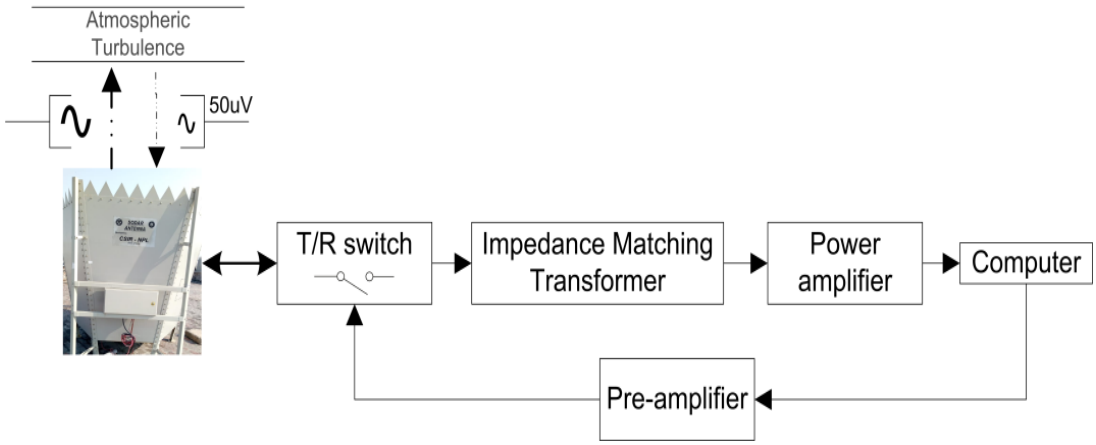

Figure 3.5: Block diagram of SODAR system

The designed ULNA and DABP filter, as shown in Figure 3.6, has advantages of improved gain and noise performance, for analog signal processing of SODAR.

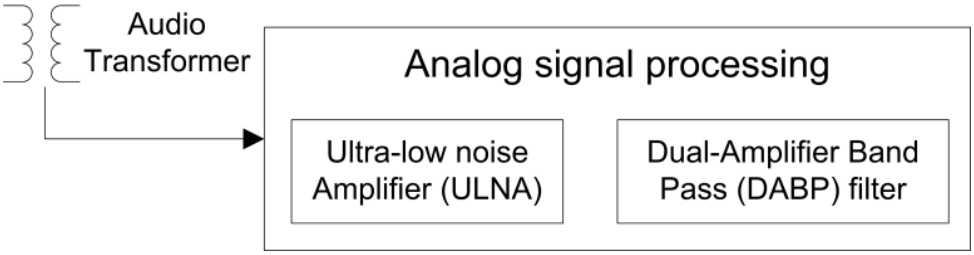

Figure 3.6: Proposed analog signal processing of SODAR

The operating parameters for SODAR are listed in Table 3.2. The backscattered signal received from the transducer is highly noisy and very low in amplitude. The processing of low amplitude signals is a challenging task due to high noise. Consequently, intrinsic noise and impedance matching have been carefully considered in the design of the amplifier.

Table 3.2: Operating parameters for SODAR system

Parameters	
Transmitting electrical power P_e $(Watt)$	$50-60$
Transmitting acoustical signal intensity P_i (dB)	$130-140$
Pulse width t_w (sec)	1.0
Pulse repetition rate T (sec)	10.0
Maximum range R $(meter)$	1000
Receiver bandwidth BW (Hz)	50
Central frequency f_c (Hz)	2250

The input impedance of the selected transducer (Ahuja PA Driver Unit $60\ W$ RMS AU-60) is very low *i.e.* $16\ \Omega$. The audio transformer is a popular technique for impedance matching in the acoustic field. The T/R switch directs the backscattered signal to the audio transformer which matches the impedance of the transducer to the amplifier selected for ULNA design. The amplification gain of $65\ dB$ is achieved from ULNA in two stages using summing amplifier configuration followed by inverting amplifier configuration.

Moreover, both amplification stages utilize the OPA27 operational amplifier. Further, this amplified signal has been processed with the DABP filter to eliminate the undesired frequency signals. The DABP filter is configured to provide an additional amplification gain of $2\ dB$ from each stage. In this work, 2-stage DABP filter design has been used for

better noise performance. Figure 3.7 depicts the consolidated schematic diagram of SODAR consisting of N-stage ULNA amplification and narrow DABP narrow-band-pass filter. The detailed discussion of ULNA and DABP circuit designing has been discussed in chapter 3.1.

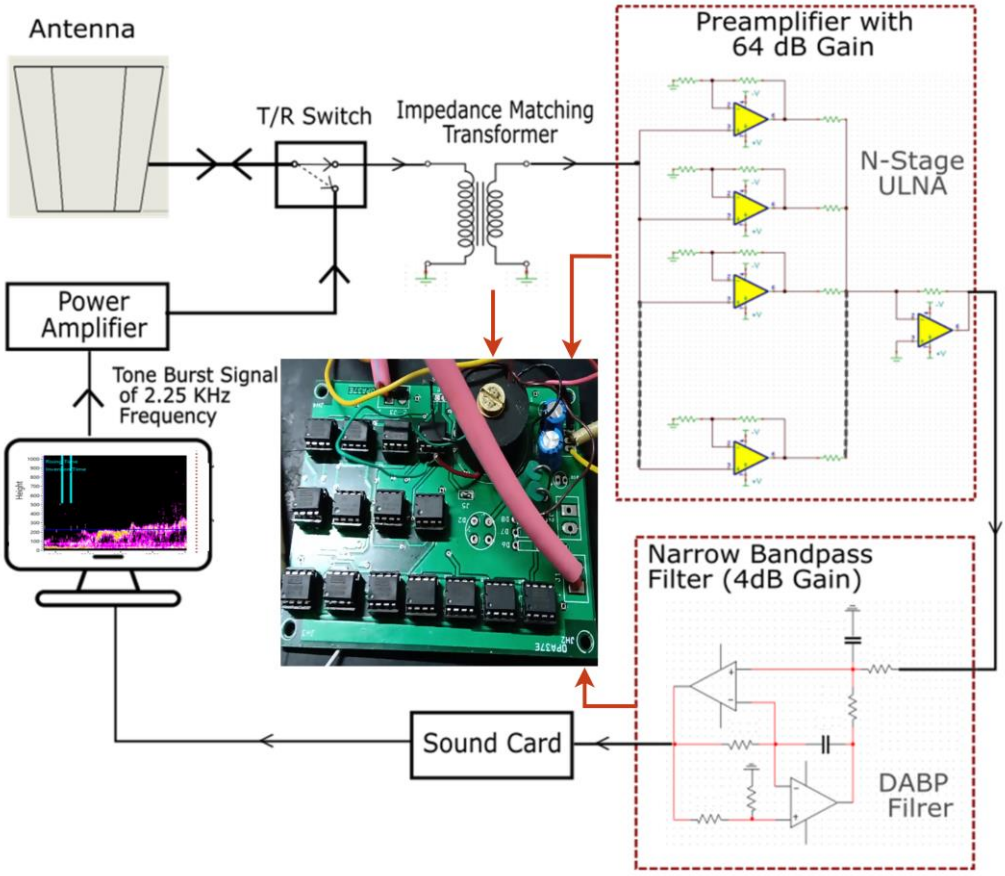

Figure 3.7: Schematic diagram of proposed analog signal processing of SODAR

3.2.2.2 Digital Signal Processing and Data Processing

The Digital Signal Processing, data representation, and IoT process, shown in Figure 3.8, are critical components for the effective implementation of IoT-SN. The digital signal processing unit consists of ADC, digital filtering, data manipulation, and noise cancellation. In the first stage, an Analog signal has been converted into digital samples with a higher sampling rate of 44.5 kHz for a better-quality signal.

The pulse repetition rate (T) for SODAR operation is 10 sec., as mentioned in Table 3.2, is used. The higher sampling rate and long repetition cycle mean more data points to process. It needs further digital filtering and data processing for extracting crucial

information from the signal. The digital FIR band-pass filter with 50 Hz bandwidth has been used to eliminate the undesired frequency component from the signal.

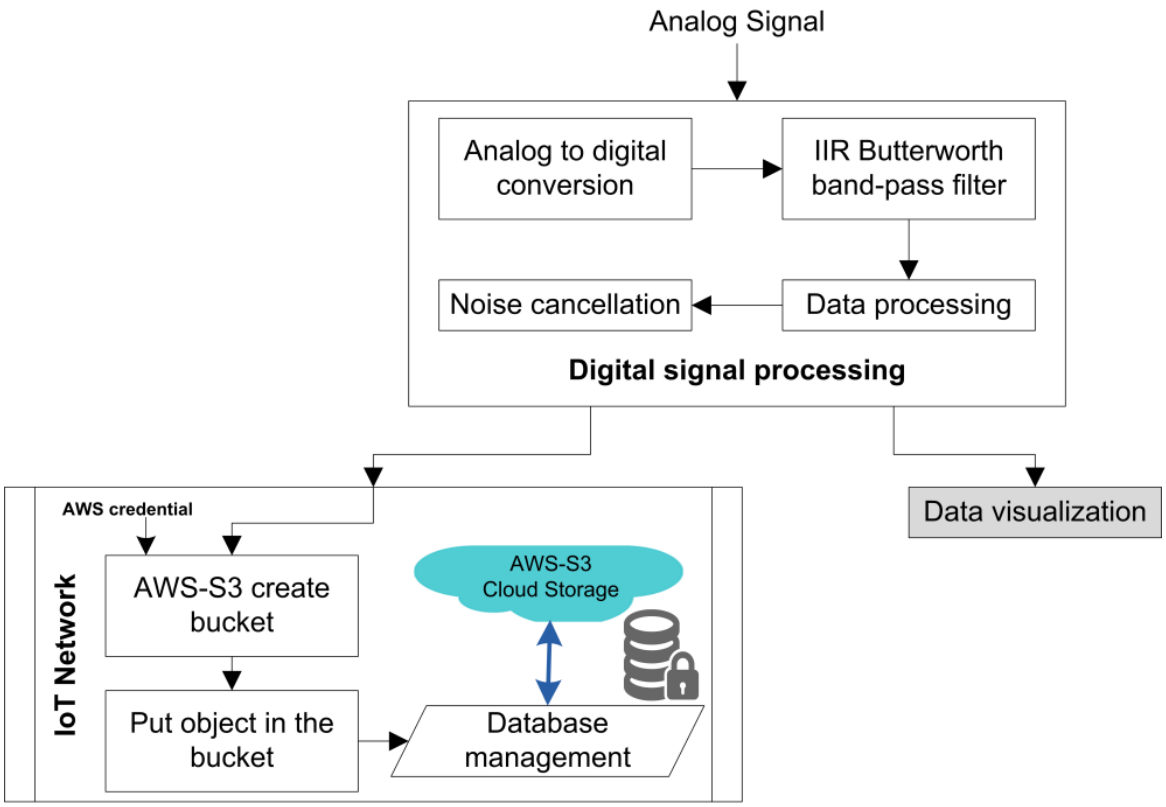

Figure 3.8: Flow chart of proposed digital signal processing of SODAR

Further, the filtered signal has been divided into small packets. In the data processing stage, the peak detection method has been used to expel the undesired peaks of small packets by setting the width and height threshold values. The mean value has been calculated of the remaining peak value and stored in the one dimension (1D) array. Similar operations have been performed on every packet of data and appended to the 1D array. This processed data also consist of environmental noise. To eliminate the noise, environmental noise data has been recorded from the transducer before starting each cycle of operation. These noise samples are also processed and the mean value has been calculated in 1D array of the same size. The noise mean value has been subtracted from the received signal mean value for the final data presentation.

The processed data representing the atmospheric boundary layer information has been presented by an intensity graph. Data networking is an important component of IoT-SN for Airshed management planning. The Labview and AWS-S3 platform has been selected for the networking and cloud services respectively. The AWS-S3 utilizes in-built tools to

create the bucket, put object bucket, and database management for the networking process. The create bucket requires the AWS credential to create the online bucket in AWS-S3. The put object block transmits the real-time data into the bucket. In database management, a day-wise folder is automatically created for data storage. The new file has been created with timestamps value as the file name in case of any interruption.

It has been observed that the IoT-SN conventional process of data transmission results in a sluggish response which leads to data loss. The transmission of large data is a time-taking process and requires reliable Internet services. Under such circumstances, the transmission of suitable data packet size plays a significant role in reliable information sharing on IoT-SN. Therefore, the proposed IoT-SN transmits data at each alternative cycle and utilizes the other cycle to complete the data transmission process. This method of data transmission reduces the data size of the echogram of IoT-SN and helps to manage the available resources effectively. The ABL height has been determined by analysing the echogram acquired from the IoT-SN data and has been verified in the later section.

3.2.2.3 Installation of SODAR

The geographical locations of SODAR site for delineation of Airshed management in Delhi-NCR, India have been presented in Figure 3.9. The installation, commissioning, and development at the multiple sites in Northern India of the IoT-SN have been completed. The expert team of CSIR-NPL in the field of atmospheric science, acoustics antenna, and instrumentation has the responsibility to design and install the SODAR system. In this system, SODAR is working as a sensor node, computer and digital signal processing as a data acquisition device, local Wi-Fi connection as a gateway, and AWS-S3 cloud services have been selected as cloud storage.

3.2.2.4 Real-Time Data Acquisition and Visualization Software

The proposed IoT-SN can share multiple location SODAR data to cloud storage using the AWS-S3. However, it remains a challenge to remotely access and visualize the data in real-time which is beneficial for Airshed management. Figure 3.10 presents the flow chart of the real-time data acquisition and visualization process. In this process, the data has been accessed using the access bucket of AWS-S3. The list-folder function of AWS-S3 opt the specific folder data from the bucket and the get-object bucket fetch all the

containing files in that folder. All the containing files in that folder are arranged in time sequence.

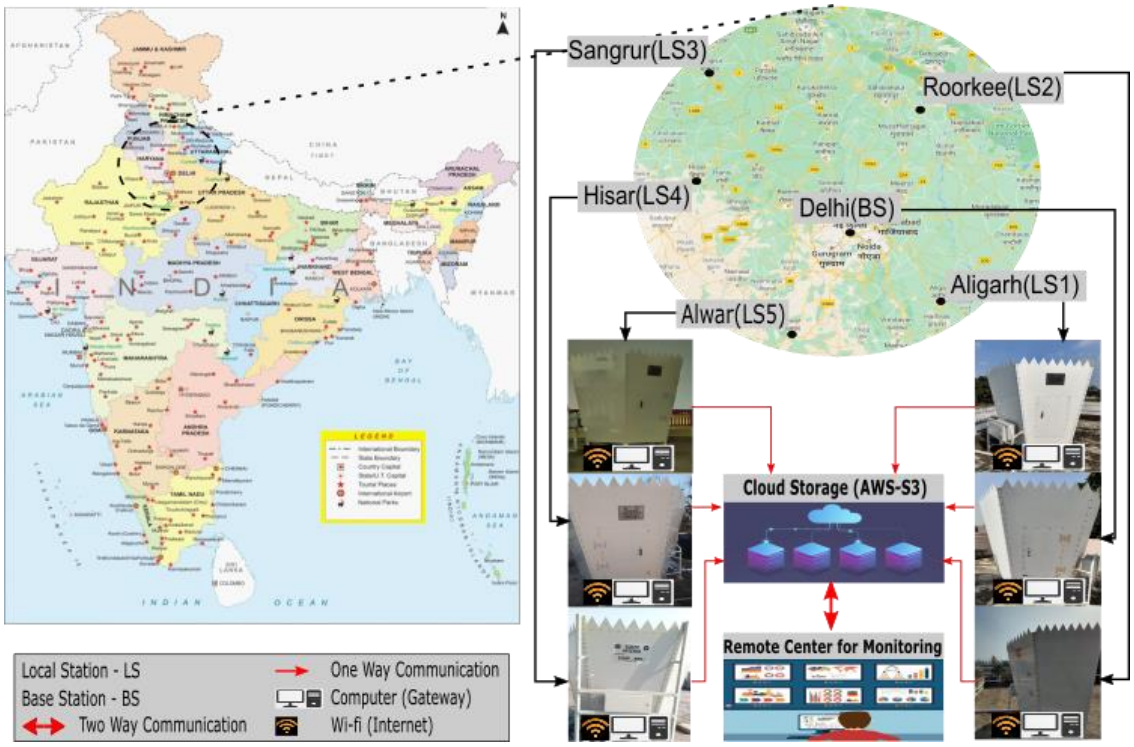

Figure 3.9: Installation location of IoT based SODAR network

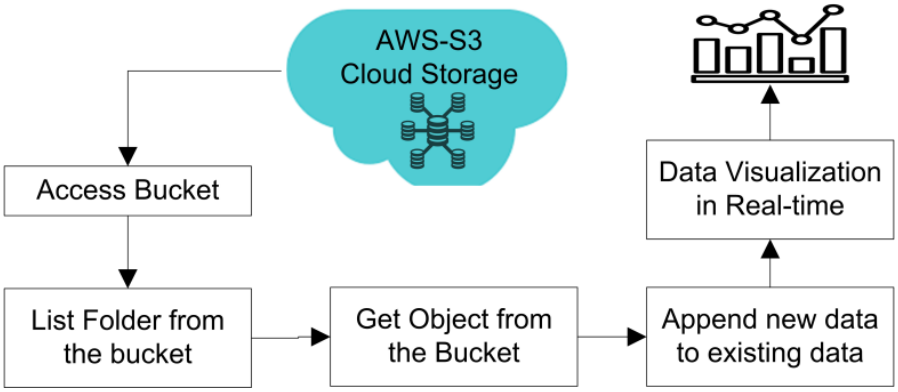

Figure 3.10: Flow chart of proposed real-time data acquisition software of SODAR

3.2.2.5 Data Validation

In the data validation stage, the ABL structures acquired from IoT-SN have been verified with the local station data. Figure 3.11 presents the flow chart of the complete data validation process of IoT-SN. The proposed digital signal processing has been implemented on NI-Labview. The data validation process has been divided into two parts. Firstly, the received data points from the developed IoT-SN have been validated with

local station data. The received data is a 2-dimensional array in comma separate value format, which has been used to plot the ABL structure. This process verifies the accuracy of received data points and the shape of the ABL structure. The second part of data validation is focused on the accuracy of the estimated ABL height value from IoT-SN. The ABL height has been calculated with the help of ABL structures. The file contents are updated automatically with freshly received data packets. The data visualization software has been modified for the real-time monitoring of SODAR data.

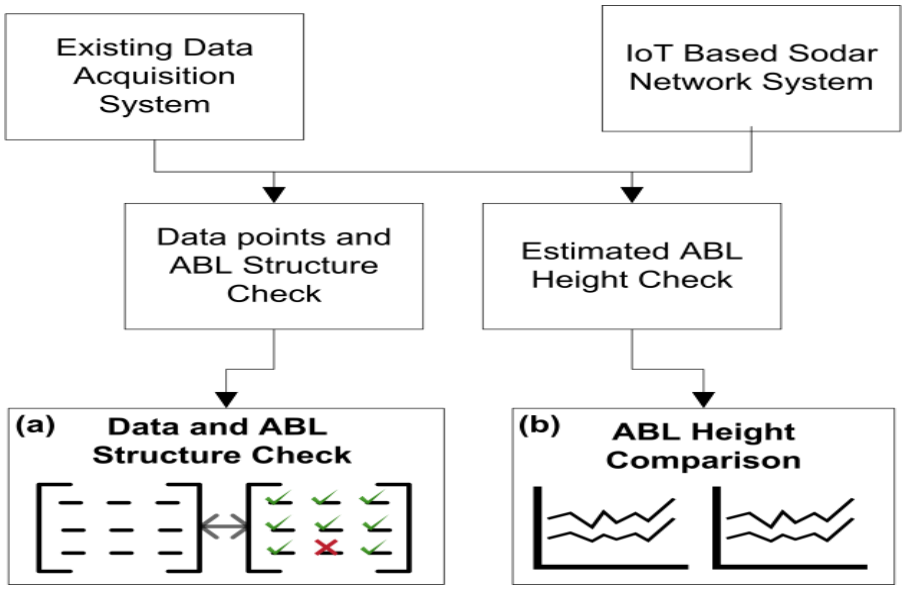

Figure 3.11: Data validation process chart (a) Data transmission accuracy check process of the ABL structure (b) Comparative analysis of ABL height

3.3 Integration of Meteorological Sensor with IoT-Based SODAR Network

Sonic Detection and Ranging (SODAR) is essential for the continuous and real-time measurement of ABL height/mixing-height. This section describes an Internet of Things (IoT)-capable SODAR-based meteorological sensor network (SMSN). The SMSN integrates temperature, relative humidity, and wind sensors with SODAR and deploys them in seven Northern India locations. The sensors with IoT infrastructure have been considered sensor nodes and make real-time air quality monitoring accessible to users.

3.3.1 IoT-SODAR and Meteorological Sensor Network (IoT-SMSN)

In the last decade, the IoT describes the capacity of the Internet to touch people's everyday lives through a wireless network of uniquely identifiable objects [23]. The IoT technique improves the decision-making of the controlling authorities to predict and promote the entire process and planning of air pollution monitoring for sustainable growth [22]. This work focuses on the IoT application in the new generation of air pollution informatics by integrating meteorological parameters such as mixing-height, wind profile, ambient temperature, and relative humidity with local air pollutants and provides a new paradigm for environmental monitoring and management in the future. Figure 3.12 depicts the basic block diagram of the integrated SODAR and meteorological sensor system.

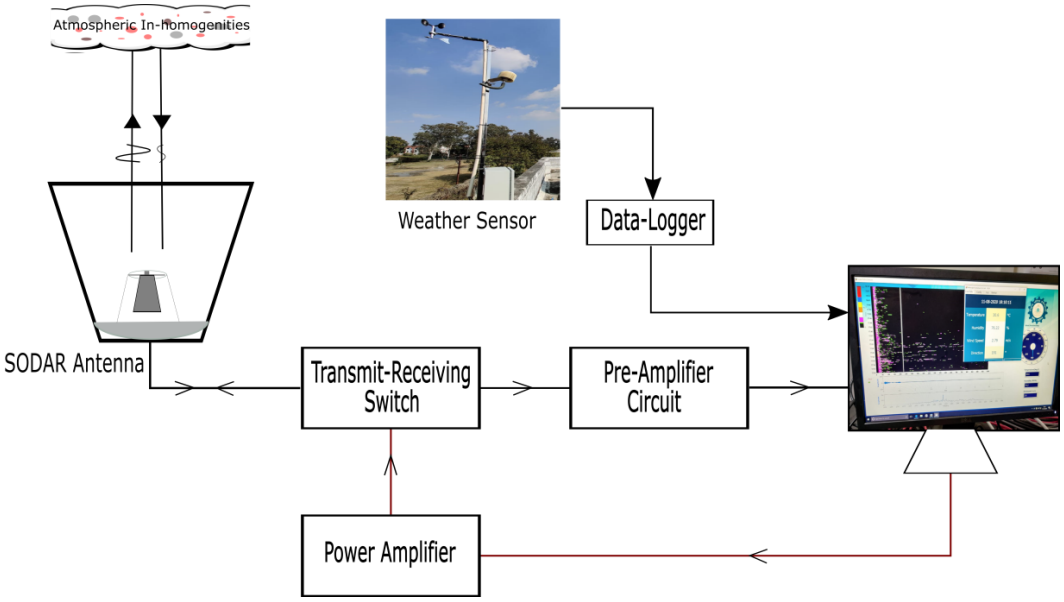

Figure 3.12: Block diagram of SODAR and meteorological sensor network

The COVID-19 outbreak and nationwide lockdown across the world improves the air pollution conditions, which gave some time to regulatory authorities, the scientific community, and the public to re-examine the environment monitoring approach [139 - 140]. Integration of air pollution monitoring and management methods based on IoT is an imperative and active topic for all stakeholders. IoT-based monitoring network covers various issues and involves multiple computer and information science technologies [150].

The integration of SODAR with a meteorological sensor is also essential to analyse and study environmental pollution. There is significant development of the SODAR

technology and meteorological sensor network for the air pollution monitoring and management system. The advancement in SODAR and integrated meteorological sensor networks and their applications have some apparent shortcomings. Firstly, multi-sources of data and information are constantly expanding. Multi-sensors data from multiple locations require effective acquisition and processing. Secondly, practical database management is necessary to tackle a large amount of data from integrated meteorological sensor networks in real time for remotely monitoring the environmental parameters. Thirdly, the influential association and fusion between multi-sensors and their real-time data acquisition is another important topic that is rarely studied in the existing literature. Lastly, adapting multidimensional and multi-scale applications under different tasks and cloud services is another challenge with the next-generation integrated sensor network system [56, 139].

The development of integrated, smart, and sustainable network systems for practices in air pollution, the environment, and sustainable engineering based on IoT is imperative for the near future. Based on this, a novel IoT-based integrated sensor network consisting of SODAR and meteorological sensors such as wind, temperature, and humidity is developed on a single platform for regional air pollution monitoring and management system. The IoT-based single platform solution is installed and commissioned in seven different Northern India locations to improve the decision-making of the air pollution monitoring system for Delhi. The subsequent section discusses the detailed theory and design methods for IoT-SMSN.

3.3.2 Theory and Design of IoT-SMSN

The increasing trend in IoT technologies has laid the foundation for integrating multiple sensors for air pollution monitoring systems. Here, a single platform solution to create SMSN has been designed for regional air pollution monitoring based on the framework of IoT. Figure 3.13 shows the methodology's four steps *i.e.*, design and development, calibration and testing, installation and real-time data acquisition, and monitoring. A detailed discussion of the proposed methodology has been presented in the following subsections.

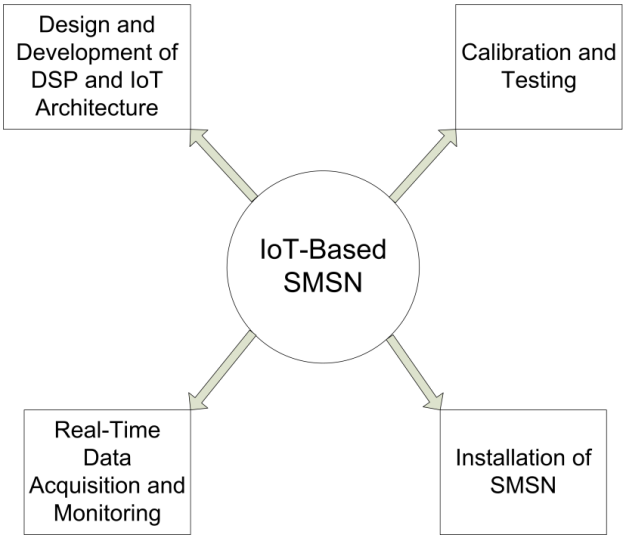

Figure 3.13: SMSN architecture

The designing and development of digital signal processing software for IoT networking is a critically important segment of the system. The first part focuses on designing a digital signal processing for SODAR and then integrating it with meteorological sensor data for local data acquisition and monitoring of the sensor data.

3.3.2.1 Digital Signal Processing

The wind, temperature, and humidity sensors along with the data acquisition card are procured from Schelt Technology, Noida, India. Data acquisition card digitally processes the sensor's signal, and the local server monitors the processed data using the local-monitoring interface. Figure 3.14 shows the sensor data acquisition card, and monitoring interface for the meteorological sensors.

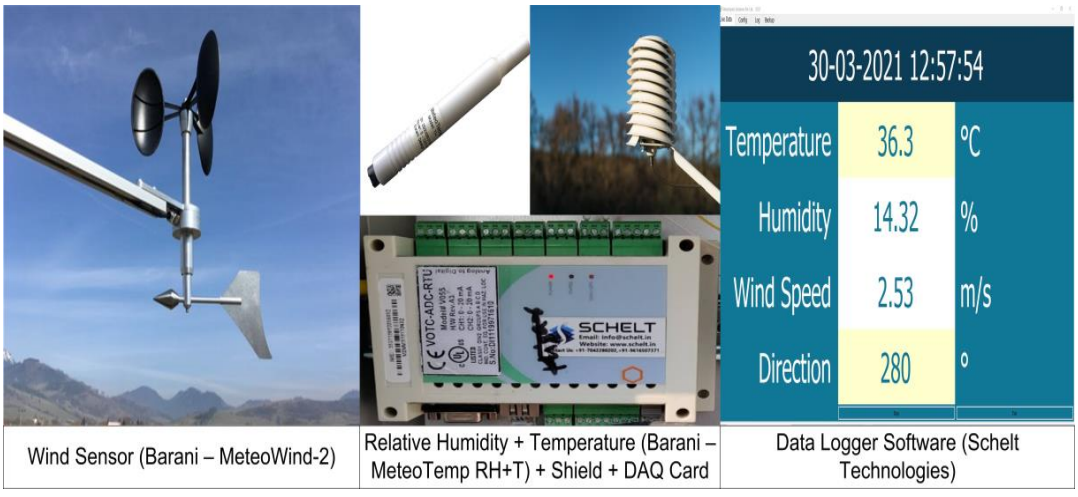

Figure 3.14: Data acquisition system of meteorological sensors

The SODAR system used has been designed and developed in the CSIR-NPL, Delhi. SODAR's digital signal processing consists of analog to digital conversion (ADC), filtering, data processing, and noise cancellation stages. The preamplifier and data logger are powered by a 12 volt DC power supply. The high-powered acoustic pulse of $130 - 140\ dB$ intensity and $2.25\ kHz$ frequency has been transmitted in the atmosphere using an acoustic transducer. SODAR receives the backscattered signal every 10 seconds (Pulse repetition cycle = $10\ sec$). To capture the complete depth of the temporal ABL structure, a fast DSP is required with a high sampling-rate ADC of $44.5\ kHz$. The advantage of a higher sampling rate is significant data points. However, it further increases the demand for digital filtering and data processing to extract crucial information from the signal.

The signal is passed from the digital FIR band-pass filter of 50 Hz bandwidth to eliminate the unwanted frequency component from the signal. These filtered data points are divided into small packets and processed using the peak detection method to expel the undesired peaks. The standard mean has been calculated of data points from each small and stored in the 1D array. Similar operations have been performed on every packet of data and appended to the 1D array. This data represents the height of the received signal in a single operating cycle. To eliminate environmental noise, atmospheric echoes have been recorded from the SODAR transducer before every operating cycle. The blank atmospheric echoes are the environmental noise directly subtracted from the original signal. The DSP system of the proposed design integrated the SODAR and meteorological sensor data and stored the combined SMSN data in a single file. This data has been monitored using the Labview-based software in the local server room. The combined digital signal processing of SODAR and meteorological sensors are shown in Figure 3.15.

3.3.2.2 IoT Architecture

Figure 3.16 shows the IoT architecture of the SMSN comprises four components, namely applications and analytics, infrastructure, integration, and security. The applications and analytics layer process and display the collected information via IoT-based SMSN. It includes data analysis tools and visualization capabilities. The Labview-based data acquisition software has been used for data processing and representation. The infrastructure layer consists of physical devices namely: sensors, communication networks, servers/controllers, and cloud storage. The SODAR, wind

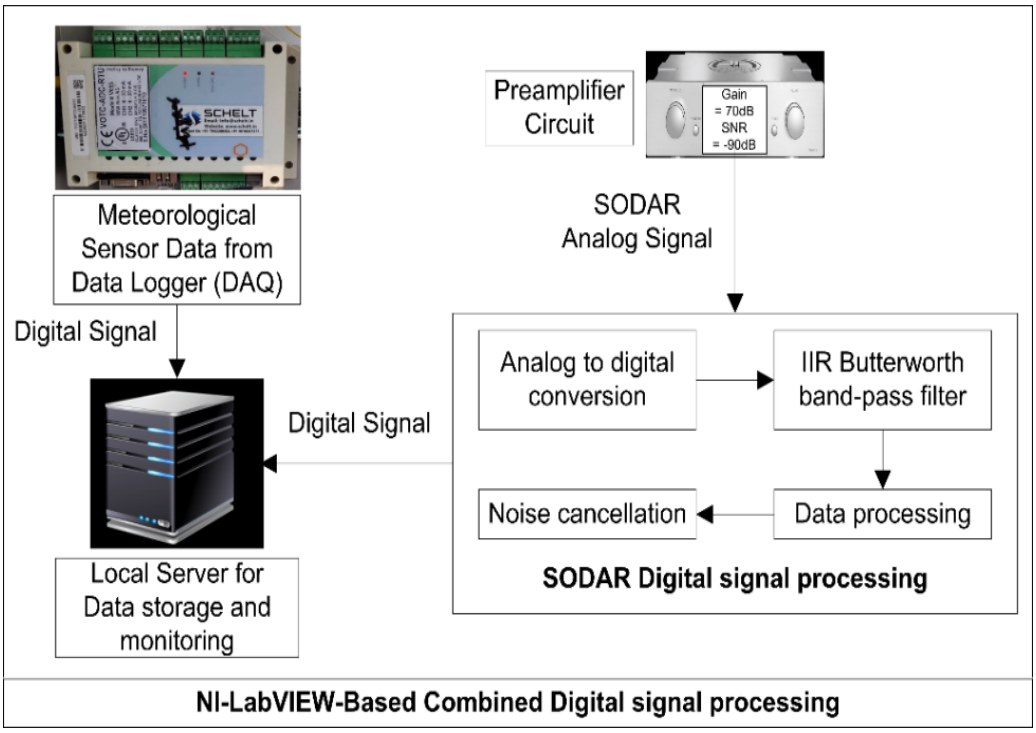

Figure 3.15: Digital signal processing of SMSN

sensor (MeteoWind-2), temperature, and relative humidity sensor (MeteoTemp + RH) have been used as primary sensing devices. A wired connection has been established between the sensors and the local server. The combined sensors and local server system have been considered as a single sensor node. Another communication network is required for connecting each sensor node and remote server via cloud services. The high-end computer of the 9th Generation Intel Core i5-9400 Processor with 4 GB of random-access memory has been used as a main controller. It consists of LabVIEW-Based User Interface (UI) and act as a server. Afterwards, AWS-S3 cloud services have been utilized to store the data into the cloud. Figure 3.17 depicts the Labview data uploading and real-time acquisition from the AWS S3 bucket using a flowchart. The entire procedure is divided into two parts. In the first part, an AWS S3 bucket is created, and the data from the sensor node is transferred to the bucket via a local gateway (Wi-Fi) using UI. In the second step, another LabView based UI is created for retrieving the data from remote location stored in the S3 bucket using Cloud Toolkit for AWS by NI-Labview.

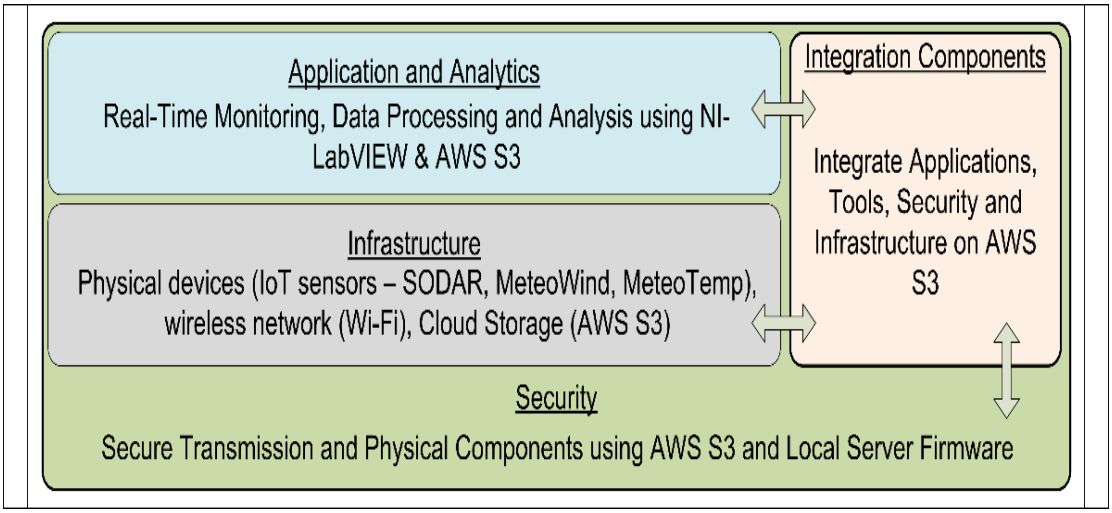

Figure 3.16: IoT architecture of proposed SMSN

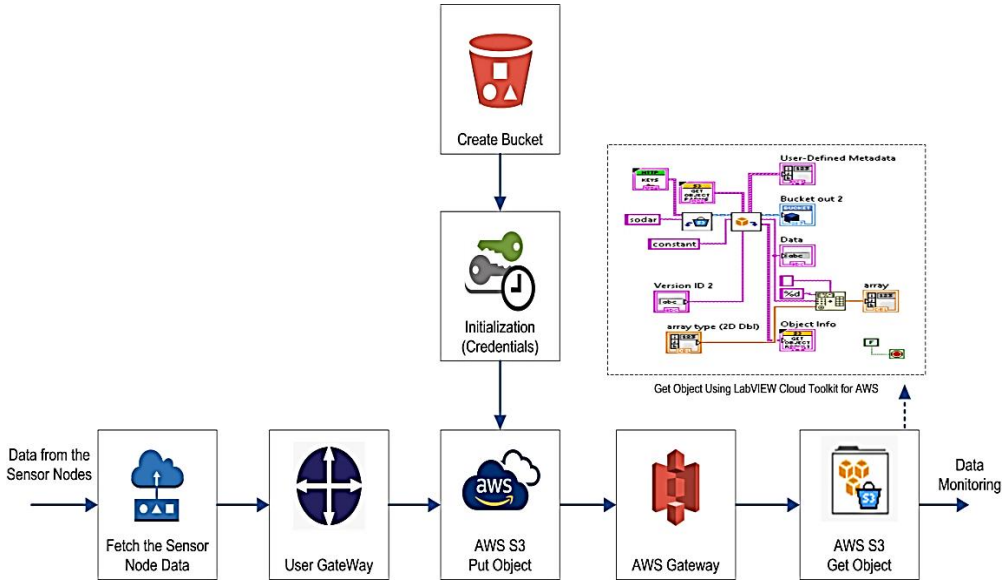

Figure 3.17: AWS S3 data communication flow chart using Labview

The data acquisition software based on Labview has been designed to represent and store the data on the local server. It establishes the data communication between the sensor node and cloud through Wi-Fi. The AWS-S3 built-in functions such as create the bucket, put-object bucket, identity, access management (IAM), and an application program interface (API) have been utilized in the software for IoT networking. The AWS create-bucket function creates a dedicated storage location in the AWS-S3. The put-object function stores the data in that location with unique vital credentials. The AWS-IAM manages the amazon S3 resources, and finally, the API ensures the object's storage and retrieval from the bucket. The Labview-based data-acquisition software also fetched the timestamps value along with the sensors s data. It transmits it over the IoT network to

update the data instantaneously in the database. The complete process of data transmission using AWS-S3 is presented in Figure 3.18.

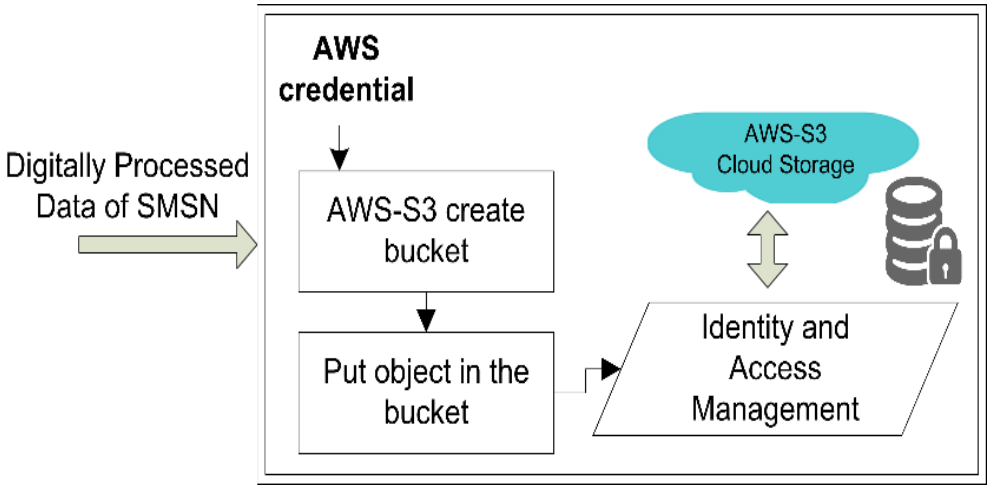

Figure 3.18: Data transmission process of SMSN parameters using AWS-S3

The IoT-based SMSN consists of each sensor node transmitting the data into the cloud and simultaneously monitoring all location data from a remote monitoring station equipped with a high-end server, Wi-Fi, and multiple-display. The complete sensor node network of the SMSN is presented in Figure 3.19. To achieve faster data communication, the alternative pulse repetition cycle is only utilized for data transmission to cloud storage. This process increases the transmission cycle time to 20 sec. It reduces the total data size of the SMSN to half, which helps to manage the available resources effectively. This sampling speed is acceptable for meteorological sensors but reduces the echogram resolution of SODAR. The estimated mixing-height data remains intact, which is the objective of the SMSN.

3.3.2.3 Calibration and Testing

Calibration is an essential part of any reliable sensor network system. The calibrated meteorological sensors have been selected for networking in this research work. The wind sensor (MeteoWind2) has been calibrated with MEASNET, IEC61400-12-1, IEC61400-12-2, ISO3966 and ISO16622 procedures with standard uncertainty of 0.2 %, standard error of 0.025 %, and correlation-coefficient of 0.999979 [55]. The temperature and humidity sensor (MeteoTemp RH+T) has been calibrated with ISO/IEC 17025:2005 procedure, with temperature uncertainty being less than 0.3ºC and 0.1% at each calibration point [56].

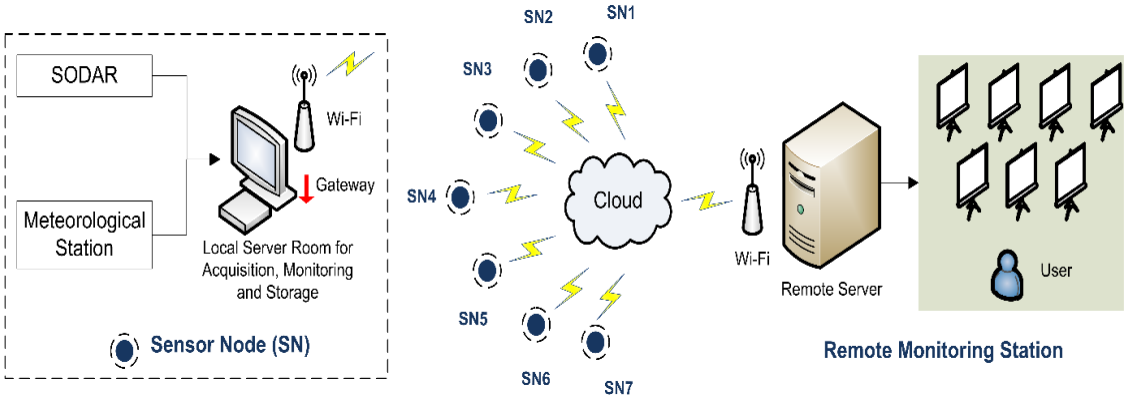

Figure 3.19: Data networking of IoT-SMSN

temperature and humidity maintained at NPL, India is validated with key comparison exercises with other National Metrology Institutes (NMIs) of the world. As such, CSIR-National Physical Laboratory Calibration and Measurement Capabilities (CMCs) of temperature and pressure are also included in prestigious Bureau International des Poids et Mesures (BIPM) Key Comparison Data base (KCDB) website since the year 2009. Figure 3.20 presents the calibration results of the temperature and humidity sensor. The expanded measurement uncertainty is $\pm 0.2\ ^{o}C$ and $\pm 0.4\ \%$ for the temperature and relative humidity, respectively.

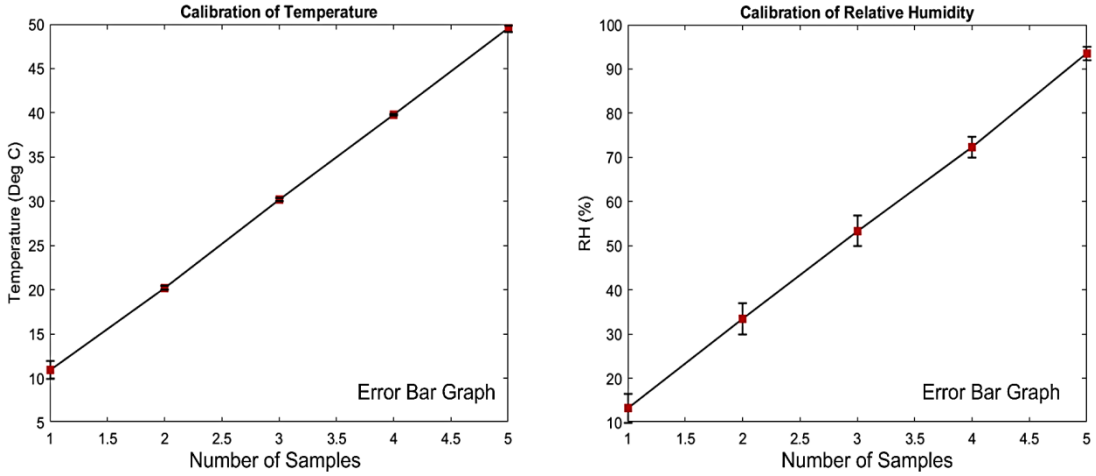

Figure 3.20: Calibration graph of the temperature and humidity sensor

3.3.2.4 Installation and Commissioning

In this research work, Delhi and the surrounding part of Northern India have been selected. Delhi is considered one of the fastest-growing cities in the world and is known for its vulnerability to climate change and air pollution. The in-depth knowledge of the

intensity of transported pollutants is essential for regional sustainable development in the area. The installation locations of Northern India selected for the study purpose are shown in Figure 3.21. The SODAR has been installed along with other meteorological sensors such as wind, temperature, and relative humidity at the CPCB, New Delhi, IIT Roorkee, AMU Aligarh, IMD Hisar, RPCB Alwar, PPCB Sangrur locations. This SODAR based meteorological sensor network helps the regulatory authorities for better and more effective air-pollution monitoring over Delhi.

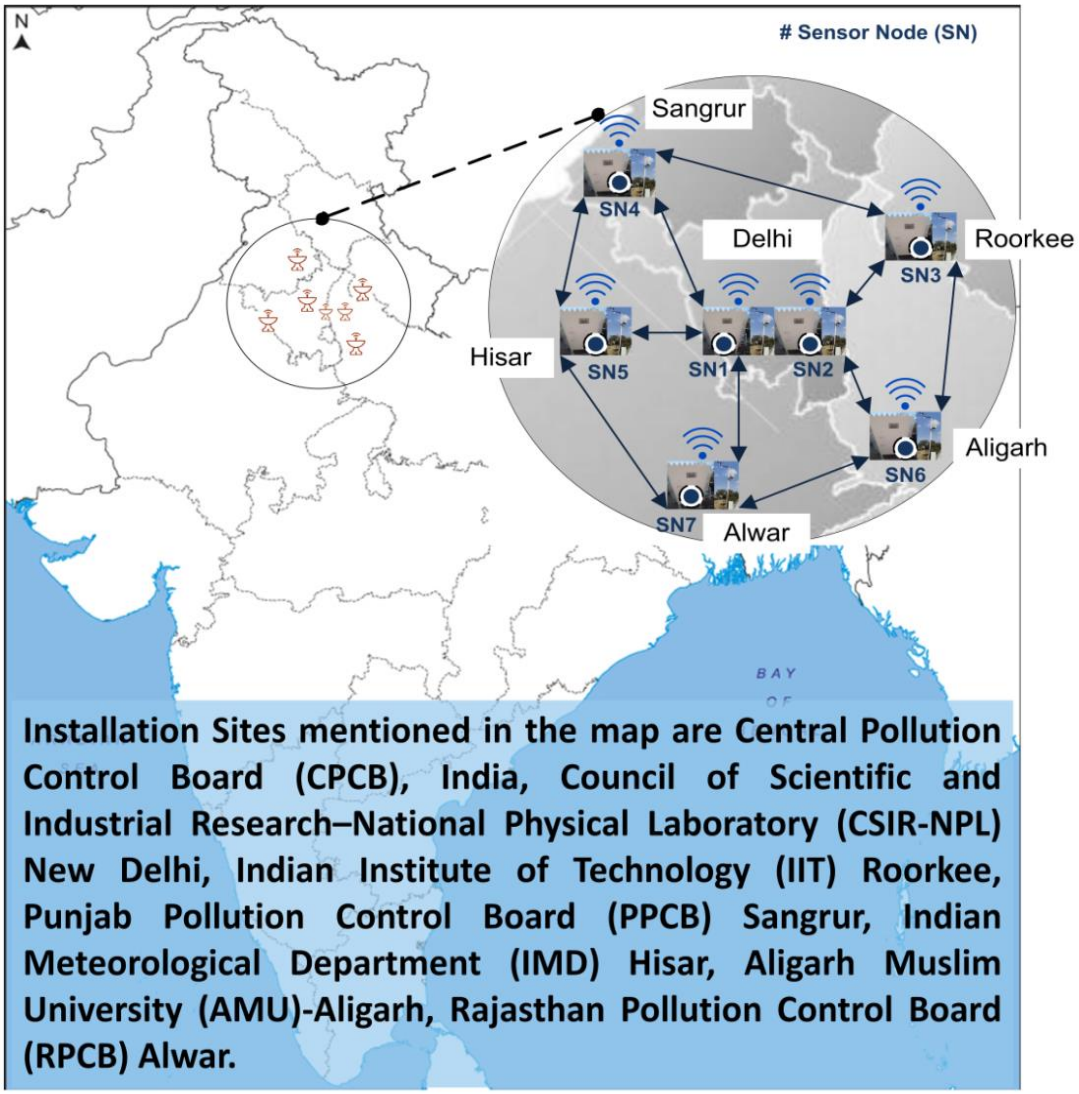

Figure 3.21: Installation sites of the SODAR based meteorological sensor network

3.3.2.5 Real-Time Data Acquisition and Monitoring

The installed sensors at each location work as a sensor node. The SODAR system and attached weather station gather all meteorological information, including wind speed, direction, temperature, and relative humidity in addition to ABL height. The proposed

SMSN shares the data from multiple sensor nodes to central monitoring stations using the IoT platform. However, it remains a challenge to process a large amount of data for remotely accessing and visualizing in real-time. In this work, the AWS-S3 and Labview-based real-time data acquisition software has been designed for data visualization and further analysis. Figure 3.22 presents the complete process of AWS-S3 and Labview-based real-time data acquisition of SMSN. The AWS-S3 cloud stores the sensor node data from multiple locations with unique credentials. This credential is used for accessing the data in the access-bucket function of AWS. Later, the list folder searches the current date and time folder from the specific bucket. The get-object function fetches the file from the bucket and appends it with the existing file of the same day. Finally, the Labview-based software has been used for plotting all the parameters in near real-time. The file contents are updated automatically with fresh data and simultaneously plotted in the software.

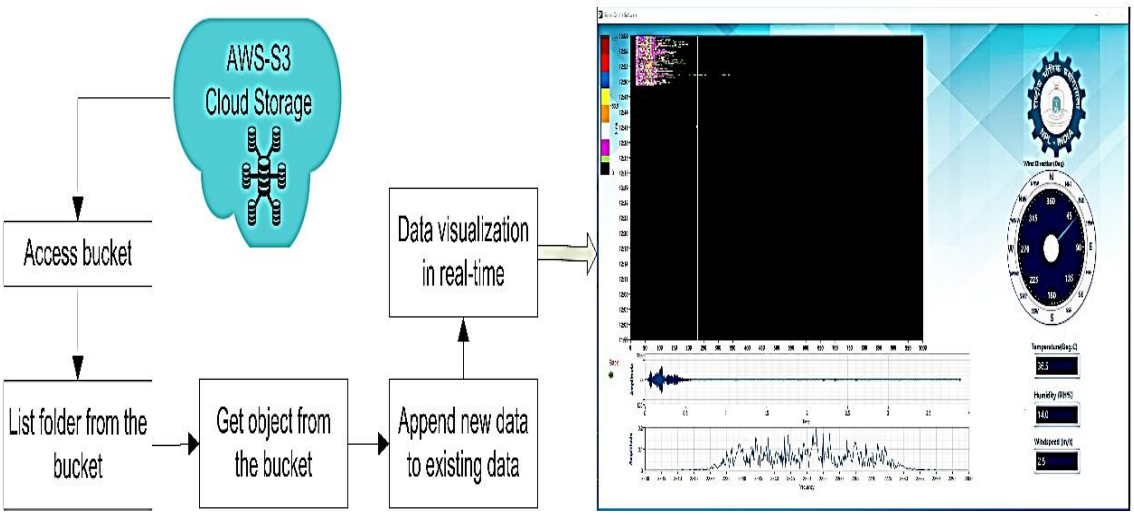

Figure 3.22: Real-time data acquisition system block diagram

This chapter focused on the theory and design methodologies of analog and signal conditioning systems for SODAR, as well as integrating essential technologies from in-situ and remote sensing meteorological sensors and the Internet of Things in a typical air pollution monitoring system. IoT-SMSN has broad prospects in both scientific and industrial areas, as SMSN is a good solution and provides integrated platforms for performing complex environmental tasks. The features of IoT are precisely suitable for data collection, processing, and analysis to improve decision-making in real-time. SMSN and IoT solutions provide competitive advantages among the application fields and play important roles in air pollution monitoring and management in the defined area. Furthermore, taking the regional pollutants sources and their ecological responses as an example provides a paradigm for environmental sciences research.

Chapter 4
Results and Discussions

This chapter presents the SODAR IoT-Networking results, performance analysis, and discussions. The results are divided into three sections: analysis of analog signal conditioning systems for SODAR, performance evaluation of digital signal processing and data acquisition systems of IoT-SN, and uncertainty estimation of integrated IoT-SMSN.

4.1 Analog Signal Processing of SODAR

The experimental analysis of analog signal conditioning system for SODAR demonstrates the performance of the signal conditioning circuits. The frequency range between 10 Hz to 1 MHz has been selected for frequency, noise, and transient analysis of analog system. Based on the comparative analysis, the top-performing design has been selected. Then, the raw signal is collected from the installation location of SODAR and transient response has been estimated. Each component of the SODAR has been calibrated at CSIR-NPL, New Delhi. The antenna has been calibrated in the reverberation chamber of CSIR-NPL. The disc and transducer assembly have been calibrated in the CSIR-NPL's anarchic chamber facility [14]. The finalized circuit design has been installed with SODAR located at CSIR-NPL, New Delhi. The gain and frequency response of the design has been compared with the SLNA-SV design.

4.1.1 Frequency Analysis of DABP, MFBP, and SV Designs

The frequency analysis has been performed primarily for two purposes, *i.e.*, determining the gain of the circuit and determining the selectivity of the frequency response. The greater attenuation at cut-off frequencies increases the circuit's selectivity. The parameters presented in Table 3.1 are used in the amplifier and filter designs. The gain has been measured at the centre, stop band, and pass band frequencies, as shown in Figure 4.1, and is tabulated in Table 4.1. The first stage of amplification consists of a parallel branch of amplifiers, whereas the second stage consists of a single amplifier. In terms of frequency analysis, the DABP structure outperforms the MFBP and SV designs. Compared to the MFBP and SV designs, the DABP design provides better gain ($65.52\ dB$) and attenuation ($3\ dB$) at pass band and stop band frequencies.

High gain and sharp attenuation at pass band and stop band frequencies are desirable properties for cancelling out atmospheric noise [13, 87]. The frequency analysis reveals that both the MFBP and SV designs are acceptable. Comprehensive noise analysis has been conducted on the design to select the optimal circuit for SODAR.

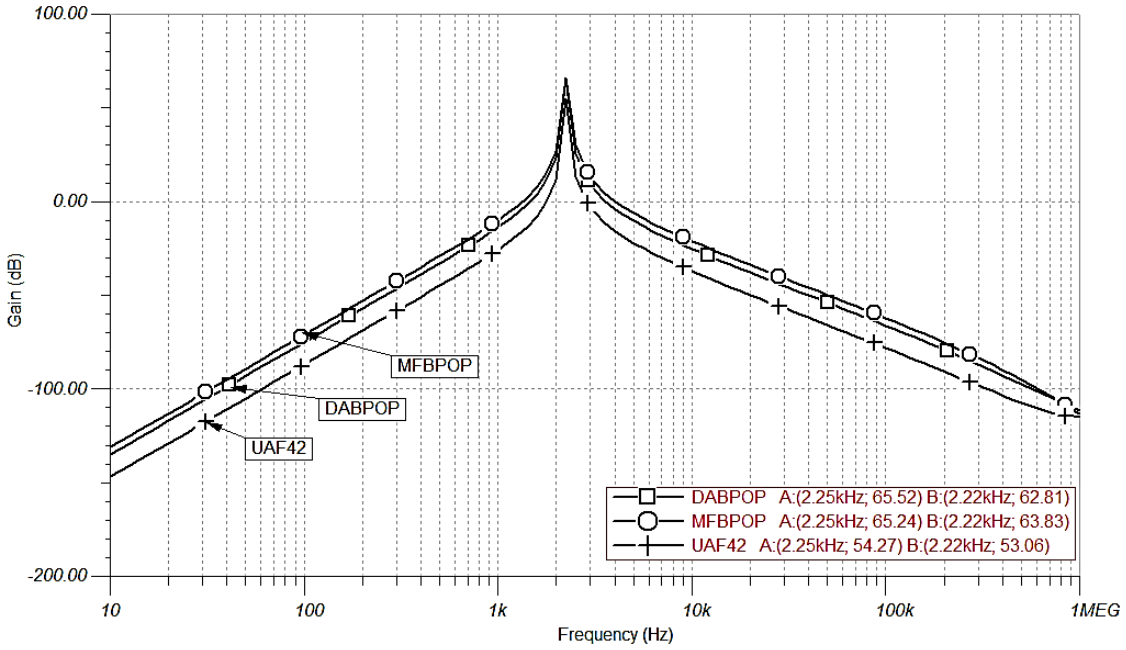

Figure 4.1: Frequency response of ULNA with MFBP, DABP and SV filters

Table 4.1: Measured gain value at center frequency, pass band frequency and stop band frequency of DABP, MFBP and SV filter designs

Filter Type	Gain (dB)				
	$Gain_{f_{lsb}}{}^{A}$	$Gain_{f_{lpb}}{}^{B}$	$Gain_{f_c}{}^{C}$	$Gain_{f_{hpb}}{}^{D}$	$Gain_{f_{hsb}}{}^{E}$
DABP	40.57	62.81	65.52	62.31	41.55
MFBP	43.18	63.83	65.24	64.47	48.20
SV	29.22	53.06	54.27	50.52	29.26

[A] $Gain_{f_{lsb}} = Lower\ stopband\ frequency\ (Hz)$: [B] $Gain_{f_{lpb}} = Lower\ passband\ frequency\ (Hz)$
[C] $Gain_{f_c} = Center\ frequency\ (Hz)$: [D] $Gain_{f_{hpb}} = Higher\ passband\ frequency\ (Hz)$
[E] $Gain_{f_{hsb}} = Higher\ stopband\ frequency\ (Hz)$

4.1.2 Noise Analysis of DABP, MFBP, and SV Designs

Three noise features, *i.e.* SNR response, output noise, and total noise, have been observed for noise analysis. The complete noise analysis of the systems is depicted in Figure 4.2, and the findings are summarized in Table 4.2.

Table 4.2: Measured output noise, total noise, and SNR of the ULNA circuit with DABP, MFBP and SV filter designs

Filter Type	Noise Analysis		
	Output Noise ($\mu V/\sqrt{Hz}$)	Total Noise (μV)	SNR (dB)
DABP	2.22	27.37	92.71
MFBP	183.67	1790	54.92
SV	2.62	32.41	91.08

4.1.2.1 SNR Response

The SNR value has been measured in the frequency range of 1 Hz to 1 MHz, as presented in Figure 4.2(a). The ULNA has been combined with all designs for the analysis. Table 4.2 shows the SNR calculated at the central frequency to evaluate noise performance in the operating frequency range. The SNR is an essential noise characteristic in the design of the SODAR preamplifier, and it dominates the selection criteria for the analog signal conditioning stage. The DABP design has the best SNR response, followed by the SV design. The MFBP performs poorly in this part and is unsuitable for SODAR system. Simultaneously, the output noise and total noise have been investigated.

4.1.2.2 Output Noise

The output noise has been measured in the frequency range of $1\,Hz – 1\,MHz$, as seen in Figure 4.2(b). The graph's scale is expressed in $\mu V/\sqrt{Hz}$. The output noise obtained from the DABP and SV designs is highly impressive in comparison to the MFBP design. The output noise of the MFBP design is approximately 60 times higher than the DABP and SV.

4.1.2.3 Total Noise

Figure 4.2(c) illustrates the total noise of each of the three filter designs. The graph's scale is expressed in mV. The total noise is the sum of the noise contributions from each component of the circuit [113]. The total noise study indicates a similar trend to the

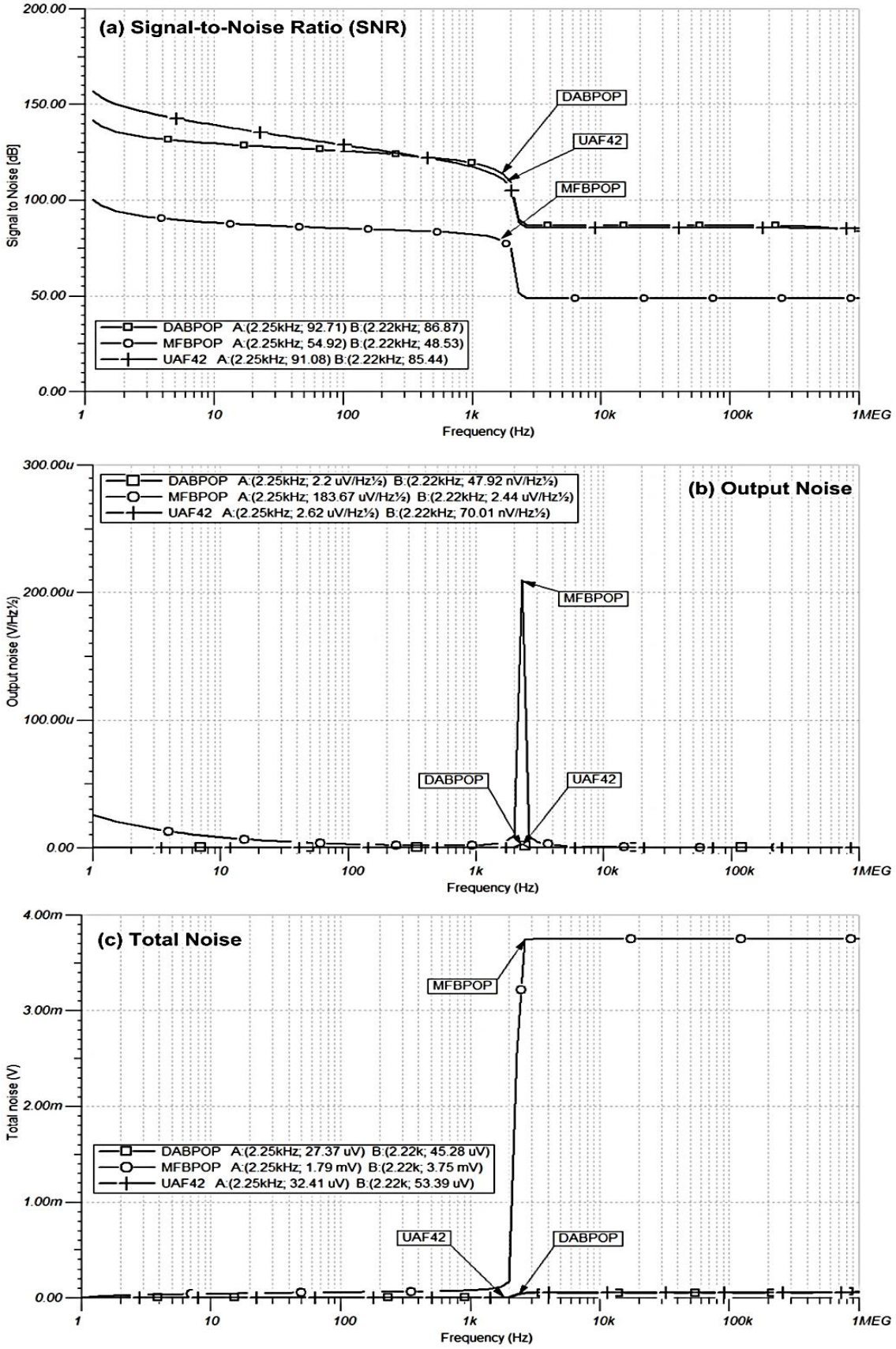

Figure 4.2: Noise comparison analysis of ULNA with DABP, MFBP and SV Filter designs for (a) Signal-to-noise ratio (dB), (b) Output noise ($\mu V/\sqrt{Hz}$), and (c) Total noise (mV)

SNR and output noise analysis. The DABP and SV designs have substantially lower total noise than the MFBP designs. SODAR's noise performance is the most important aspect of its analog signal processing. The noise analysis of the chosen filter designs in conjunction with the ULNA amplification stage demonstrates the DABP's superiority.

4.1.3 Transient Response Analysis

Figure 4.3 depicts the transient response of the proposed circuits. The transient analysis demonstrates the output voltage's performance in terms of stability. A standard unit-step signal is applied as an input. Minor oscillations have been observed from the DABP circuit response and thus have negligible effect on the performance of proposed designs.

As determined by the analysis, DABP and SV designs have distinct advantages over MFBP, such as high gain, sharp attenuation, comprehensive noise performance, and stable output response. Figure 4.4 depicts the comprehensive flowchart of the circuit analysis and the performance comparison chart. As the MFBP design has been considered inadequate for the SODAR system, it has been excluded from the remainder of the analysis.

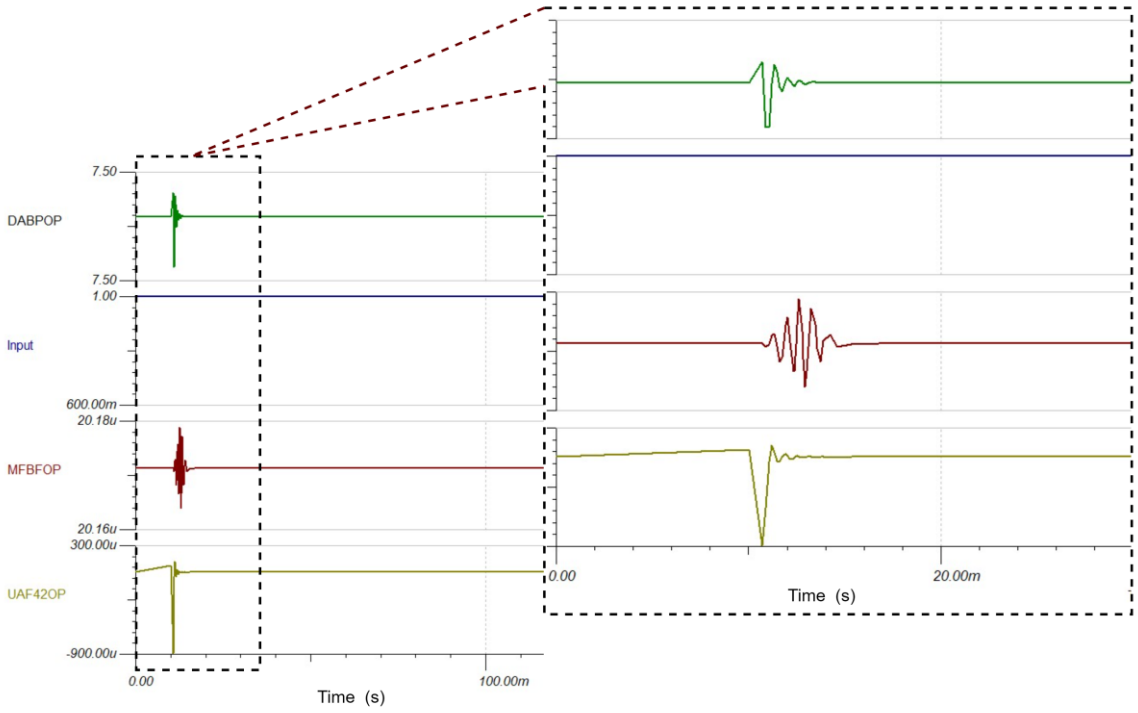

Figure 4.3: Transient response (normal and enlarged) analysis of ULNA with DABP, MFBP and SV filters for unit-step input

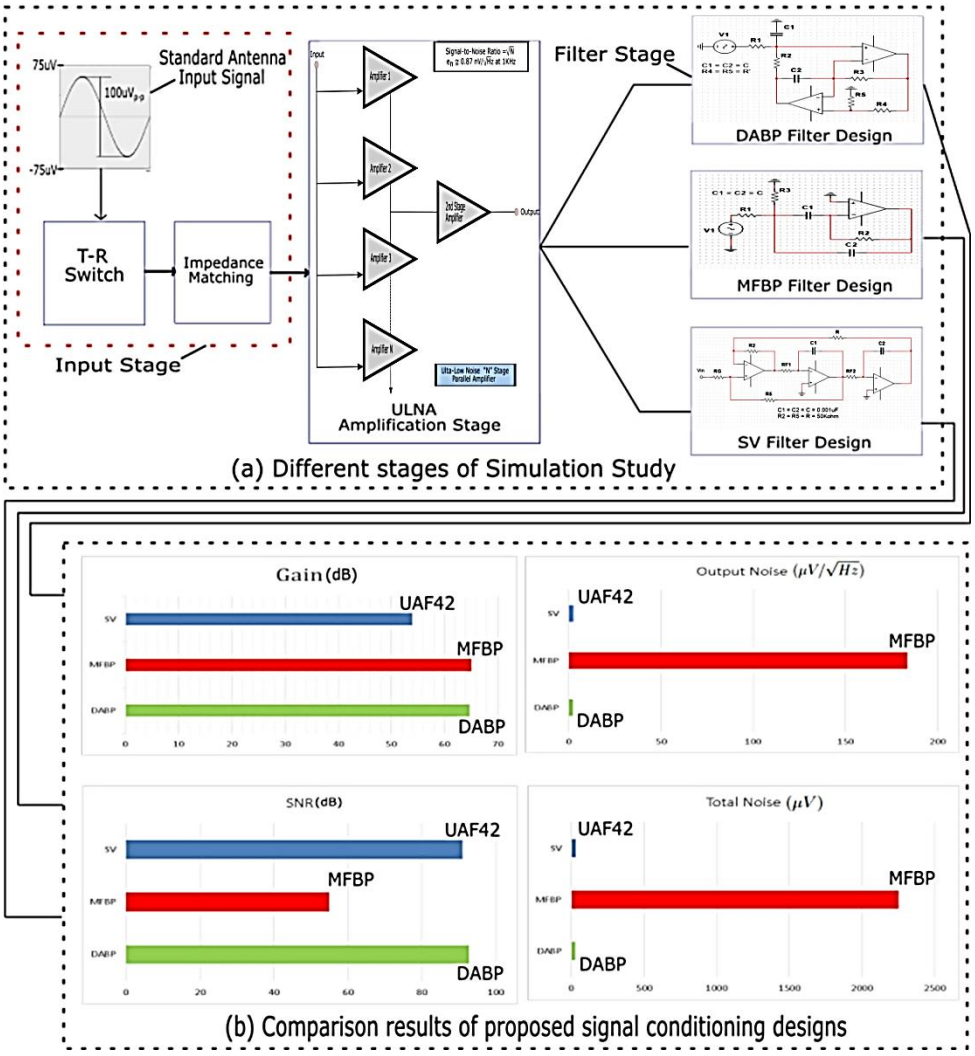

Figure 4.4: (a) Different simulation stages for analysis, (b) comparative experimental result analysis of multiple feed-back band-pass (MFBP), dual-amplifier band-pass (DABP), and state variable (SV) designs

4.1.4 SODAR Transient Analysis Under Practical Considerations

CSIR-NPL SODAR transducer has been used as an input device (signal source) to record backscattered acoustic signals for transient analysis. This signal has been acquired using digital storage oscilloscope (Digilent Analog Discovery-2 Kit) directly from a SODAR transducer and imported into TINA software as a piece-wise input. Later, it has been used to simulate the response of the DABP filter. The transducer is enclosed in an acoustic shield to minimize the surrounding noise, but still, ambient noise modulates the original signal along its propagation path. Figure 4.5 presents the process chart and output response of the transient analysis. The significant noise is visible in the input signal, which is further processed through the ULNA and DABP filters later to remove the noise. The ULNA and DABP remove the unwanted peaks from the signal, and smooth voltage

waveforms have been acquired. This work strongly manifests the implementation of the DABP filter with ULNA for the SODAR signal conditioning stage.

4.1.5 Comparative Frequency Analysis of Preamplifier Circuit

The frequency response has been evaluated in the AC/DC Metrology section of CSIR-NPL, New Delhi. The Fluke 5700A calibrator has been used as a standard input supply, and the Fluke 8846A precision multimeter has been used for measuring the output signal. The fixed 1 mV input supply is given with a frequency that varies from 10 Hz to 10 kHz. The ULNA and SLNA preamplifier circuit voltage responses have been recorded and plotted, shown in Figure 4.6. The preamplifier circuit consisting of ULNA and DABP filters provides 11 dB additional gain compared to the SLNA-SV design. Also, the DABP filter yields a better NBP response with sharp attenuation at cut-off frequencies. These features show the advantages in the signal processing of SODAR.

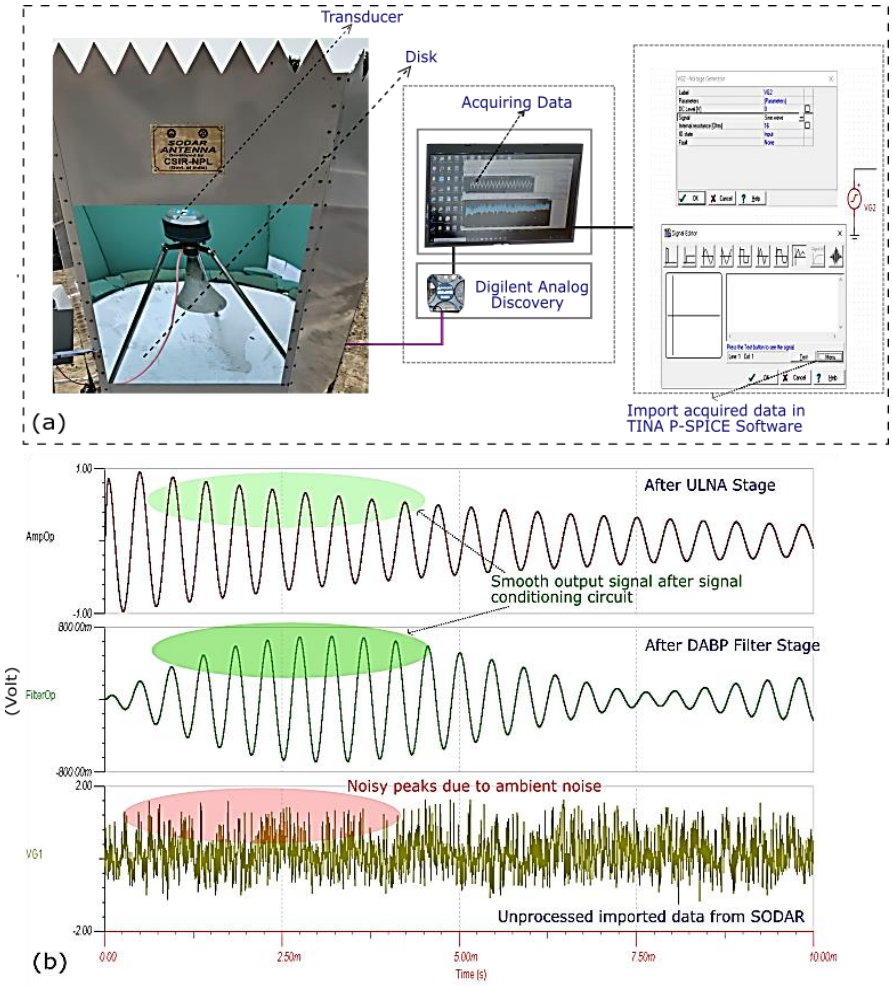

Figure 4.5: (a) Data acquiring process from practical SODAR at CSIR-NPL, New Delhi, (b) transient response of the case study.

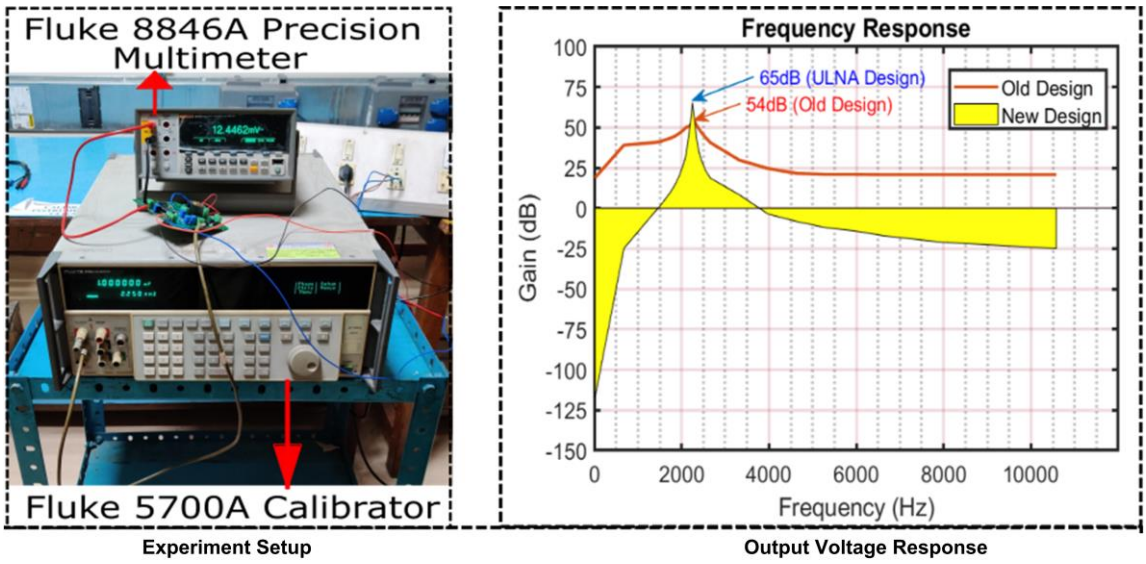

Figure 4.6: Experiment setup for frequency response comparison of the ULNA-DABP and SLNA-SV circuit

4.1.6 Echogram Structure Analysis

The updated preamplifier has been successfully installed with the SODAR system located at CSIR-NPL and now providing continuous real-time data. The ABL structure obtained from the updated SODAR system has been processed using the data acquisition software developed in the NI-Labview framework. The echogram is a graphical representation of the prevalent meteorological conditions and a qualitative measurement of the diurnal variation of the atmospheric dispersion capabilities. The echogram has been generated from the backscattered signals of the SODAR. Since 1970, SODAR is used to record the atmospheric boundary layer as an echogram [65]. These echogram structures are extremely reliant on the geographical location and climatic conditions, including temperature, relative humidity, and wind profiles. The ABL height is calculated using an approximation approach.

SODAR system has been calibrated with standards for accurate results. The testing has been conducted at CSIR-NPL, New Delhi [13, 26, 69]. The updated system's echogram structure was compared to the old SODAR system that had been previously utilized at CSIR-NPL. The various echogram structures of updated and old system are depicted in Figures 4.7(a) and 4.7(b), respectively. The echogram structures have been derived from old and updated systems in various time periods. The updated SODAR design is able to effectively produce a variety of well-known ABL structures [25]. Different colours have

been assigned to new structures. These colour intensities determine the amplitude of the backscattered signals.

Figure 4.8 depicts user interface for real-time data acquisition. It displays the plots the echogram, filtered backscattered signal, and frequency response plot. The frequency response demonstrates the filter's efficacy, as the signal amplitude drastically decreases outside the operational frequency range.

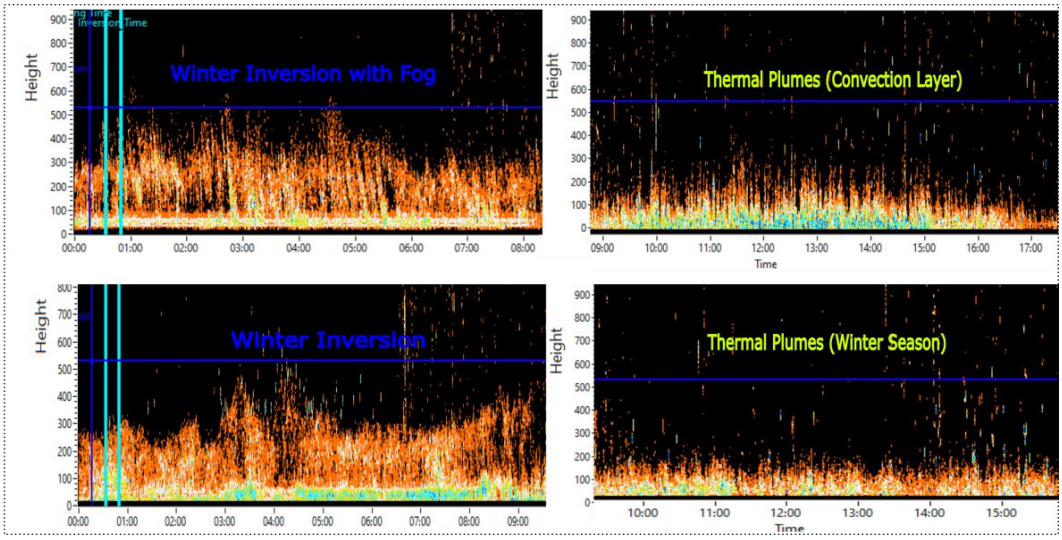

(a) Various echogram structures of updated design.

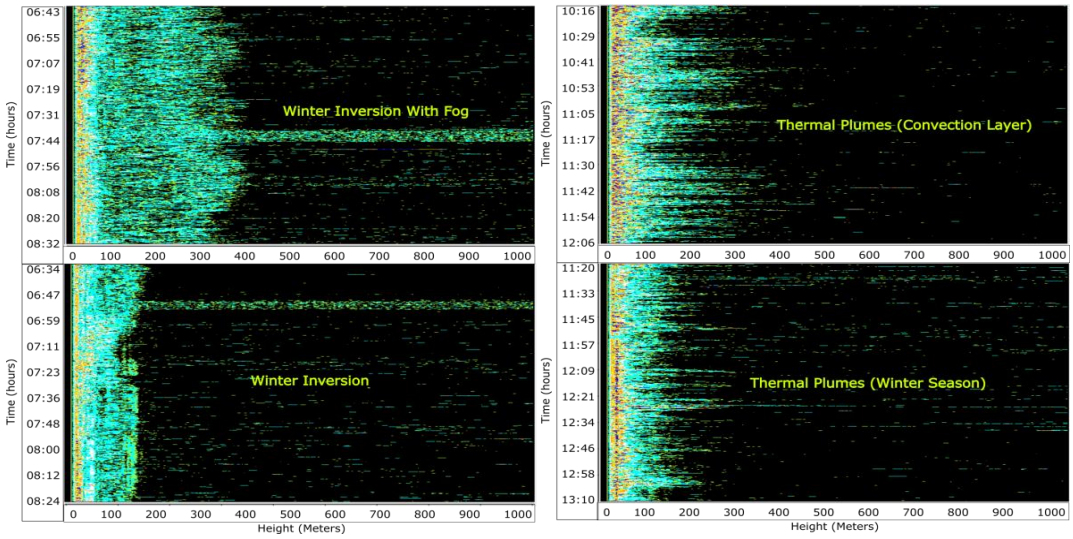

(b) Various echogram structures of old design

Figure 4.7: Standard echogram structures (winter-inversion, thermal plumes, winter inversion and thermal plumes) of updated design and old design

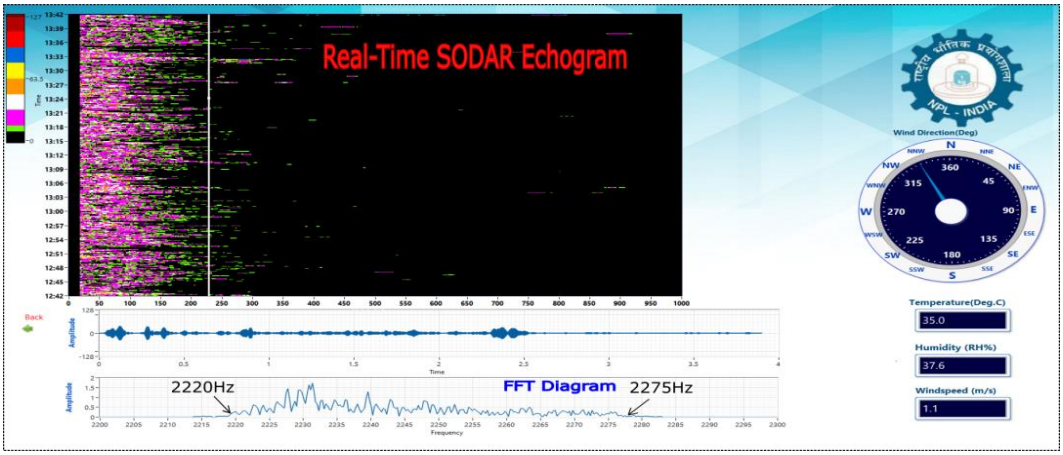

Figure 4.8: Graphical user interface of the real-time SODAR software

4.2 IoT-Based SODAR Network

Figure 4.9 shows the testing part of performance analysis of analog signal processing, digital signal processing and data validation of the network. In the first phase, the gain performance of the analog system for IoT-SN has been observed and compared with the existing SLNA-SV based analog system. The research work has been performed at the acoustic and vibration department of CSIR-NPL, New Delhi with fluke 5700A calibrator, fluke 8846A precision multi-meter. The second phase is focused on the data collection and data validation of IoT-SN system. Last phase is focused on analysis of ABL height from multiple locations using IoT-SN and compared with the estimated ABL height at the local station.

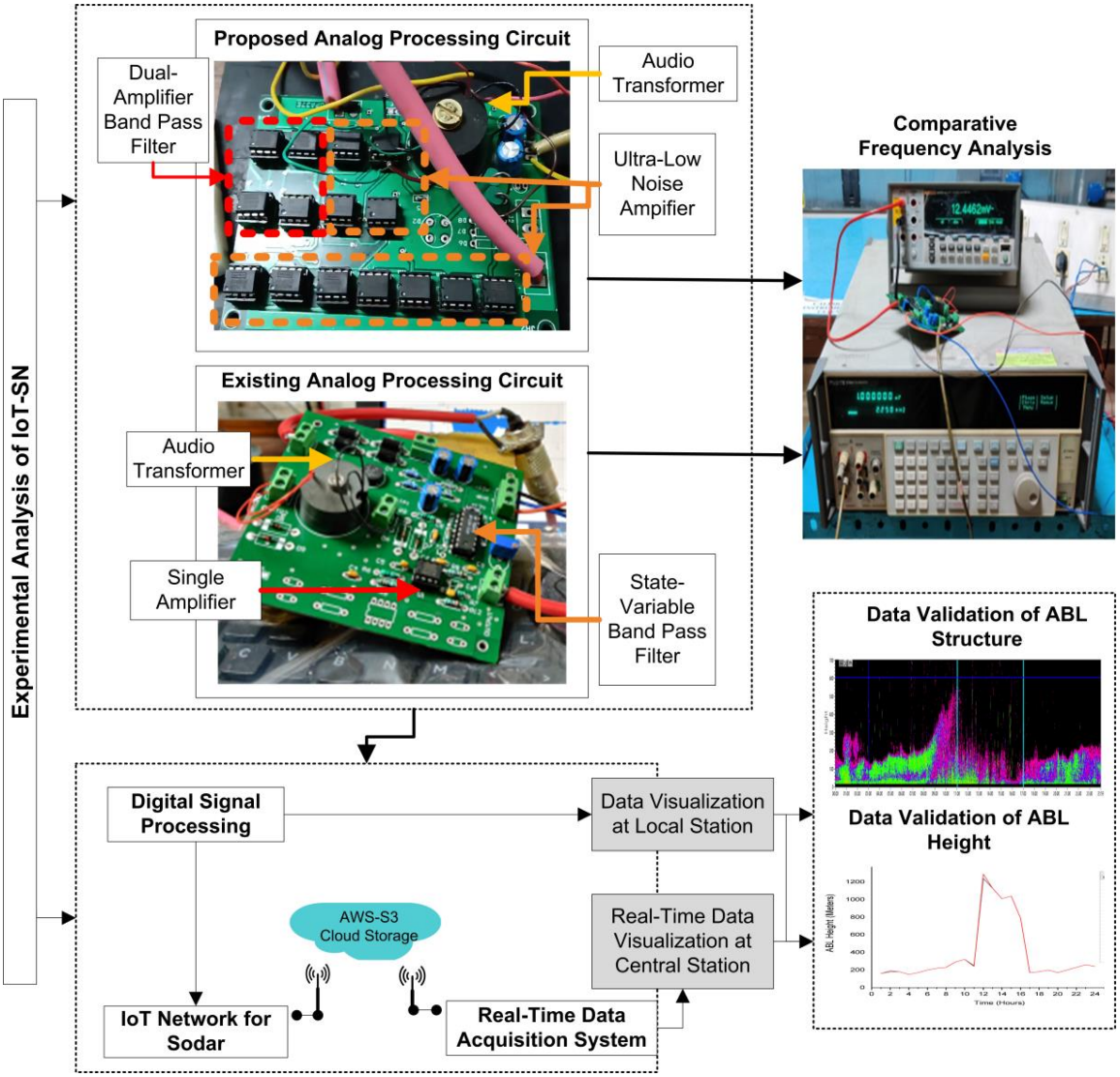

Figure 4.9: Experimental analysis of IoT based SODAR network

4.2.1 Frequency Analysis of Analog System

The frequency analysis has been performed to evaluate the gain performance of the analog systems with the SLNA-SV. An input signal of 100 mV is provided in frequency range $20\ Hz\ to\ 20\ kHz$ with octave increment. Thereafter, the gain in dB is calculated using equation 4.1.

$$Gain(dB) = 20log\frac{Output\ Voltage}{Input\ Voltage} \qquad 4.1$$

Figure 4.10 depicts the gain verses frequency plot where black and red line represents the gain of the updated and SLNA-SV design, respectively. The analog circuit offers better

gain of 65.44 dB at center frequency 2.25 kHz and sharp attenuations of −13.38 dB and −11.51 dB at cutoff frequencies at 2.2 kHz at 2.3 kHz, respectively. The sharp attenuation outside the desired operating frequency range 2.2 kHz to 2.3 kHz shows the better noise elimination characteristics of the analog system. The SODAR transducer is highly sensitive to atmospheric turbulence and a high gain amplifier and NBP filter design of analog circuit help to capture the highly sensitive backscattered signal from the atmosphere [28].

4.2.2 ABL Structure Analysis

The ABL structures are the atmospheric backscattered signal, acquired from the SODAR data acquisition system in real-time. The data of 24-Hours duration has been taken from the IoT-SN and local station of CSIR-NPL, as a reference for further analysis. The ABL structure obtained from the IoT-SN has been compared with the reference ABL structures, as shown in Figure 4.11. The echogram of IoT-SN has been plotted using half data points only in comparison to data for local station ABL structure. The comparative analysis has been performed for 24-Hours, 5-Hours and 3-Hour ABL Structure data to observe the resolution of the ABL structures. The number of data points used for plotting the 24-Hour ABL structure from reference station is 6747520.

In contrast, the number of data points in the IoT-SN for plotting the same ABL structures is reduced to 3365120. It has been observed that the IoT-SN have received 8640 less data points from the intended data points with accuracy of 99.74 %. The shape of the ABL structure acquired from the IoT-SN is same as the reference ABL structure besides the denseness of the graph. In the 24-hour data, very minor changes have been observed in the density of the reference structure, and the shape remains same in both cases.

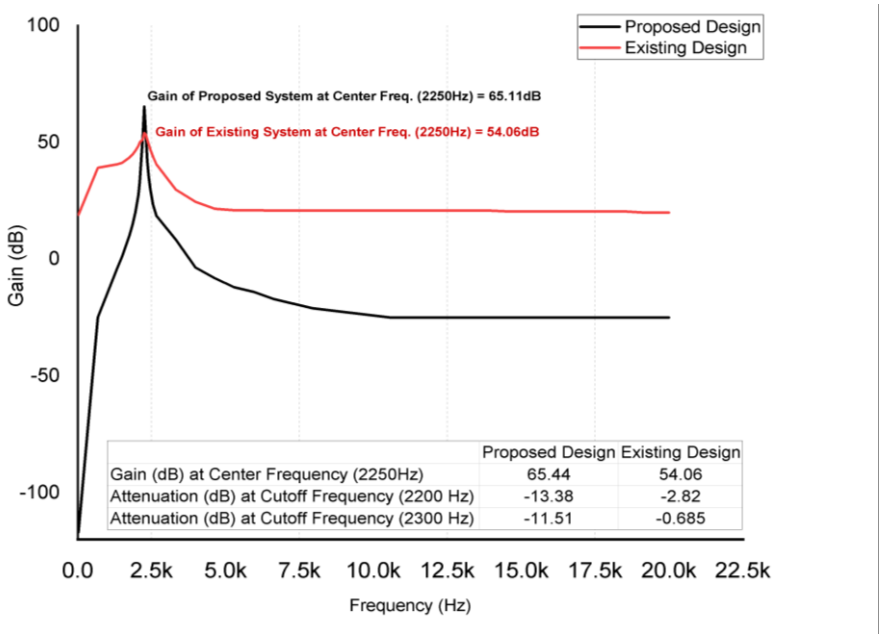

Figure 4.10: Comparative gain (dB) analysis of proposed and SLNA-SV designs

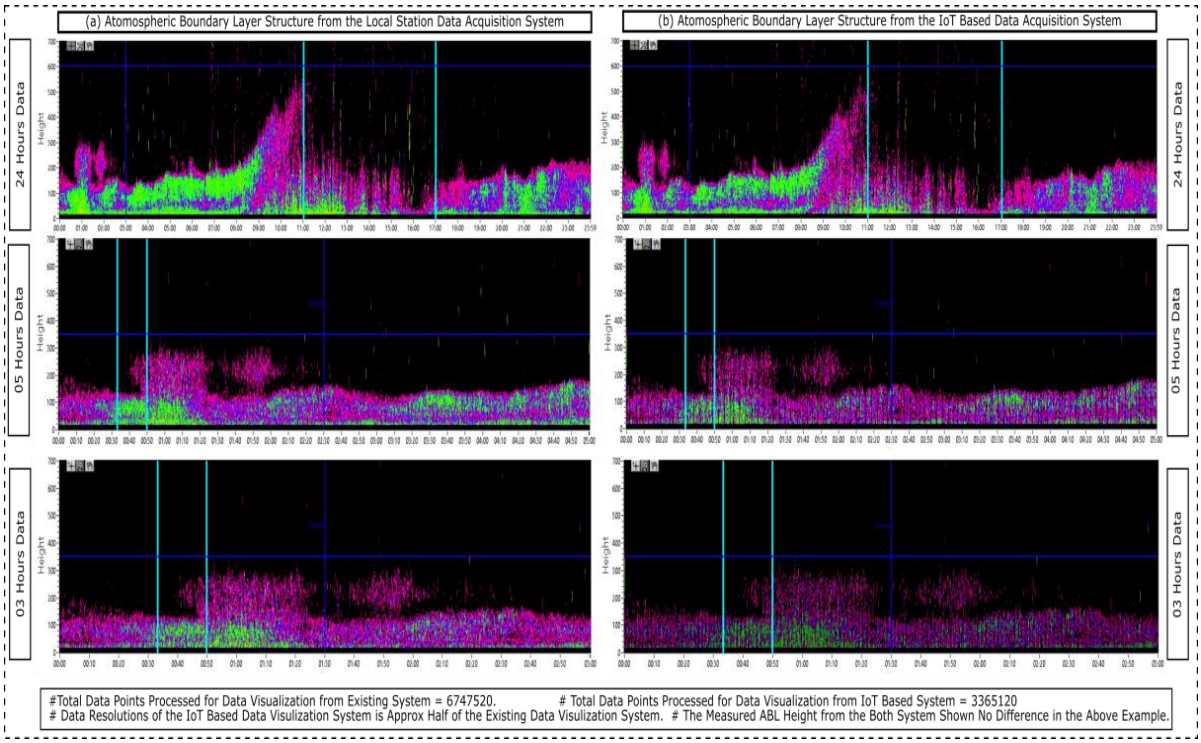

Figure 4.11: ABL structure of 24-hour data, 5-hour data, and 3-hour data from the proposed and local system

The 5 hour data gives more clarity about the density of the graph, as the small gapes are visible in the graph. The low density of ABL structure is visible in the 3 hour data, where gapes between the data points are further increased.

4.2.3 ABL Height Analysis

The objective of acquiring the ABL structures is to estimate the ABL height. The ABL height from the IoT-SN data and reference data has been estimated for the comparative analysis. Several dynamic elements have been included in the process of estimating ABL height from the ABL structure. The observer needs to broadly classify the data into two categories namely inversion-time and convection-time. The other classifications of ABL structure are fog-layer, rising-layer, and multi-layer and each classified structure demands a different approach for the ABL height estimation.

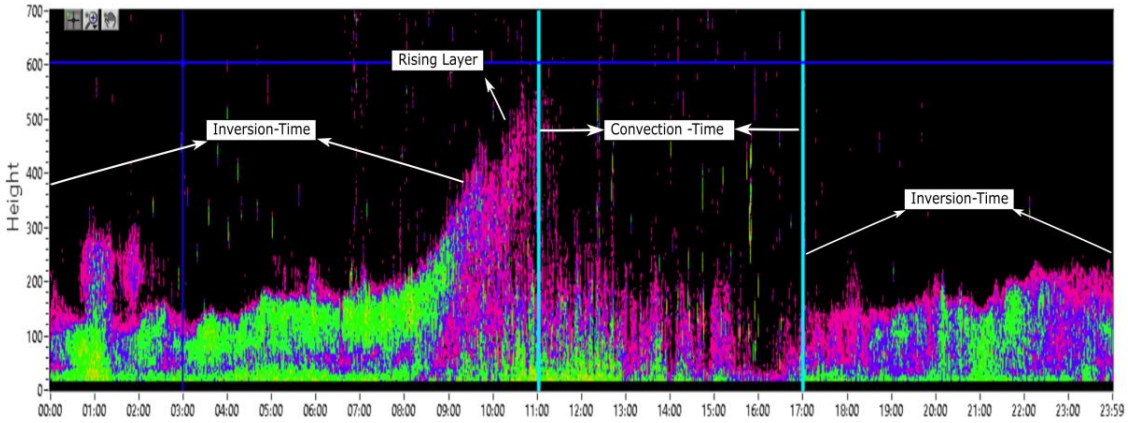

Figure 4.12: ABL structure classification as inversion-time, convection-time, and rising layer

Figure 4.12 presents an example of classified ABL structure data of 20th December 2020 obtained from CSIR-NPL SODAR, New Delhi. The ABL height has been estimated under the supervision of atmospheric science experts of CSIR-NPL, New Delhi. During inversion time, the ABL height is calculated directly using the graph's highest stable point. However, during the convection period, height is determined using the empirical relation $y = 4.24x + 95$ [28]. The actual height in this case is x. Figure 4.12 presents a clear categorization of inversion and convection time. Therefore, the height during convection time is significantly higher than the height during inversion time. ABL height is calculated using both locally acquired echogram structure and structure obtained from an IoT-based system. Figure 4.13 gives the comparison chart of ABL height estimated from the IoT-SN and reference data. The comparative analysis shows the 95.57 % accuracy of estimated ABL height from the IoT-SN with an error of less than $\pm$ 5 %. The estimated value with error has a variation from the true value of less than $\pm$ 13 %. The estimation process of ABL height is analytical work and an error of less than $\pm$ 5 % is in lies within the permissible limit [152]. Further, a similar comparative analysis has been

performed on multiple location data and presented in Figure 4.13. The estimation of ABL height gives the accurate vertical excursion of the unstable parcel and is highly useful in Airshed management planning. Precise Airshed in a defined area is unlikely due to its dependency on several atmospheric conditions [153]. The ABL height data from multiple locations using IoT-SN is instrumental for the Airshed management planning effectively from a central location.

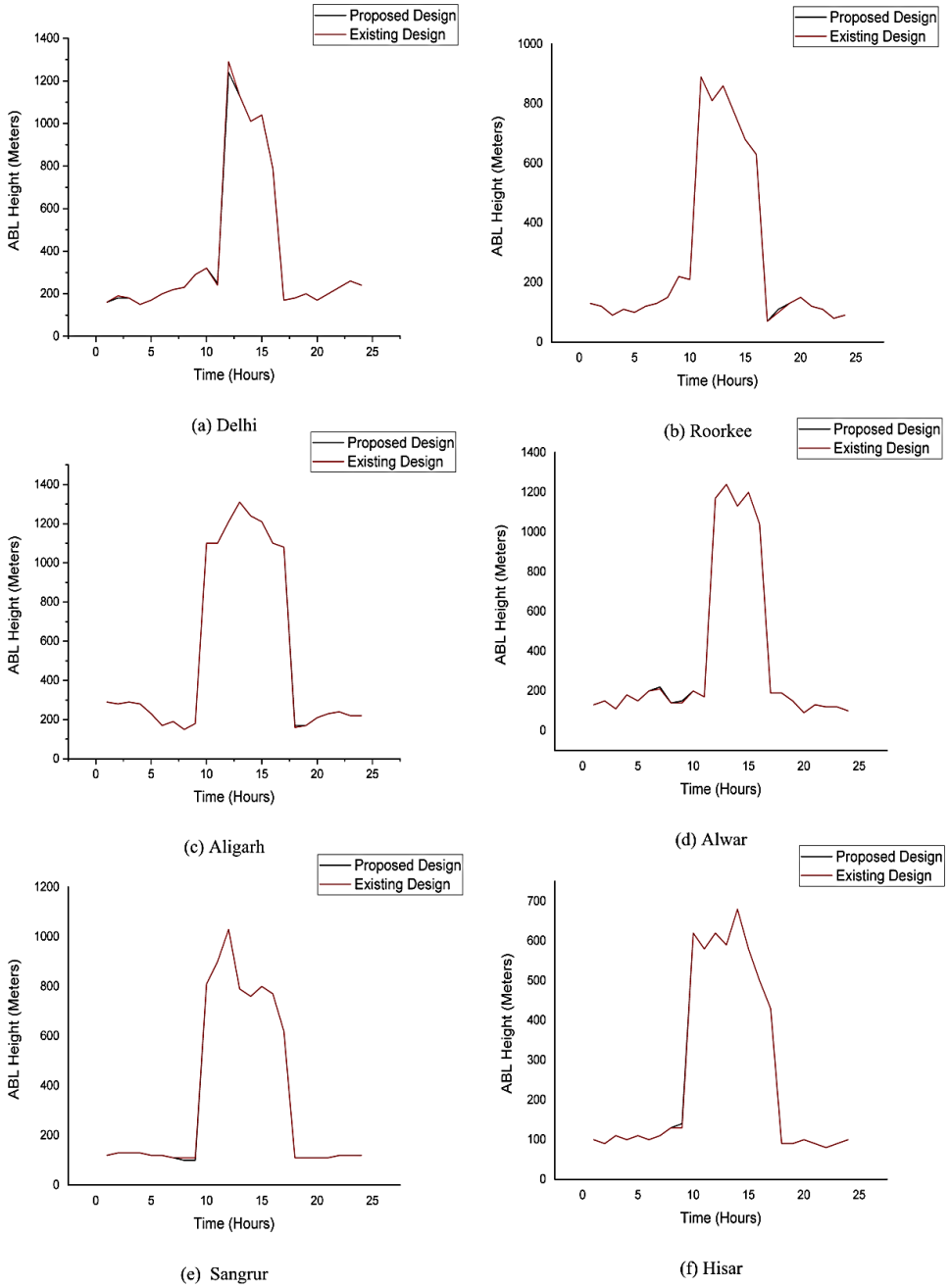

Figure 4.13: ABL height comparison for all stations

4.3 Integrated IoT-Based SODAR and Meteorological Sensor Network (IoT-SMSN)

The integrated SMSN has been established to monitor the mixing-height and affect meteorological parameters in Northern India. To ensure the reliability of the IoT-SMSN, the data collection has been done at the testing laboratory (CSIR-NPL) and validated with the local data acquisition software. Thereafter, the data has been collected from all sensor nodes (installation sites), and the correlation is analyzed between the mixing-height and other meteorological parameters. In a similar context, the combined impact of all the sensor nodes' data on air pollution has been also studied.

4.3.1 IoT Enabled SMSN Data Analysis

The first sensor node has been established in the CSIR-NPL for testing purposes and later installed in all locations. The data has been collected from all locations using IoT-SMSN. The collected data points have been compared with the expected number of data points to check system reliability. The standard uncertainty of the network has been calculated in the first stage of analysis. The mathematical expressions used for calculating the standard uncertainty are as follows:

$$Standard\ Uncertainty\ (u) = \frac{\sigma}{\sqrt{N}} \qquad 4.2$$

where σ = Standard Deviation

$$\sigma = \sqrt{\frac{(x_i - \mu)^2}{N}}$$

where, N is the number of data points, x is the per day percentage accuracy, μ is the mean of percentage accuracy, and $= 1,2,$ up to N ;

To calculate the accuracy percentage, the daily received data points have been compared to the predicted data points. The six months data from September 2020 to February 2021 have been analyzed. Afterward, the standard uncertainty has been estimated from daily percentage accuracy values for all the parameters at all sensor nodes. Table 4.3 depicts the calculated standard uncertainty results of the IoT-SMSN system. The combined uncertainty has been calculated for every sensor node to estimate the overall network performance. The combined uncertainty results lie well within the acceptance range. The

minimum combined uncertainty is found at 0.1011 from SN4, whereas maximum uncertainty is observed in SN6, *i.e.*, 0.3370. The standard uncertainty for meteorological parameters has been excluded due to inconsistencies in sensor node data from the IIT Roorkee and AMU Aligarh installation sites. The overall results show excellent consistency with significantly low uncertainty.

The second part of the analysis has been focused on the measurement of SMSN parameters from a remote server. The one-hour standard mean has been calculated from temperature, relative humidity, wind-speed, and prominent direction considered for wind-direction. The estimating process of mixing-height from the ABL structure is a bit complex work. The data acquired from IoT-SMSN has been reduced to half to manage the resources effectively. In this analysis, the measured parameters from the IoT network are compared with the local data acquisition system. The comparative result shows 95 % accuracy with less than 5 % error which lies well within the feasible range considering the manual estimating process of mixing-height. An IoT-SMSN with low network uncertainty is a reliable solution for regional air pollution monitoring.

Table 4.3: Standard uncertainty of the IoT-SMSN

Sensor Nodes (SN)	SMSN Parameters Standard Uncertainty (u)					u_c
	Mixing-height	Temperature	Relative Humidity	Wind Speed	Wind Direction	
SN1	0.15	0.02	0.02	0.02	0.02	0.1591
SN2	0.19	0.03	0.03	0.03	0.02	0.2028
SN3	0.13	*NA*	*NA*	*NA*	*NA*	0.1347
SN4	0.10	*NA*	*NA*	*NA*	*NA*	0.1011
SN5	0.22	0.09	0.03	0.05	0.03	0.2442
SN6	0.28	0.10	0.08	0.11	0.10	0.3370
SN7	0.23	0.03	0.03	0.02	0.02	0.2382

SN1 = CPCB Delhi, SN2 = NPL Delhi, SN3 = IIT Roorkee, SN4 = Aligarh, SN5 =Hisar, SN6 = Sangrur, SN7 = Alwar
MH = Mixing-height, Temp = Temperature, RH = Relative Humidity, WS = Wind Speed, WD = Wind Direction

$$Combined\ Uncertainty\ (u_c) = \sqrt{{u_{MH}}^2 + {u_{Temp}}^2 + {u_{RH}}^2 + {u_{WS}}^2 + {u_{WD}}^2}$$

4.3.2 Correlation Analysis Between Meteorological Parameters and Mixing-Height

The meteorological parameters are significantly crucial for observing the mixing-height pattern of the atmosphere. A correlation study has been performed between the mixing-height data and meteorological parameters. From March 2020 to February 2021, data from all installation sites have been manually collected for analysis. The purpose of the developing SMSN is to observe the regional impact of meteorological parameters on

Delhi air quality. Figure 4.14 shows the correlation-coefficient matrix between sensor nodes for each parameter, where dark-red and dark-blue color indicates a strong positive and negative correlation, respectively. It is evident from the correlation-coefficient matrix that mixing-height, temperature, relative humidity, and wind speed exhibit a significantly strong positive correlation across the sites.

The wind direction is very unpredictable in nature due to local geographical conditions. As a result, it has a negligible correlation with any other sensor node locations. Consequently, the overall strong correlation between Delhi's significant metrics and other sensor nodes indicated that monitoring via IoT-SMSN is certainly beneficial for improved and more effective decision-making. In comparison to other sensor nodes, the Sangrur parameters have a lower level of correlation. The data have been analyzed for one year, which is insufficient to make any meaningful conclusion. The network makes a strong case for the importance of mixing-height in regional meteorological studies.

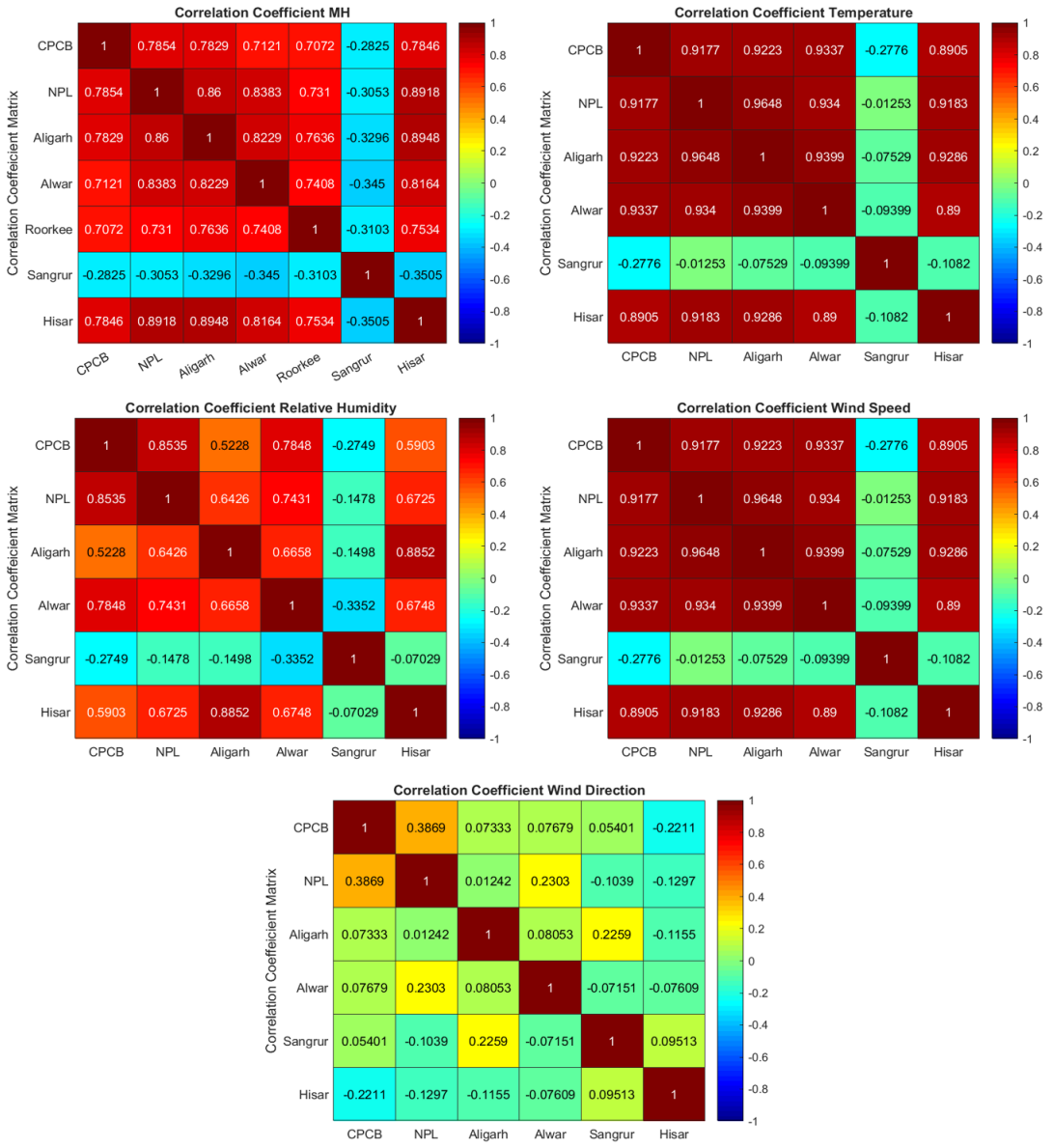

Figure 4.14: Correlation-coefficient matrix between sensor node locations of SMSN parameter

4.3.3 Correlation Analysis of SMSN Parameters for Air Pollutants

The intricate behavior of the atmosphere and the multitude of factors involved in determining air quality in an area necessitate the use of a regional approach for better planning and management. A comprehensive approach is necessary for analyzing the regional impact of air pollution in Delhi. This approach should involve the evaluation and quantification of pollution sources, their emissions, transformations, and the broader effects of meteorology on air pollution for all surrounding regions. In particular, a correlation study is an essential component of this approach. For analysis, the key air-pollutants such as $PM2.5, PM10, O_3, SO_2$ and NO_2 have been selected for analysis. The

data from March-2020 to Feb-2021 has been collected from the CPCB, India, continuous air-quality monitoring stations nearest sensor node locations. The Delhi SMSN parameters along with the air pollutant data have been analyzed with the other sensor node pollutants. Figure 4.15 presents the correlation-coefficient matrix between the SMSN and air-pollutant data of Delhi to all sensor node locations. The correlation analysis displays the notable correlation between mixing-height and O_3 across all the sensor node locations except Hisar. The strongest correlation is found with the Aligarh data highlighted in the purple box in Figure 4.15. The O_3 pollutant is considered the prime air-pollutant for smog creation, which is a major issue in Delhi during the winter season.

Moreover, Delhi's $PM_{2.5}$, PM_{10}, and NO_2 air pollutants exhibit a strong correlation with the pollutant data of other sensor node locations. Among all the locations, Aligarh has shown the strongest correlation with pollutant data. However, a comprehensive analysis is required for understanding the overall impact of each sensor node locations meteorological parameters and pollutants on Delhi's air quality. This research emphasizes the significance of advanced techniques like IoT for establishing a network of multiple sensors to enhance the monitoring and regulation of air quality in a particular area.

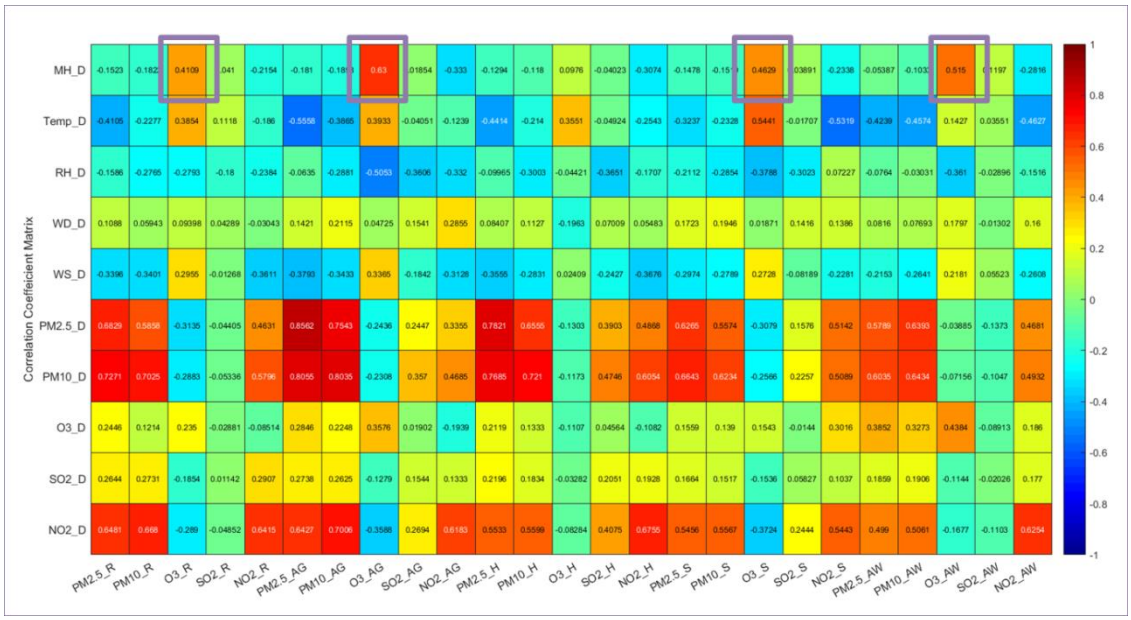

Figure 4.15: Correlation-coefficient matrix between Delhi SMSN parameters and air-pollutants with other senor-node air-pollutants

A novel signal conditioning circuit aided the SODAR in its investigation of the lower atmosphere. Due to its excellent SNR and gain performance, the ULNA design in combination with the DABP filter was selected for the analog signal conditioning system of SODAR based on frequency and noise analyses. Furthermore, the new analog signal conditioning circuit was compared to the current circuit, which includes SLNA and SV amplifier and filter designs. The second section presents the results of the intended IoT-based SODAR network. It promotes information sharing, which is important for Airshed management and planning. The data received from the IoT network was validated by comparing it to data from the local station. IoT-SN echograms have also been plotted using half data points. Finally, a calibrated SMSN with IoT features is established. The SMSN, which is IoT-enabled, estimates the mixing height in real-time as well as the meteorological parameters. The IoT-SMSN's estimated standard uncertainty is excellent, ensuring the system's reliability. The data validation results show more than 95 % accuracy. The significant relationship between SMSN parameters and air pollutants across sensor nodes shows the importance of regional monitoring systems for air quality management.

Chapter 5

Conclusions and Future Recommendations

5.1 Conclusion

The Atmospheric Boundary Layer (ABL) plays a significant role to express the air-quality index of an environment. It determines the environmental capacity for the diffusion of atmospheric pollutants. The air quality in a designated area is influenced by the local air pollution as well as the transported pollutants from remote locations. Estimation of ABL height helps to determine the volume of space in which the emitted pollutants are dispersed. The continuous and effective monitoring of ABL height in real-time is a major concern for the research community. SODAR is crucial for real-time and continuous determination of mixing-height. SODAR provides vital information about atmospheric parameter information such as ABL height, inversions, and stability class. These parameters have a substantial impact on monitoring the hazardous conditions of air pollution.

In the IoT-based SODAR network research, a novel signal conditioning circuit has been designed to study the lower atmosphere. The ULNA design was combined with the DABP filter and performance was compared with the SLNA-SV designs. The performance evaluation of the ULNA and DABP designs shows the better gain and higher selectivity in comparison to the SLNA and SV designs. The updated SODAR system was installed at CSIR NPL, New Delhi, and was used to reflect the ABL structure of Delhi.

Thereafter, digital signal processing and an IoT network have been created for SODAR. The Labview programming language was used for digital signal processing and AWS-S3 was utilized for cloud storage. The echogram structure was plotted using the IoT-based SODAR network. The network accuracy of the received data points has been calculated against the transmission data points. The exhaustive analysis of the developed network shown promising accuracy of 99.74 %. These echograms have been further used for ABL height estimation and the observations are compared with the local data. The comparative analysis showed that the IoT-based SODAR network depicts an accuracy of 95.57 % and variation $\pm$ 13 % from the actual value. These observations assure the IoT-SN is suitable

to provide interconnectivity of multiple SODAR sites effectively, which can be useful in airshed management and planning.

Additionally, a study was conducted to integrate the IoT-based SODAR network with meteorological sensors, referred as IoT-based SMSN. The standard uncertainty of the network was calculated in the first stage of analysis. The combined uncertainty was calculated for every sensor node to estimate the overall network performance. The combined uncertainty results are well within the range of acceptability. It was observed that the Sangrur had the lowest combined uncertainty of 0.1011, while Aligarh has the greatest, of 0.3370. Overall, the results exhibit excellent consistency and a marked reduction in uncertainty.

A correlation study was also performed between the ABL height data and meteorological parameters. The purpose of the developing SMSN was to observe the regional impact of meteorological parameters on Delhi meteorology. According to the correlation coefficient matrix, ABL height, temperature, relative humidity, and wind speed exhibit a strong positive correlation across all sites. The Delhi SMSN parameters, along with the air pollutant data, have been analyzed with the other sensor node pollutants. The air-pollutants such as those $PM2.5, PM10$ and NO_2 of Delhi show a strong correlation with other sensor node locations' pollutant data. It was observed that air pollutants from different sensor nodes are also responsible for the Delhi air pollution. However, a rigorous study on the topic will be helpful to determine detailed characteristics of meteorological parameters across all locations. The integration of IoT with SODAR and meteorological parameters is important for improving the overall decision-making and planning of Delhi's air quality for the regulatory authorities.

5.2 Future Recommendations

For future work, the following suggestions are made to improve the performance of the IoT-based SODAR Network:

- Real-time estimation of the anomalies presents in the atmosphere structure obtained from SODAR can be done by artificial intelligence and machine learning (AI/ML) techniques. Overall, AI/ML may improve the decision-making of regulatory authorities for atmospheric monitoring.
- Doppler-SODAR is useful for monitoring the complete wind profile. The integration of IoT and AI/ML capabilities with Doppler-SODAR can be more useful for airshed management and planning.

Publications

SCI Publications

1. Parag Chourey, Nirbhow Jap Singh, Kirti Soni, & Ravinder Agarwal. (2022). A Novel Signal Conditioning System for SODAR. **Measurement Science and Technology**, vol. 33, pp. 13, 2022, [DOI: https://doi.org/10.1088/1361-6501/ac83e0]
2. Parag Chourey, Kirti Soni, Nirbhow Jap Singh, & Ravinder Agarwal. (2022). IoT-SODAR network for airshed management planning. **IETE Journal of Research**, pp. 1-15, 2022, [DOI: https://doi.org/10.1080/03772063.2022.2026826]
3. Parag Chourey, Nirbhow Jap Singh, Kirti Soni, & Ravinder Agarwal. (2022). SODAR Based Meteorological Sensor Network for Air Pollution Monitoring in Northern India. **Journal of Metrology Society of India**, pp. 1-15, 2022, [DOI: https://doi.org/10.1007/s12647-022-00569-y]

Book Chapters Publications

1. Parag Chourey, Nirbhow Jap Singh, Kirti Soni, & Ravinder Agarwal. (2022). IoT-Enabled Sensor Node for Environmental Monitoring. Recent Advances in Metrology. Lecture Notes in Electrical Engineering, vol 906, **Springer Singapore**. [DOI: https://doi.org/10.1007/978-981-19-2468-2_38]
2. Kirti Soni, Parag Chourey, Kumar, N., Nirbhow Jap Singh, Ravinder Agarwal., & Nair, A. (2022). Fusion of Smart Meteorological Sensors, Remote Sensing Techniques and IoT in Context of Industry 4.0, Handbook of Metrology and Applications, **Springer Singapore**. (Accepted).
3. Kirti Soni, Nair, A., Kumar, N., Parag Chourey, Nirbhow Jap Singh, & Ravinder Agarwal. (2022). Development of calibrated and validated SODAR with reference of Air Quality Management, Handbook of Metrology and Applications, **Springer Singapore**. (Accepted).
4. Kirti Soni, Kumar, N., Nair, A., Parag Chourey, Nirbhow Jap Singh, & Ravinder Agarwal. (2022). Artificial Intelligence: Implementation and Obstacles in Industry 4.0, Handbook of Metrology and Applications, **Springer Singapore**. [DOI: https://doi.org/10.1007/978-981-19-1550-5_54-1]

Journal Publications (Non-SCI)

1. Parag Chourey, Kirti Soni, Nirbhow Jap Singh, Mahavir Singh, & Ravinder Agarwal. (2019). Analyzing sound absorption coefficient of echo wood material with different air gap thickness. THE JOURNAL OF ACOUSTICAL SOCIETY OF INDIA, 57.

International/National Conferences

1. Parag Chourey, Kirti Soni, Nirbhow Jap Singh, Nishant Kumar, & Ravinder Agarwal. (2022). Forecasting of Atmospheric Boundary Layer Height using LSTM. 11th International Conference on “Advances in Metrology”, pp. 188, 2022.
2. Parag Chourey, Kirti Soni, Nirbhow Jap Singh, Mahavir Singh & Ravinder Agarwal. (2019). Study of Atmospheric Boundary layer of Delhi during the dust storm in May 2018 using SODAR and its impact on the Air Quality, National Symposium on Acoustics, India, 17-19 October 2019, Cuttack.
3. Nishant Kumar, Parag Chourey, Rohan Kamra, Priyanka Singh, Anjali S. Nair, Mamta Devi, Kirti Soni and Mahavir Singh. (2020). Design Considerations and Ambient Noise Problem in SODAR System. 6th National Conference on “Advances in Metrology – 2020, CSIR-NPL, New Delhi.

References

[1] S. P. Singal, S. K. Aggarwal, D. R. Pahwa, and B. S. Gera, "Stability studies with the help of acoustic sounding," *Atmospheric Environment*, vol. 19, no. 2, pp. 221–228, 1985.

[2] S. P. Singal and S. K. Aggarwal, "Sodar & radiosonde studies of thermal structure of the lower atmosphere at Delhi," 1979.

[3] S. P. Singal, B. S. Gera, D. R. Pahwa, and S. K. Aggarwal, "Studies of sodar surface-based shear echo structures," *Atmospheric Research*, vol. 20, no. 2–4, pp. 125–131, 1986.

[4] M. S. Pekour and M. A. Kallistratova, "SODAR study of the boundary layer over Moscow for air pollution applications," *Appled Physics*, vol. B57, pp. 49–55, 1993.

[5] M. E. Chang and C. Cardelino, "Application of the urban airshed model to forecasting next-day peak ozone concentrations in Atlanta, Georgia," *Journal of the Air & Waste Management Association*, vol. 50, no. 11, pp. 2010–2024, 2000.

[6] N. Zirnhelt *et al.*, "Airshed Management," in *Air Quality Management*, Springer, 2014, pp. 329–348.

[7] J. M. Wilczak, E. E. Gossard, W. D. Neff, and W. L. Eberhard, "Ground-based remote sensing of the atmospheric boundary layer: 25 years of progress," pp. 321–349, 1996.

[8] D. Biswas, "Assessment of Impact to Air Environment: Guidelines for Conducting Air Quality Modelling," *Central Pollution Control Board(CPCB), New Delhi*, vol. 70, p. 42.

[9] R. B. Stull, *An introduction to boundary layer meteorology*, vol. 13. Springer Science & Business Media, 2012.

[10] P. Seibert, F. Beyrich, S.-E. Gryning, S. Joffre, A. Rasmussen, and P. Tercier, "Review and intercomparison of operational methods for the determination of the mixing height," *Atmospheric Environment*, vol. 34, no. 7, pp. 1001–1027, 2000.

[11] E. N. Kadygrov, *Operational aspects of different ground-based remote sensing observing techniques for vertical profiling of temperature, wind, humidity and cloud structure: A Review*, no. WMO/TD-No. 1309. World Meteorological Organization, Geneva, Switzerland, 2006.

[12] S. P. Singal, *Acoustic remote sensing applications*, vol. 69. Springer, 2006.

[13] M. M. S. S. P. Singal, B. S. Gera, S. K. Aggarwal, "Use of Monostatic Sodar in Probing the Lower Atmosphere," *Indian Jouirnal of Radio Space Physics*, vol. 4, pp. 146–156, 1975.

[14] N. Kumar, K. Soni, and R. Agarwal, "Design and Development of SODAR Antenna Structure," *MAPAN*, pp. 1–9, 2021.

[15] S. P. Singal and B. S. Gera, "Acoustic remote sensing of the boundary layer," *Proceedings of Indian Academics Science Section C: Engineering Science*, vol. 5, no. 2, pp. 131–157, 1982.

[16] S. P. Singal, B. S. Gera, and S. K. Agarwal, "Determination of structure parameters using sodar," *Boundary-Layer Meteorology*, vol. 23, no. 1, pp. 105–114, 1982.

[17] S. D. Danilov *et al.*, "Acoustic calibration of sodars," *Measurement Science Technology*, vol. 3, no. 10, p. 1001, 1992.

[18] G. W. Gilman, H. B. Coxhead, and F. H. Willis, "Reflection of sound signals in the troposphere," *Journal of Acoustics Society of America*, vol. 18, no. 2, pp. 274–283, 1946.

[19] R. L. Coulter and M. A. Kallistratova, "Two decades of progress in SODAR techniques: a review of 11 ISARS proceedings," *Meteorology Atmospheric Physiocs*, vol. 85, no. 1, pp. 3–19, 2004.

[20] R. I. S. Pereira, S. C. S. Juca, P. C. M. Carvalho, and C. P. Souza, "IoT Network and

Sensor Signal Conditioning for Meteorological Data and Photovoltaic Module Temperature Monitoring," *IEEE Latin America Transactions*, vol. 17, no. 06, pp. 937–944, 2019.
[21] Z. Idrees, Z. Zou, and L. Zheng, "Edge computing based IoT architecture for low cost air pollution monitoring systems: a comprehensive system analysis, design considerations & development," *Sensors*, vol. 18, no. 9, p. 3021, 2018.
[22] Y. Hajjaji, W. Boulila, I. R. Farah, I. Romdhani, and A. Hussain, "Big data and IoT-based applications in smart environments: A systematic review," *Computer Science Rev.*, vol. 39, p. 100318, 2021.
[23] J. Wang, M. K. Lim, C. Wang, and M.L. Tseng, "The evolution of the Internet of Things (IoT) over the past 20 years," *Computers & Industrial Engineering*, vol. 155, p. 107174, 2021.
[24] M. A. Khan and K. Salah, "IoT security: Review, blockchain solutions, and open challenges," *Future Generation Computer Systems*, vol. 82, pp. 395–411, 2018.
[25] N. Kumar *et al.*, "SODAR pattern classification and its dependence on meteorological parameters over a semiarid region of India," *International Journal of Remote Sensing*, vol. 38, no. 11, pp. 3466–3482, 2017.
[26] D. Saha, K. Soni, M. N. Mohanan, and M. Singh, "Long-term trend of ventilation coefficient over Delhi and its potential impacts on air quality," *Remote Sensing Applications: Society and Environment*, vol. 15, no. 100234, pp. 1–11, 2019.
[27] M. Mishra and S. R. N. Reddy, "ESENSE: Design & Development of an IoT based Environment Monitoring System," in *2020 IEEE International Conference on Computing, Power and Communication Technologies (GUCON)*, 2020, pp. 368–372.
[28] S. P. Singal, B. S. Gera, M. A. Kallistratova, and I. V Petenko, "Sodar aspect sensitivity studies in the convective boundary layer," *International Journal of Remote Sensing*, vol. 18, no. 8, pp. 1809–1819, 1997.
[29] S.-S. Sharifi, V. Rezaverdinejad, V. Nourani, and J. Behmanesh, "Multi-time-step ahead daily global solar radiation forecasting: performance evaluation of wavelet-based artificial neural network model," *Meteorology and Atmospheric Physics*, vol. 134, no. 3, pp. 1–14, 2022.
[30] P. C. S. Devara, P. Ernest Raj, B. S. Murthy, G. Pandithurai, S. Sharma, and K. G. Vernekar, "Intercomparison of nocturnal lower-atmospheric structure observed with lidar and sodar techniques at Pune, India," *Journal of Applied Meteorology Climatology*, vol. 34, no. 6, pp. 1375–1383, 1995.
[31] X. Y. Wang and K. C. Wang, "Estimation of atmospheric mixing layer height from radiosonde data," *Atmospheric Measurement Techniques*, vol. 7, no. 6, pp. 1701–1709, 2014.
[32] G. Tang *et al.*, "Mixing layer height and its implications for air pollution over Beijing, China," *Atmospheric Chemistry and Physics*, vol. 16, no. 4, pp. 2459–2475, 2016.
[33] T. Partal, "Comparison of wavelet based hybrid models for daily evapotranspiration estimation using meteorological data," *KSCE International Journal of Civil Engineering*, vol. 20, no. 5, pp. 2050–2058, 2016.
[34] E. Taylor and A. McMillan, *Air quality management: Canadian perspectives on a global issue*. Springer Science & Business Media, 2013.
[35] CPCB, "Air Quality Monitoring, Emission Inventory and Source Apportionment Study for Indian Cities: National Summary Report," 2011.
[36] CPCB, "National Ambient Air Quality Status & Trends in India-2010," 2012.
[37] CPCB, "Continuous Ambient Air Quality." 2016.
[38] S. Mahato, S. Pal, and K. G. Ghosh, "Effect of lockdown amid COVID-19 pandemic on air quality of the megacity Delhi, India," *Science of the Total Environment*, vol. 730, p.

139086, 2020.
[39] S. K. Jha *et al.*, "Domain Adaptation-Based Deep Calibration of Low-Cost $PM_{2.5}$ Sensors," *IEEE Sensors Journal*, vol. 21, no. 22, pp. 25941–25949, 2021.
[40] B. R. Gurjar, K. Ravindra, and A. S. Nagpure, "Air pollution trends over Indian megacities and their local-to-global implications," *Atmospheric Environment*, vol. 142, pp. 475–495, 2016.
[41] D. Saini, U. R. Darla, D. H. Lataye, V. M. Motghare, and A. A. Shingare, "Effect on Ambient Air Quality in Nagpur due to lockdown to contain the spread of COVID-19 pandemic in the year 2020: a case study," *Sadhana*, vol. 47, no. 2, pp. 1–11, 2022.
[42] P. Pant *et al.*, "Monitoring particulate matter in India: recent trends and future outlook," *Air Quality, Atmosphere, and Health*, vol. 12, no. 1, pp. 45–58, 2019.
[43] G. Beig *et al.*, "Objective evaluation of stubble emission of North India and quantifying its impact on air quality of Delhi," *Science of the Total Environment*, vol. 709, p. 136126, 2020.
[44] R. Sawlani *et al.*, "The severe Delhi SMOG of 2016: A case of delayed crop residue burning, coincident firecracker emissions, and atypical meteorology," *Atmospheric Pollution Research*, vol. 10, no. 3, pp. 868–879, 2019.
[45] CPCB, "NAQI Status of Indian Cities in 2015–16," 2016.
[46] "AIR QUALITY INDEX A Guide to Air Quality and Your Health," 2020.
[47] A. Boubrima, W. Bechkit, and H. Rivano, "Optimal WSN deployment models for air pollution monitoring," *IEEE Transactions on Wireless Communications*, vol. 16, no. 5, pp. 2723–2735, 2017.
[48] A. C. Rai, "End-user perspective of low-cost sensors for outdoor air pollution monitoring," *Science of the Total Environment*, vol. 607, pp. 691–705, 2017.
[49] Z. Idrees and L. Zheng, "Low cost air pollution monitoring systems: A review of protocols and enabling technologies," *Journal of Industrial Information Integration*, vol. 17, p. 100123, 2020.
[50] N. M. Patil, R. Jain, S. Sankhe, K. Vichare, and A. Wankhede, "IoT based Environment Pollution Monitoring System," *International Journal on Recent and Innovation Trends in Computing and Communication*, vol. 6, no. 4, pp. 150–153, 2018.
[51] X. Yang, L. Yang, and J. Zhang, "A WiFi-enabled indoor air quality monitoring and control system: The design and control experiments," in *2017 13th IEEE International Conference on Control & Automation (ICCA)*, 2017, pp. 927–932.
[52] M. Lobur, D. Korpyljov, N. Jaworski, M. Iwaniec, and U. Marikutsa, "Arduino Based Ambient Air Pollution Sensing System," in *2020 IEEE XVIth International Conference on the Perspective Technologies and Methods in MEMS Design (MEMSTECH)*, 2020, pp. 32–35.
[53] S. Dhingra, R. B. Madda, A. H. Gandomi, R. Patan, and M. Daneshmand, "Internet of Things mobile-air pollution monitoring system (IoT-Mobair)," *IEEE Internet of Things Journal*, vol. 6, no. 3, pp. 5577–5584, 2019.
[54] B. Guanochanga *et al.*, "Real-time air pollution monitoring systems using wireless sensor networks connected in a cloud-computing, wrapped up web services," in *Proceedings of the future technologies conference*, 2018, pp. 171–184.
[55] M. Malhotra, I. K. Aulakh, N. Kaur, and N. S. Aulakh, "Air Pollution Monitoring Through Arduino Uno," in *ICT Systems and Sustainability*, Springer, 2020, pp. 235–243.
[56] R. Kiruthika and A. Umamakeswari, "Low cost pollution control and air quality monitoring system using Raspberry Pi for Internet of Things," in *2017 International Conference on Energy, Communication, Data Analytics and Soft Computing (ICECDS)*, 2017, pp. 2319–2326.

[57] Y. Yang, Z. Zheng, K. Bian, Y. Jiang, L. Song, and Z. Han, “Arms: A fine-grained 3D AQI realtime monitoring system by UAV,” in *GLOBECOM 2017-2017 IEEE Global Communications Conference*, 2017, pp. 1–6.
[58] I. Kalamaras, “Visual analytics for exploring air quality data in an AI-enhanced IoT environment,” in *Proceedings of the 11th International Conference on Management of Digital EcoSystems*, 2019, pp. 103–110.
[59] P. Velasquez, L. Vasquez, C. Correa, and D. Rivera, “A low-cost IoT based environmental monitoring system. A citizen approach to pollution awareness,” in *2017 CHILEAN conference on electrical, electronics engineering, information and communication technologies (CHILECON)*, 2017, pp. 1–6.
[60] B. Maag, Z. Zhou, and L. Thiele, “A survey on sensor calibration in air pollution monitoring deployments,” *IEEE Internet Things J.*, vol. 5, no. 6, pp. 4857–4870, 2018.
[61] W. Tsujita, A. Yoshino, H. Ishida, and T. Moriizumi, “Gas sensor network for air-pollution monitoring,” *Sensors & Actuators, B: Chemical*, vol. 110, no. 2, pp. 304–311, 2005.
[62] M. A. Zaidan, “Intelligent calibration and virtual sensing for integrated low-cost air quality sensors,” *IEEE Sensors Journal*, vol. 20, no. 22, pp. 13638–13652, 2020.
[63] M. Z. Jacobson, “Studying the effects of aerosols on vertical photolysis rate coefficient and temperature profiles over an urban airshed,” *Journal of Geophysical Research: Atmospheres*, vol. 103, no. D9, pp. 10593–10604, 1998.
[64] Y. Levi, U. Dayan, I. Levy, and D. M. Broday, “On the association between characteristics of the atmospheric boundary layer and air pollution concentrations,” *Atmospheric Research*, vol. 231, p. 104675, 2020.
[65] S. P. Singal, B. S. Gera, S. K. Aggarwal, and M. Saxena, “Use of monostatic sodar in probing the lower atmosphere,” *Indian Journal of Radio & Space Physics*, vol. 4, no. 2, pp. 146–156, 1975.
[66] C. G. Little, “Acoustic methods for the remote probing of the lower atmosphere,” *Proceedings of the IEEE*, vol. 57, no. 4, pp. 571–578, 1969.
[67] M. Zhou, “Development of Sodar Detection and Its Application for Studies of Atmospheric Boundary Layer in Beijing , China,” 1997.
[68] A. M. Obukhov, “Sound scattering in a turbulent flow,” in *Proceedings of the USSR Academy of Sciences*, 1941, pp. 611–614.
[69] M. A. Kallistratova, “Sodar sounding of the atmospheric boundary layer: Review of studies at the Obukhov Institute of Atmospheric Physics, Russian Academy of Sciences,” *Izvestiya, Atmospheric and Oceanic Physics*, vol. 54, no. 3, pp. 242–256, 2018.
[70] J. C. Kaimal and D. A. Haugen, “An acoustic Doppler sounder for measuring wind profiles in the lower boundary layer,” *Journal of Applied Meteorology and Climatology*, vol. 16, no. 12, pp. 1298–1305, 1977.
[71] P. L. Finkelstein, J. C. Kaimal, J. E. Gaynor, M. E. Graves, and T. J. Lockhart, “Comparison of wind monitoring systems. Pad II: Doppley. Sodars,” *Journal of Atmospheric and Oceanic Technology*, vol. 3, no. 4, pp. 594–604, 1986.
[72] S. P. Singal, B. S. Gera, and D. R. Pahwa, “Application of sodar to air pollution meteorology,” *Remote Sensing*, vol. 15, no. 2, pp. 427–441, 1994.
[73] W. D. Neff and R. L. Coulter, “Acoustic remote sensing,” in *Probing the Atmospheric Boundary Layer*, Springer, 1986, pp. 201–239.
[74] T. J. Moulsley, D. N. Asimakopoulos, R. S. Cole, and B. A. Crease, “Design of arrays for acoustic sounder antennas,” *Journal of Physics E: Scientific Instruments*, vol. 11, no. 7, p. 657, 1978.
[75] G. Elisei, “Implementation of a multiaxial Doppler sodar system with advanced data

processing," *Atmos. Res.*, vol. 20, no. 2–4, pp. 109–118, 1986.
[76] S. P. Singal, E. W. D. Lewthwaite, and D. S. Wratt, "Estimating atmospheric stability from monostatic acoustic sounder records," *Atmospheric Environment*, vol. 23, no. 10, pp. 2079–2084, 1989.
[77] B. S. Gera and S. P. Singal, "Sodar in air pollution meteorology," *Atmospheric Environment. Part A. General Topics*, vol. 24, no. 8, pp. 2003–2009, 1990.
[78] B. S. Gera, "Instrumentation and computer capabilities for improving sodar data acquisition," *International Journal of Remote Sensing*, vol. 32, no. 17, pp. 4807–4817, 2011.
[79] E. Mursch-Radlgruber *et al.*, "NOAA's portable, high-frequency minisodar design and first results," *Remote Sensing*, vol. 15, no. 2, pp. 325–332, 1994.
[80] G. Mihalakakou, M. Santamouris, J. O. Lewis, and D. N. Asimakopoulos, "On the application of the energy balance equation to predict ground temperature profiles," *Solar Energy*, vol. 60, no. 3–4, pp. 181–190, 1997.
[81] D. N. Asimakopoulos, C. G. Helmis, and M. Petrakis, "Mini acoustic sounding, a powerful tool for ABL applications: Recent advances," in *Acoustic Remote Sensing Applications*, Springer, 1997, pp. 117–132.
[82] S. von Hunerbein, S. G. Bradley, B. J. Piper, and others, "UpWind: integrated wind turbine design-Salford final summary on WP 6.1, WP. 6.2, WP 6.3 And WP 6.4," 2011.
[83] P. Behrens, S. Bradley, and S. Von Hunerbein, "A scanning bi-static SODAR," in *IOP Conference Series: Earth and Environmental Science*, 2008, p. 12010.
[84] A. G. Triantafyllou *et al.*, "Evaluation of an atmospheric model with surface and ABL meteorological data for energy applications in structured areas," *Theoretical and Applied Climatology*, vol. 135, no. 3, pp. 1227–1242, 2019.
[85] N. Elansky, Y. Verevkin, N. Ponomarev, V. Rakitin, and others, "Air quality and pollutant emissions in the moscow megacity," in *11th International Conference on Air Quality Science and Application. Proceedings*, 2018.
[86] S. W. Li, Z. Z. Hu, P. W. Chan, and G. Hu, "A study on the profile of the turbulence length scale in the near-neutral atmospheric boundary for sea (homogeneous) and hilly land (inhomogeneous) fetches," *Journal of Wind Engineering & Industrial Aerodynamics*, vol. 168, pp. 200–210, 2017.
[87] S. V Anisimov, S. V Galichenko, K. V Aphinogenov, and A. A. Prokhorchuk, "Evaluation of the atmospheric boundary-layer electrical variability," *Boundary-Layer Meteorology*, vol. 167, no. 2, pp. 327–348, 2018.
[88] H. T. Friis, "Noise figures of radio receivers," *Proc. IRE*, vol. 32, no. 7, pp. 419–422, 1944.
[89] F. A. Levinzon, "Noise of the JFET amplifier," *IEEE Transactions on Circuits and Systems I: Fundamental Theory and Applications*, vol. 47, no. 7, pp. 981–985, 2000.
[90] S. P. Singal, "Noise problem in the design of SODAR system," *Indian Journal of Radio & Space Physics*, vol. 16, no. 2, pp. 225–231, 1987.
[91] G. H. Crescenti, "The degradation of Doppler sodar performance due to noise: A review," *Atmospheric Environment*, vol. 32, no. 9, pp. 1499–1509, 1998.
[92] D. Singh, R. R. Yadav, and A. K. Tiwari, "Ultrasonic attenuation in semiconductors," 2002.
[93] H. S. Ryait, A. S. Arora, and R. Agarwal, "Interpretations of wrist/grip operations from SEMG signals at different locations on arm," *IEEE Transactions on Biomedical Circuits and Systems*, vol. 4, no. 2, pp. 101–111, 2010.
[94] B. S. . S. P. S. Gera, "Design of a microcomputer-based monostatic sodar system," *Indian Journal of Radio & Space Physics*, vol. 22, no. 1, pp. 296–300, 1993.
[95] G. Maxim, D. R. W. Leipold, B. Scott, and R. C. Nieri, "Low noise amplifier." Google

Patents, 2017.
[96] B. Scott, G. Maxim, D. R. W. Leipold, and K. K. T. Yan, “Low noise amplifier (LNA) system.” Google Patents, 2018.
[97] J. C. Hartung, “Low noise amplifier.” Google Patents, 1976.
[98] L. Dauphinee and L. M. Burns, “Amplifier assembly including variable gain amplifier, parallel programmable amplifiers, and AGC.” Google Patents, 2008.
[99] F. A. Levinzon, “Ultra-low-noise high-input impedance amplifier for low-frequency measurement applications,” *IEEE Transactions on Circuits and Systems I: Regular Papers*, vol. 55, no. 7, pp. 1815–1822, 2008.
[100] Q. Huynh, “Ultra Low Noise Preamplifier Design for Magnetic Particle Imaging,” Electrical Engineering and Computer Sciences University of California, Berkeley, 2018.
[101] B. Vogel, *Simulation Models and Other Spice Related Problems*, no. i9783030112295. Springer, 2019.
[102] C. Maag and L. Parker, “Parallel preamplifier and equalizer.” Google Patents, 1998.
[103] S. Bradley, T. Mikkelsen, S. von Hünerbein, M. Legg, and others, “Precision measurements of wind turbine noise using a large aperture microphone array,” in *Proc. Berlin Beamforming Conference*, 2016, pp. 1–11.
[104] M. Legg, “Multi-frequency clutter-rejection algorithms for acoustic radars,” University of Auckland, 2007.
[105] J. Molina and R. M. Stitt, “Filter design program for the UAF42 universal active filter,” *Burr-Brown*, vol. 746–7592, no. 602, pp. 1–15, 1993.
[106] P. O. Bobbie, C. Z. Arif, H. Chaudhari, and S. Pujari, “Electrocardiogram (EKG) data acquisition and wireless transmission,” *World Scientific and Engineering Academy and Society Transactions on ComputersGreece*, vol. 3, no. 8, pp. 2665–2672, 2004.
[107] A. Polo, P. Narvaez, and C. Robles Algarin, “Implementation of a cost-effective didactic prototype for the acquisition of biomedical signals,” *Electronics*, vol. 7, no. 5, pp. 77–100, 2018.
[108] S. la Pena, A. Polo, and C. Robles-Algarin, “Implementation of a portable electromyographic prototype for the detection of muscle fatigue,” *Electronics*, vol. 8, no. 619, pp. 1–15, 2019.
[109] K. Orłowska, P. Słupski, P. Świkatkowski Michałand Kunicki, A. Sankowska, and T. Gotszalk, “Light intensity fibre optic sensor for MEMS displacement and vibration metrology,” *Optics & Laser Technology*, vol. 65, pp. 159–163, 2015.
[110] T. Nonthaputha and M. Kumngern, “Programmable universal filters using current conveyor transconductance amplifiers,” *Journal of Circuits, Systems, and Computers*, vol. 26–7, no. 1750121, pp. 1–23, 2017.
[111] A. B. Williams and F. J. Taylor, *Electronic filter design handbook*, no. i9780071471718. MCGraw-Hill companies, New York, 2006.
[112] R. P. Sallen and E. L. Key, “A practical method of designing RC active filters,” *IRE Transactions on Circuit Theory*, vol. 2, no. 1, pp. 74–85, 1955.
[113] H. Zumbahlen, *Linear circuit design handbook*, no. i9780750687034.
[114] T. Sullivan and H. Schnell, “Programmable multi-tone voice message starting system.” Google Patents, 1998.
[115] T. Ikeda and H. Miyagi, “Broadcast Signal Receiving Apparatus.” Google Patents, 2008.
[116] T. Ikeda and H. Miyagi, “Antenna input tuning circuit.” Google Patents, 2009.
[117] D. Vasić, V. Bilas, and A. J. Peyton, “Scaled experimental verification of single-well induction conductivity measurement through nonmagnetic casing,” *IEEE Transactions on Instrumentation and Measurement*, vol. 62, no. 5, pp. 1199–1206, 2013.
[118] S. Mantha and M. A. Rani, “Effect of Catastrophic faults in an Analog System,” in *2017 IEEE 7th International Advance Computing Conference (IACC)*, 2017, pp. 535–539.

[119] J. Tow, “Active RC filters -- A state-space realization,” *Proceedings of the IEEE*, vol. 56, no. 6, pp. 1137–1139, 1968.
[120] B. J. Kim, K. B. Lee, J. M. Lee, S. H. Hwang, D. H. Heo, and K. H. Han, “Design of optimal digital filter and digital signal processing for a CdZnTe high resolution gamma-ray system,” *Applied Radiation and Isotopes*, vol. 162, no. 109171, pp. 1–17, 2020.
[121] P. Kendrick and S. von Hünerbein, “Fixed Echo Rejection in Sodar Using Noncoherent Matched Filter Detection and Gaussian Mixture Model--Based Postprocessing,” *Journal of Atmospheric and Oceanic Technology*, vol. 36, no. 1, pp. 3–16, 2019.
[122] Y. Neuvo, G. Rajan, and S. Mitra, “Design of narrow-band FIR bandpass digital filters with reduced arithmetic complexity,” *IEEE Transactions on Circuits and Systems*, vol. 34, no. 4, pp. 409–419, 1987.
[123] D. Koracin and R. Berkowicz, “Nocturnal boundary layer height: Observations by acoustic sounding and predictions in terms of surface layer parameters,” *Boundary Layer Meteorology*, vol. 43, no. 43, pp. 65–83, 1988.
[124] S. J. Caughey, “Observed characteristics of the atmospheric boundary layer,” *Atmospheric turbulence and air pollution modelling*, vol. 43, no. 43, pp. 107–158, 1982.
[125] J. Walczewski, “Application of sodar in urban air-quality monitoring systems,” in *Acoustic Remote Sensing Applications*, Springer, 1997, pp. 385–394.
[126] G. C. Holzworth, “Mixing Depths, Wind Speeds and Air Pollution Potential for Selected Locations in the United States.,” *Journal of Applied Meteorology*, vol. 6, no. 6, pp. 1039–1044, Dec. 1967.
[127] R. L. Coulter and K. H. Underwood, “Some Turbulence and Diffusion Parameter Estimates within Cooling Tower Plumes Derived from Sodar Data,” *Journal of Applied Meteorology Climatol.*, vol. 19, no. 12, pp. 1395–1404.
[128] N. O. Jensen and E. L. Petersen, “The box model and the acoustic sounder: A case study,” *Atmospheric Environment*, vol. 13, pp. 717–720, 1979.
[129] T. J. Moulsley and R. S. Cole, “The evaluation of acoustic sounder returns from a methane plume,” *Atmospheric Environment*, vol. 14, pp. 1063–1066, 1980.
[130] G. Brusasca, G. Elisey, M. Malni, and A. Marzorati, “The evaluation of acoustic sounder returns from a methane plume,” *Proceedings of 2nd international symposium on acoustic remote sensing and associated techniques of the atmosphere and oceans, Rome, Italy*, vol. XXI, pp. 1–12, 1983.
[131] B. S. Gera and N. Saxena, “Sodar data—A useful input for dispersion modeling,” *Atmospheric Environment*, vol. 30, no. 21, pp. 3623–3631, 1996.
[132] A. Salam, “Internet of Things for Environmental Sustainability and Climate Change,” in *Internet of Things for Sustainable Community Development*, Springer, 2020, pp. 33–69.
[133] H. T. Reda, P. T. Daely, J. Kharel, and S. Y. Shin, “On the application of IoT: Meteorological information display system based on LoRa wireless communication,” *IETE Technical Review*, vol. 35, no. 3, pp. 256–265, 2018.
[134] S. Fang *et al.*, “An integrated system for regional environmental monitoring and management based on internet of things,” *IEEE Transactions on Industrial Informatics*, vol. 10, no. 2, pp. 1596–1605, 2014.
[135] Dieter Westermann and H. Westermann, “Measnet Anemometer Calibration Procedure.” 2018.
[136] B. Keswani, “Adapting weather conditions based IoT enabled smart irrigation technique in precision agriculture mechanisms,” *Neural Computing & Applications*, vol. 31, no. 1, pp. 277–292, 2019.
[137] C. Xiaojun, L. Xianpeng, and X. Peng, “IOT-based air pollution monitoring and forecasting system,” in *2015 international conference on computer and computational*

sciences (ICCCS), 2015, pp. 257–260.
[138] H. Tran-Dang, N. Krommenacker, P. Charpentier, and D.-S. Kim, "The Internet of Things for Logistics: Perspectives, Application Review, and Challenges," *IETE Technical Review*, vol. 35, no. 2, pp. 205–220, 2020.
[139] P. P. Ray, "A survey of IoT cloud platforms," *Future Computing and Informatics Journal*, vol. 1, no. 1–2, pp. 35–46, 2016.
[140] S. Andreozzi, L. Magnoni, and R. Zappi, "Towards the Integration of StoRM on Amazon Simple Storage Service (S3)," in *Journal of Physics: Conference Series*, 2008, pp. 33–40.
[141] B. Bitzer and T. Kleesuwan, "Cloud-based smart grid monitoring and controlling system," in *2015 50th International Universities Power Engineering Conference (UPEC)*, 2015, pp. 33837–33863.
[142] A. K. Sharma and K. K. Kim, "Real-Time ECG Signal Acquisition and Processing Using LabVIEW," *Journal of Sensor Science and Technology*, vol. 29, no. 3, pp. 162–171, 2020.
[143] C. E. Mej'ia Mayancela, "Development of remote monitoring solutions for wind resources using the SODAR technique".
[144] J. Vega, "Source resistance and noise considerations in amplifiers," *Analog Applications Journal*, vol. 2Q2012, no. SSZZ022C, pp. 23–28, 2012.
[145] "PA Driver Units," no. AU60 60Watt/16Ohm. 2015.
[146] R. C. D. de Paiva, J. Pakarinen, V. Välimäki, and M. Tikander, "Real-time audio transformer emulation for virtual tube amplifiers," *Eurasip Journal on Advances in Signal Processing*, vol. 2011, no. 1, pp. 1–15, 2011.
[147] ISO1996-2:S, "Acoustics — Description, measurement and assessment of environmental noise — Part 2: Determination of sound pressure levels," *International Organization for Standardization (ISO), Geneva, Switz.*, 2017.
[148] CPCB, "IMPACT OF LOCKDOWN ON AMBIENT AIR QUALITY," 2020.
[149] G. K. Sharma, A. Tewani, and P. Gargava, "Comprehensive analysis of ambient air quality during second lockdown in national capital territory of Delhi," *Journal of Hazardous Materials*, vol. 6, p. 100078, 2022.
[150] C. Zhang and Y. Chen, "A review of research relevant to the emerging industry trends: Industry 4.0, IoT, blockchain, and business analytics," *Journal of Industrial Integration and Management*, vol. 5, no. 01, pp. 165–180, 2020.
[151] N. Kumar, K. Soni, and R. Agarwal, "A comprehensive study of different feature selection methods and machine-learning techniques for SODAR structure classification," *Modeling Earth Systems and Environment*, pp. 1–12, 2020.
[152] S.E. Gryning, F. Beyrich, and E. Batchvarova, "The determination of the mixing height. Current progress and problems," 1997.
[153] B. C. Roisin, "Local air pollution," *Environmental Transport and Fate*, vol. Winter, pp. 181–209, 2012.